الجمهورية الجزائرية الديمقراطية الشعبية

République Algérienne démocratique et Populaire

وزارة التعليم العالي والبحث العلمي

Ministère de l'Enseignement Supérieur et de la Recherche Scientifique

جامعة الشهيد حمة لخضر الوادي

Université Elchahid Hamma Lakhdar - El Oued

Faculté de Technologie
Département de Génie Électrique
Filière d'Électrotechnique

Thèse de doctorat

Présentée par

Miloud GATI

Pour l'obtention du diplôme de Doctorat LMD en électrotechnique

Option optimisation et gestion d'énergie

Titre

Contribution à la commande sans capteur mécanique de la machine synchrone à réluctance variable

---

Thèse soutenue publiquement le (25/01/ 2025) devant le jury composé de

Prénom et nom	Grade	Institution d'affiliation	Designation
Mr Abderrahim Allal	Professeur	Université Elchahid Hamma Lakhdar - El Oued	Président
Mr Hicham Serhoud	Professeur	Université Elchahid Hamma Lakhdar - El Oued	Directeur de thèse
Mr Youcef Bekakra	Professeur	Université Elchahid Hamma Lakhdar - El Oued	Examinateur
Mr Ridha Kechida	MCA	Université Elchahid Hamma Lakhdar - El Oued	Examinateur
Mr Amor Ounissi	Professeur	Université Mostefa Ben Boulaïd - Batna 2	Examinateur
Mr Youcef Harbouche	MCA	Université Mostefa Ben Boulaïd - Batna 2	Examinateur

الجمهورية الجزائرية الديمقراطية الشعبية
People's Democratic Republic of Algeria
وزارة التعليم العالي والبحث العلمي
Ministry of Higher Education and Scientific Research
جامعة الشهيد حمة لخضر الوادي
Elchahid Hamma Lakhdar University of El Oued

Faculty of Technology
Department of Electrical Engineering
Electrotechnics branch

DOCTORAL THESIS

Presented by

Miloud GATI

With a view to obtaining the doctoral diploma in 3rd Cycle Doctoral (D-LMD)

Specialty: Optimisation and Energy Management

Topic

Contribution to the Sensorless Mechanical Control of a Variable Reluctance Synchronous Machine

---

Thesis publicly defended on (25/01/ 2025) before the jury composed of

Last and first name	Grade	Institution of affiliation	Designation
Mr Abderrahim Allal	Professor	Elchahid Hamma Lakhdar University of El Oued	President
Mr Hicham Serhoud	Professor	Elchahid Hamma Lakhdar University of El Oued	Supervisor
Mr Youcef Bekakra	Professor	Elchahid Hamma Lakhdar University of El Oued	Examiner
Mr Ridha Kechida	MCA	Elchahid Hamma Lakhdar University of El Oued	Examiner
Mr Amor Ounissi	Professor	Mostefa Ben Boulaïd University of Batna 2	Examiner
Mr Youcef Harbouche	MCA	Mostefa Ben Boulaïd University of Batna 2	Examiner

بسم الله الرحمن الرحيم

اللهم لك الحمد حمدًا أبلغ به رضاك، أؤدي به شكرك وأستوجب به المزيد من فضلك.. اللهم لك الحمد على حلمك بعد علمك، ولك الحمد على عفوك.. اللهم لك الحمد كما أنعمت علينا نعمًا بعد نعم.. اللهم لك الحمد بالإسلام، ولك الحمد بالقرآن، ولك الحمد بالأهل والمال والمعافاة، ولك الحمد بالسراء والضراء، ولك الحمد بالشدة والرخاء، ولك الحمد على كل حال، ولك الحمد فوق كل شعور.. اللهم لك الحمد كما ينبغي لجلال وجهك وعظيم سلطانك.. اللهم لك الحمد حمدًا لا ينفد أوله ولا ينقطع آخره.. اللهم لك الحمد فأنت أهل أنت تُحمَد وتُشكَر وتُعبَد.

Acknowledgements

I begin by offering my heartfelt thanks to Allah, whose strength, guidance, and unwavering support have sustained me throughout my academic journey. Without His countless blessings, this achievement would not have been possible.

*I wish to express my sincere gratitude to my supervisor, **Pr. Serhoud Hicham**, for his steadfast support, invaluable guidance, and insightful advice. Your mentorship has been instrumental in shaping this research, and I am deeply thankful for the knowledge and wisdom you have shared with me. I would like to extend my heartfelt thanks to the esteemed members of the jury for the honour of evaluating my work **Prof.Abderrahim Allal**, **Prof.Youcef Bekakra** and **Prof.Ounissi Amor**, **Dr.Rida Khechida**, and **Dr.Youcef Harbouche**. Your time, expertise, and valuable insights are deeply appreciated, and I am truly grateful for your thoughtful consideration and constructive feedback.*

I am profoundly grateful to my family, particularly my wife and children, for their boundless love, encouragement, and patience. Your unwavering support has been my greatest source of strength, and I feel truly privileged to have you beside me.

To my colleagues and friends, thank you for your friendship, encouragement, and belief in me. You have lightened the burden of this academic journey and made it more enjoyable.

I would also like to express my sincere thanks to the distinguished gentlemen who have graciously agreed to chair the defence committee, and to the members of the jury for taking the time to read and evaluate this thesis.

Finally, I extend my gratitude to all those who, either indirectly or directly, have contributed to this academic endeavour. Your combined support has had a lasting impact on this work.

As I present this thesis, I am fully aware of the collaboration and support that have made it possible. I hope that this contribution serves to benefit the university world and beyond.

Gati Miloud

Dedicates

I dedicate this thesis to my loved ones that served as my columns of strength and motivation along my academic career:

To the loving memory of my dear parents, who have passed away: Though you are no longer with me, your unwavering support and faith continue to light my path. You instilled in my heart the spirit of resilience and commitment, and for that I will always be grateful.

To the memory of my brother Sami,
To my brothers Hamza and Fouad, and my sister Hayzia (Jazira): your presence has been a source of strength.

To my wife and children: Your patience and love made this trip truly unforgettable. The faith you have shown in me was a great motivator.

To my friends and colleagues: your belief in my potential and your confidence in my success have kept me going. Thank you for standing by me.

Gati Miloud

Table of contents

List of figures

List of Tables

Notations and Abbreviations

Notations

Non-exhaustive list of the main variables and parameters.

The conditions for modelling SynRM are as follows:

R_s	(Ω)	Stator resistor,
L_s	(H)	Stator inductance,
L_m	(H)	Magnetising inductivity,
l_s	(H)	Self-inductance of a stator phase,
M_0	(H)	Maximum value of the mutual inductance between the stator phase and the rotor phase,
p	(–)	Number of pole pairs,
F	(N.m.s/rd)	Coefficient due to viscous friction
T_{em}	(N.m)	Electromagnetic torque
J	(Kg.m^2)	Total moment of inertia,
K_p	(–)	Proportional component of the PI controller,
K_i	(–)	Integral component of the PI controller,

Axis reference points:

(d, q)	Park reference frame axes (rotating at synchronisation speed)
(α, β)	Concordia/Clarke reference frame axes (Park reference frame fixed to the stator),
θ_{sr} (rad)	Angular position of the rotor in relation to the stator,
θ_s (rad)	Angular position of the stator in relation to the axis (d),
θ_r (rad)	Angular position of the rotor in relation to the axis (d).

Electrical values at the stator:

$v_{s\,a,b,c}$	(V)	Three-phase stator voltages,
$v_{s\,d,q}$	(V)	Two-phase stator voltages in reference frame (d, q),
$v_{s\,\alpha,\beta}$	(V)	Two-phase stator voltages in reference frame (α, β),
$[V_s]_{3\times1} = [v_{sa}, v_{sb}, v_{sc}]^T$	(V)	Vector of stator phase voltages a, b and c,
V_s	(V)	Modulus of the stator voltage vector,
$i_{s\,a,b,c}$	(A)	Instantaneous three-phase stator currents
$i_{s\,d,q}$	(A)	Two-phase stator currents in reference frame (d, q),
$i_{s\,\alpha,\beta}$	(A)	Two-phase stator currents in reference frame (α, β),

$[I_s]_{3\times1} = [i_{sa}, i_{sb}, i_{sc}]^T$	(A)	Vector of the instantaneous currents of stator phases a, b and c,

Magnetic quantities in the stator:

$\varphi_{s\,a,\,b,\,c}$	(Wb)	Instantaneous magnetic flux at the stator,
$\varphi_{s\,\alpha,\,\beta}$	(Wb)	Two-phase stator fluxes in reference frame (α, β),
$\varphi_{s\,d,\,q}$	(Wb)	Two-phase stator fluxes in the rotating reference frame (d, q).
$[\varphi_s]_{3\times1} = [\varphi_{sa}, \varphi_{sb}, \varphi_{sc}]^T$	(Wb)	Instantaneous flux vector for stator phases a, b and c,
φ_s	(Wb)	Modulus of the stator flux vector.

Mechanical quantities:

ω_r	(rad/s)	Electrical pulsation corresponding to the speed of rotation,
ω_s	(rad/s)	Electrical pulsation of stator magnitudes (rotating field),
f	(Hz)	f (Hz) Electrical frequency of stator magnitudes,
N_s	(rpm)	Rotating field speed,
N_r	(rpm)	Nominal mechanical speed of rotation.

Transformations:

s	Laplace operator,
P (θ)	Park transformation: $X_{sa,b,c} \rightarrow X_{sd,q}$ et$X_{ra,b,c} \rightarrow X_{rd,q}$,
C_{32}	Concordia/Clarke transformation :$X_{sa,b,c} \rightarrow X_{s\alpha,\beta}$ et$X_{ra,b,c} \rightarrow X_{r\alpha,\beta}$,

SynRM control quantities:

T_{em}^*	(N.m)	Electromagnetic torque setpoint,
$\hat{\omega}$	(rad/s)	Estimated Rotor Speed,
$\hat{T}_{em}$	(N.m)	Estimated electromagnetic torque,
K_p, K_i	(−)	Proportional and integral components of the PI corrector,
T_s	(s)	Sampling period,
f_p	(Hz)	Carrier frequency,
f_r	(Hz)	Reference frequency,
δ	(deg)	Phase shift between the stator and rotor flux vectors,
ω_n	(rad/s)	Natural pulsation,
ξ	(−)	Damping Factor,
ε	(−)	Static error,
S_a, S_b, S_c	(−)	Switching states of the inverter switches,
T_r		Resistant Couple.
Ω		SynRM Rotor Speed

Abbreviation

SynRM	:	Synchronous reluctance machine
IE1	:	Standard Efficiency.
IE2	:	High-Efficiency.
IE3	:	Premium Efficiency
IE4	:	Super Premium Efficiency
IE5	:	Ultra-Premium Efficiency
FOC	:	Field Oriented Control.
DC	:	Direct Current.
MPC	:	Model Predictive Control.
MRAS	:	Model Reference Adaptive System.
IGBT	:	Insulated Gate Bipolar Transistor.
IGCT	:	Integrated Gate Commutated Thyristor.
MOSFET	:	Metal Oxide Semiconductor Field Effect Transistor.
PMSG	:	Permanent Magnet Synchronous Generator.
PWM	:	Pulse Width Modulation.
SVM	:	Space Vector Modulation.
THD	:	Total Harmonic Distortion.
CARMA	:	Control Auto Regressive on Moving Average
NTVS	:	Nonlinear Time-Varying Systems

General Introduction

General Introduction:

The concept of an "ideal" electrical machine refers to a theoretical device that operates with perfect efficiency and without any losses, limitations, or constraints. In practice, no electrical machine can achieve this ideal state due to various factors such as resistance, hysteresis, eddy currents, and other losses associated with energy conversion processes.

Induction machines are the world's most widely used machines in industrial applications, due to their ability to be supplied directly from the mains without the need for an electronic power converter, their robustness and their low cost. The development of vector control has given them dynamic performance, particularly at medium and high speeds, their main handicap is certainly their efficiency and the losses in the rotor, which are more difficult to evacuate. Consequently, the replacement of standard-efficiency electric machines with higher-efficiency machines is assessed on the basis of considerations that differ from actual operating conditions in the industry. The United Stated Energy Policy Act of 1992, which initiated the standardisation of electric machines according to their efficiency class (hereafter referred to as ‘efficiency class’), marked an important step in improving the efficiency of electric machines, which involves the use of better magnetic materials and more copper, which obviously has an impact on the cost of the machines [1]. Since then, the categorisation of the efficiency class has improved, standardising the definitions of the International Electrotechnical Commission (IEC) [2]: IE1, IE2, IE3, IE4, IE5.

As a result, in industrial applications requiring speed or torque control, other types of machine are generally used instead of the IM, such as the permanent magnet synchronous machine (PMSM).

Synchronous machines with magnets are the best in terms of dynamic performance, efficiency and low-speed behaviour. They are therefore reserved for demanding applications in robotics and machine tools. However, they have two major drawbacks. The first is the difficulty of defluxing them, which can reduce their speed range at high speeds and pose serious safety problems in the event of power electronics failure. The second is the availability and price volatility of the rare earths needed to manufacture high-performance magnets. These two disadvantages are overcome in the case of a machine with a wound rotor, but the inertia of the rotor increases considerably and its robustness decreases accordingly.

Nevertheless, the introduction of other traction machine drive topologies could provide a means of optimising the operating parameters for a specific use case. One potentially promising solution is the adoption of synchronous electric machines with no rotor active elements. This reduces material costs, increases efficiency thanks to the absence of resistive losses in the rotor and simplifies the manufacturing process. The most popular topologies are the switched reluctance machine (SRM) and the synchronous reluctance machine (SynRM). The switched reluctance machine is growing in popularity today, but it has several drawbacks such as higher torque ripple, acoustic noise and relatively low torque density [3]. Acoustic noise and torque ripple are factors holding back the development of this type of electric machine. SynRM is subject to fewer of the disadvantages inherent in SRM. They are economical and are well suited to very low or very high speeds. SynRMs are a serious competitor to the induction machine in variable speed applications. These machines have minimal or no Joule losses in the rotor and are more compact and more efficient than asynchronous machines of the same power. They generally have a higher torque-to-volume ratio compared to induction machines. This means that for a given physical size, a SynRM can deliver higher torque output. This feature can be advantageous in applications where space is limited, and high torque density is required. Their main disadvantage is their power factor, which can lead to the static converter feeding them being oversized. Flux barrier machines minimise this problem, but at a higher cost and with less robust rotors.

The first design of the synchronous reluctance machine (SynRM) indeed had some limitations, including low efficiency and low torque. Additionally, the machine required cage windings for self-starting when connected directly to the power grid. [4]

Low efficiency in early SynRM designs was primarily due to factors such as suboptimal magnetic circuit design, inefficient rotor configurations, and less sophisticated control algorithms. These issues resulted in higher power losses and reduced overall machine efficiency.

Low torque output was another challenge in the initial designs. Synchronous reluctance machines rely on the principle of magnetic reluctance to generate torque. However, early designs struggled to maximize the torque output due to suboptimal rotor shapes and insufficient utilization of magnetic materials.

To address the self-starting issue, the initial SynRM designs incorporated cage windings. These windings were added to the rotor of the machine, allowing it to generate the necessary starting torque. The cage windings helped overcome the lack of initial magnetic field during startup and facilitated the machine's ability to begin rotating when directly connected to the power grid.

Since the early designs, significant advancements have been made in SynRM technology. Modern SynRM designs employ improved magnetic circuit configurations, optimized rotor geometries, advanced materials, and enhanced control algorithms. These advancements have led to improved efficiency, higher torque output, and reduced reliance on cage windings for self-starting.

The selection of machine type depends on the specific requirements of the application, such as energy efficiency goals, control requirements, cost considerations, and the availability of suitable technology in the market. Industrial users should evaluate the benefits and trade-offs of both induction machines and SynRM machines to determine the most appropriate solution for their particular needs. Nevertheless, variable reluctance synchronous machines offer many advantages and are often an excellent compromise.

The fact that the SynRM has been used in variable speed drive systems (VSD) is due to technological developments, particularly in semiconductors, which have made it possible to build high power converters capable of delivering high performance voltages or currents of adjustable amplitude and frequency. [7]

Current scientific research has focused on the operation of regulated drives without mechanical speed sensors, without altering their dynamic or static performance. Estimating the rotor speed of a sensorless synchronous reluctance machine (SynRM) can be achieved using various methods:

1. High-frequency injection: Injecting a high-frequency signal into the stator windings of the SYNRM can induce a secondary voltage at the rotor [5], [6]. By analysing the response of the induced voltage, the rotor speed can be estimated. High-frequency injection methods can be based on techniques such as voltage model injection (VMI) or current model injection (CMI).
2. Magnetic saturation analysis: SYNRM's magnetic saturation level can provide information about the rotor position and speed. By analysing the machine's magnetic characteristics, such as inductance or flux linkage, variations in saturation can be correlated with rotor speed [7]. This method requires accurate measurements and a good understanding of the machine's saturation behavior.
3. Model-based methods: These methods utilize mathematical models of the machine to estimate the rotor speed. The machine model incorporates the electrical, magnetic, and mechanical characteristics of the SynRM. By observing the machine's electrical quantities such as voltage and current, the rotor speed can be estimated through model-based algorithms such as :
   - Extended Kalman filters (EKFs) which have shown excellent qualities as an optimal recursive estimation algorithm for non-linear systems, and they are very appropriate in the case of noisy measurements [8] ,[9], [10]. Unfortunately, implementation at SynRM is not easy, and the main problem is the derivation of the Jacobian matrices, which is critical when the magnetic model is based on piecewise linear interpolation of look-up tables. Other estimation techniques like Unscented Kalman Filters (UKFs) or particle filters may offer alternative solutions with different trade-offs.
   - Sliding mode observers [11] are known for their robustness against various disturbances and uncertainties, making them suitable for applications where the machine may encounter varying loads, external disturbances, or parameter variations. However, the presence of chattering, i.e. high-frequency oscillations of the control

signal around the switching surface, can lead to higher current harmonics in the machine windings, which can affect machine efficiency and cause additional losses.

- Back-EMF integration: The SYNRM generates a back-electromotive force (back-EMF) due to the rotor movement [12]. By integrating the measured back-EMF voltage, the rotor speed can be estimated. This method requires accurate voltage measurements and may be affected by noise and signal distortion.
- Luenberger observers are simple and easy to implement, but they require accurate knowledge of the system parameters and are sensitive to noise and disturbances. [13].
- Predictive control: is used to predict the future output based on historical information about the process, as well as anticipated future input. The optimization of predictive control is limited to a moving time interval and is carried on continuously on-line. PID type controllers do not perform well when applied to systems with significant time delays. Model predictive control overcomes the debilitating problems of delayed feedback by using predicted future states of the output for control.
- The Adaptive Reference Model System (MRAS) based speed estimation method [14],[15] is one of many promising techniques used for sensorless variable speed drives, due to its practical implementation, robustness and low computational complexity.

This thesis deals with the sensorless control of synchronous reluctance machine (SynRM). We chose this research topic because, on the one hand, this machine is still little studied compared with asynchronous machines and, on the other hand, at low speeds, the absence of a mechanical sensor puts its reliability at a critical point.

Our contribution to this thesis is devoted to the study of a hybrid controller, composed of a predictive model controller and an MRAS observer. The most widely used approach in the observers mentioned above is a synchronous frame proportional-integral (PI) controller. It is estimated that more than 95% of controllers used in industry are PID controllers, and most of them are PI controllers [16]- [17]. The weakness of this control scheme is the employment of multiple PI controllers in the outer and inner loops, which have numerous parameters to be set, compared to these techniques, we propose an observer that estimates speed by replacing these conventional PI controllers with a predictive control model that calculates the new speed estimate based on the MRAS scheme using only stator current and voltage measurements.

Thesis Organization

The thesis is structured into four chapters, and all of them deal with a different topic.

Chapter 1 deals with the principle of operation, the modelling of synchronous reluctance machines (SynRMs) and their representation in different frameworks, starting with the SynRM model in the

Concordia framework, then in the modified Park framework, and then examining the machine supply by a two-level voltage inverter.

Chapter 2 Examines vector control by orientation of the rotor flux on the SynRM, and also presents the study of control, which is linked to stability in the Lyapunov sense, convergence and the nature of the machine as a non-linear dynamic system.

Chapter 3 This chapter analyses predictive control, which is a combination of prediction of future process behaviour and feedback control, applied to SynRM. The process model adopted in this chapter is the CARMA structure, and the criteria for optimisation by minimising the cost function, which differs from one method to another are analysed, and finally the control parameters are defined for general predictive control.

Chapter 4 This chapter extends the previous chapters' knowledge of the synchronous reluctance machine (SynRM). It discusses the model-referenced adaptive system (MRAS) observer based on Popov's criteria for hyperstability, then optimises a voltage vector that minimises the current error. Two cascaded MRAS-MPC approaches are presented for two cost functions. The chapter concludes with a comparative analysis between MRAS-PI and MRAS-MPC and concluding remarks.

Chapter 1: Modelling of Synchronous Reluctance Machines and their power supplies

Chapter 1: Modelling of synchronous Reluctance Machine and their power supplies

1.1 Introduction

Synchronous machines are used in many fields, as in machine applications or in generator applications. The goals to have a synchronous machine model can be split into two groups: (1) to achieve further insight in the complex electro-magnetic behaviour of the machine [18], and (2) for simulation or control purposes [19], [20].

In this chapter, we examine the operating principle and modelling of the SynRM. This is followed by its representation in different reference frameworks, starting with the model of the SynRM in the Concordia framework and then in the modified Park framework. To study the dynamics and behaviour of the SynRM under transient and stable conditions, the appropriate choice of reference frame will be made according to the control or observation objectives. This chapter also presents a modelling study of the inverter and its PWM control technique.

1.2 Working Principle of SynRM

SynRM operation is based on the principle of reluctance, which is a property of magnetic circuits. The term "synchronous" refers to the machine's ability to operate at a speed directly proportional to the frequency supplied, keeping its rotation synchronised with the frequency of the power supply. The basic principle of a synchronous reluctance machine is that a magnetic object tends to move from a region of low magnetic permeability to a region of high magnetic permeability. This phenomenon is known as "reluctance".

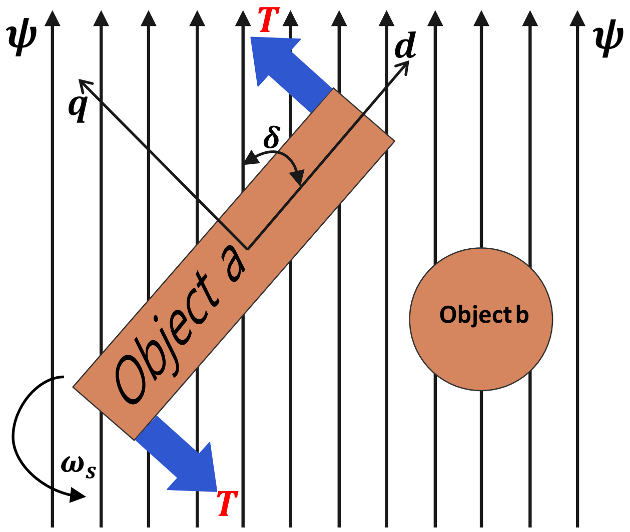

Figure 1.1 Torque production mechanism.[63]

If a magnetic field ($\boldsymbol{\Psi}$) is applied to an object **'a'** made of an anisotropic material, it creates a torque if there is an angle between the d-axis and the magnetic field lines ($\boldsymbol{\delta \neq 0}$) ***Figure 1.1.*** Or if the d-axis of object "a" is not aligned with the field.

The reluctant torque will tend to rotate the material to reduce the angle and minimise the magnetic energy. If this angle (***δ***) is kept constant by a torque control or an applied resistive torque, the electromagnetic energy is continuously converted into mechanical energy.

1.3. Influence of the L_d/L_q factor on machine performance

The saliency rate, given by the following equation, is an important parameter for monitoring the performance of a SynRM. $\zeta = \frac{L_d}{L_q}$.

To achieve a SynRM with high performance, the main goal is to obtain a high L_d value and a low L_q value, which results in maximum *d*-axis flux and minimum *q*-axis flux.

The graphic vector diagram is an essential means of displaying and understanding the operating principles and characteristics of SynRM's performance.

The d-axis and q-axis rotor magnetic flux components are differentiated in the vector diagram, d-axis corresponding to the high reluctance direction and q-axis representing the low reluctance direction. Torque is produced by changing the reluctance between these axes.

The stator current vector in the vector diagram is broken down into its *d*-axis and *q*-axis components, which are vital in determining the torque output and the machine's overall performance.

The electromagnetic steady-state torque produced by this machine is expressed as follows:

$$T_e = p.\left(L_{sd} - L_{sq}\right) I_{sd} I_{sq} \tag{1.1}$$

To boost the torque without changing the value of the current, the inductance of the direct axis (L_d) must be increased in relation to the inductance of the quadrature axis (L_q).

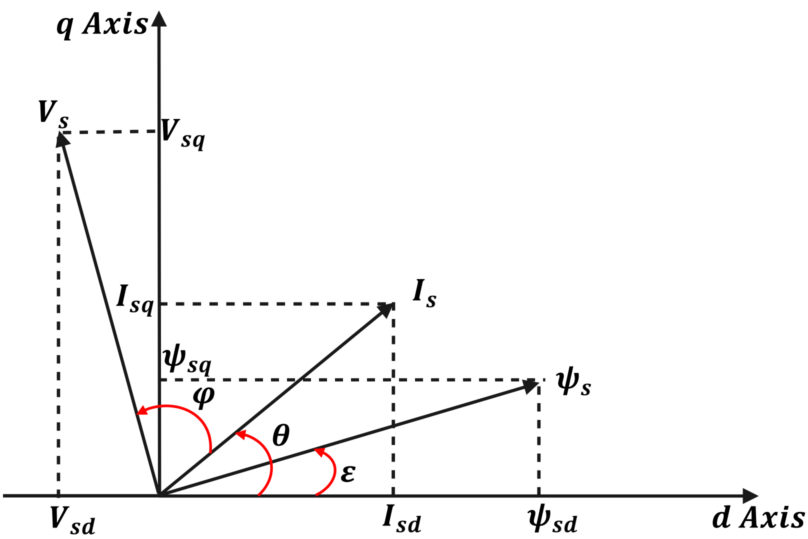

Figure 1.2. SynRM steady-state vector diagram

In other hands, to increment the torque, the saliency ratio (ζ) must be augmented [21].

The angle $\boldsymbol{\theta}$, represents the position ($\boldsymbol{I_s}$) of the stator current vector relative to the $\boldsymbol{d}$-axis. The current vector in the stator is kept fixed in steady state.

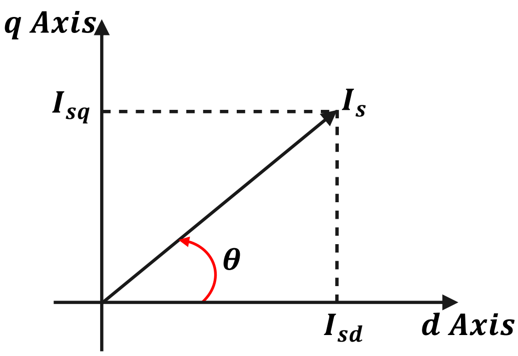

Figure 1.3. Position of the stator current on the (d - q) axis.

The amplitude of the stator current is defined by the following equation:

$$I_s = \sqrt{I_{sd}^2 + I_{sq}^2} \tag{1.2}$$

Electromagnetic torque as a function of stator current *Is and θ*:

$$T_e = p\left(L_d - L_q\right)I_s^2 \sin 2\theta \tag{1.3}$$

The preceding relationships show that when the stator current is fixed at a specific value, the maximum torque is reached at $\boldsymbol{\theta = \pi/4}$, which corresponds to $\boldsymbol{I_{sd} = I_{sq}}$, a mode of operation associated with a particular control strategy. Fixing $\boldsymbol{\theta = \pi/4}$ in equation (1.3) gives equation (1.4), which reveals the saliency ratio $\boldsymbol{\zeta}$.

$$T_e = pL_d I_s^2 . \left(1 - \frac{1}{\zeta}\right) \tag{1.4}$$

The SynRM is an AC machine designed to be supplied with three-phase sinusoidal currents in steady state. The machine's power factor, expressed as the phase shift between the fundamental of the current in the line and the respective phase-to-neutral voltage, can be defined. It also corresponds to the ratio between the apparent power absorbed by the machine and the active power. It is essential that this ratio is as close as possible to 1 in order to limit the electrical power of the source feeding the machine. By ignoring losses in the machine model, we get a simple expression for the power factor:

$$\cos\varphi = \frac{\left(\zeta - 1\right)\sin\theta}{\sqrt{\left(\zeta\right)^2 + \tan^2\theta}} \tag{1.5}$$

If a specific strategy of control is applied (requiring $\boldsymbol{\tan\theta} = \sqrt{\zeta}$), the factor of power is maximised and only depends on the ratio L_d / L_q .

The expression of the power factor is then given by the expression [22, 23] :

$$(cos\varphi)_{max} = \frac{(\zeta - 1)}{(\zeta + 1)} \tag{1.6}$$

In Figure (1.4) we can see how the power factor varies as a function of the saliency ratio ***Ld/Lq***. The power factor becomes more important for saliency ratios greater than 8. Based on equations (1.4) and (1.6), to achieve optimum machine performance, the structure of the rotor has to be chosen to reach the maximum possible value of L_d and the highest possible L_d/L_q ratio [23].

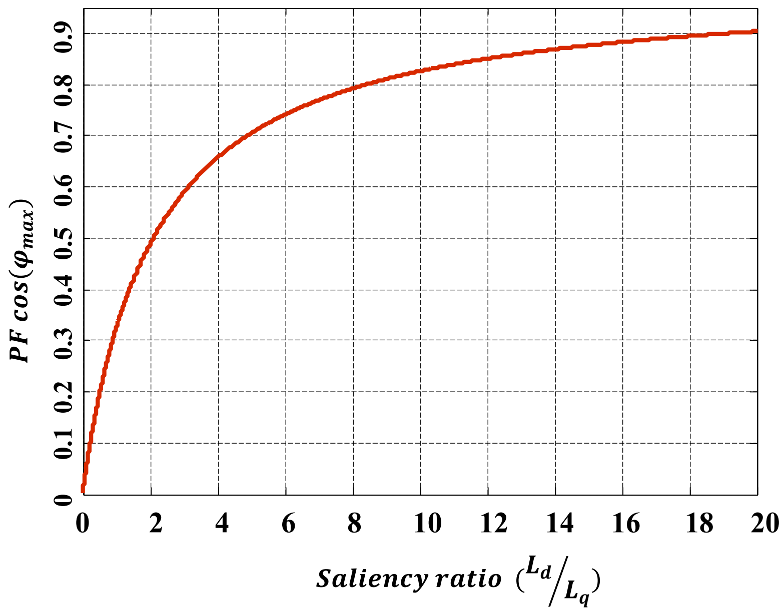

Figure 1.4. Power Factor as a relation to the saliency ratio *Ld/Lq*

1.4 Simplifying hypotheses

The synchronous machine model is based on the following assumptions:

Assumption 1.1: Stator winding currents are assumed to set up a magnetomotive force (mmf) sinusoidally distributed in space around the air gap. Therefore, the effect of space harmonics in the field distribution is neglected.

Assumption 1.2. The currents induced in the magnetic circuit (eddy currents) are assumed to be negligible, as are the phenomena of hysteresis and the skin effect.

Assumption 1.3. Saturation effects are neglected.

Assumption 1.4. The effect of temperature on resistance values is neglected.

Assumption 1.5 Notch and gap harmonics are not taken into account

1.5 Electrical equations of the machine in the abc reference frame

The electrical equations governing the operation of a synchronous machine in a fixed frame of reference linked to the stator can be written as follows:

$$[V_{abc}]=[R_s][I_{abc}]+\frac{d}{dt}[\Psi_{abc}] \tag{1.7}$$

$$[I_{abc}]=\begin{bmatrix} i_a \\ i_b \\ i_c \end{bmatrix}; \quad [V_{abc}]=\begin{bmatrix} v_a \\ v_b \\ v_c \end{bmatrix}; \quad [\Psi_{abc}]=\begin{bmatrix} \psi_a \\ \psi_b \\ \psi_c \end{bmatrix} \quad ; [R_s]=\begin{bmatrix} R_s & 0 & 0 \\ 0 & R_s & 0 \\ 0 & 0 & R_s \end{bmatrix}$$

where:

- ψ_a, ψ_b, and ψ_c are the magnetic fluxes that link each stator winding.
- v_a, v_b, and v_c are the individual phase voltages across the stator windings.
- i_a, i_b, and i_c are the currents flowing in the stator windings.
- R_s is the equivalent resistance of each stator winding.

The total fluxes of the stator phases can be written in the stator reference frame in the following matrix form:

$$[\Psi_{abc}]=[L][I_{abc}] \tag{1.8}$$

where $[L]$ is the inductance matrix which depends on the angle θ defined in ***Figure 1.5***:

$$[L]=\begin{bmatrix} L_a(\theta) & M_{ab}(\theta) & M_{ac}(\theta) \\ M_{ba}(\theta) & L_b(\theta) & M_{bc}(\theta) \\ M_{ca}(\theta) & M_{cb}(\theta) & L_c(\theta) \end{bmatrix} \quad . \tag{1.9}$$

Assuming the first space harmonic, the inductance shown in ***Figure 1.5*** varies with the position of the rotor can be expressed as follows [64]:

$$\left| \begin{aligned} L_a(\theta) &= L_l + L' + L''\cos(2\theta) \\ L_b(\theta) &= L_l + L' + L''cos\left(2\theta+\frac{2\pi}{3}\right) \\ L_c(\theta) &= L_l + L' + L''cos\left(2\theta-\frac{2\pi}{3}\right) \end{aligned} \right. \qquad \left| \begin{aligned} M_{ab}(\theta) &= M_{ba}(\theta) = M' + M''\,cos\left(2\theta-\frac{2\pi}{3}\right) \\ M_{ac}(\theta) &= M_{ca}(\theta) = M' + M''\,cos\left(2\theta+\frac{2\pi}{3}\right) \\ M_{bc}(\theta) &= M_{cb}(\theta) = M' + M''\,cos(2\theta) \end{aligned} \right.$$

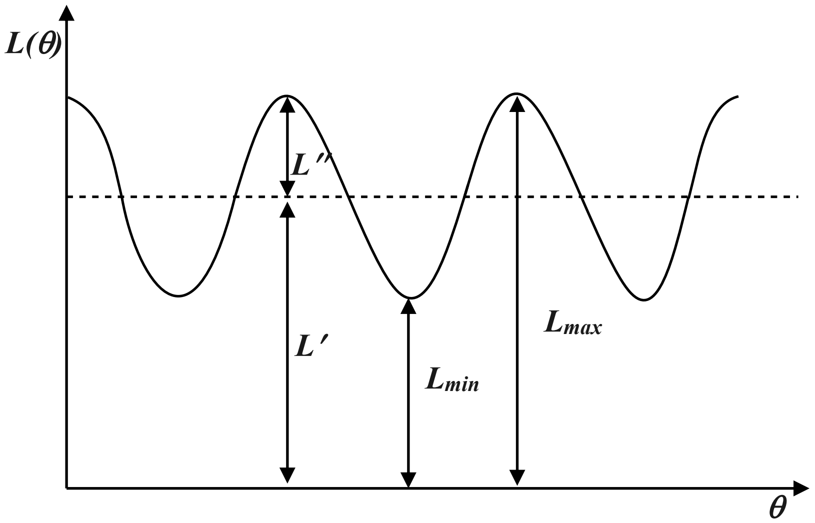

Figure 1.5. Variation in inductance as a function of rotor position

Where:

L_l: leakage inductance

L' : Constant self-inductance term for one phase

L'': Amplitude of the first harmonic of the natural inductance of a phase

$M' = -\frac{1}{2}L', M'' = L''$. [61]

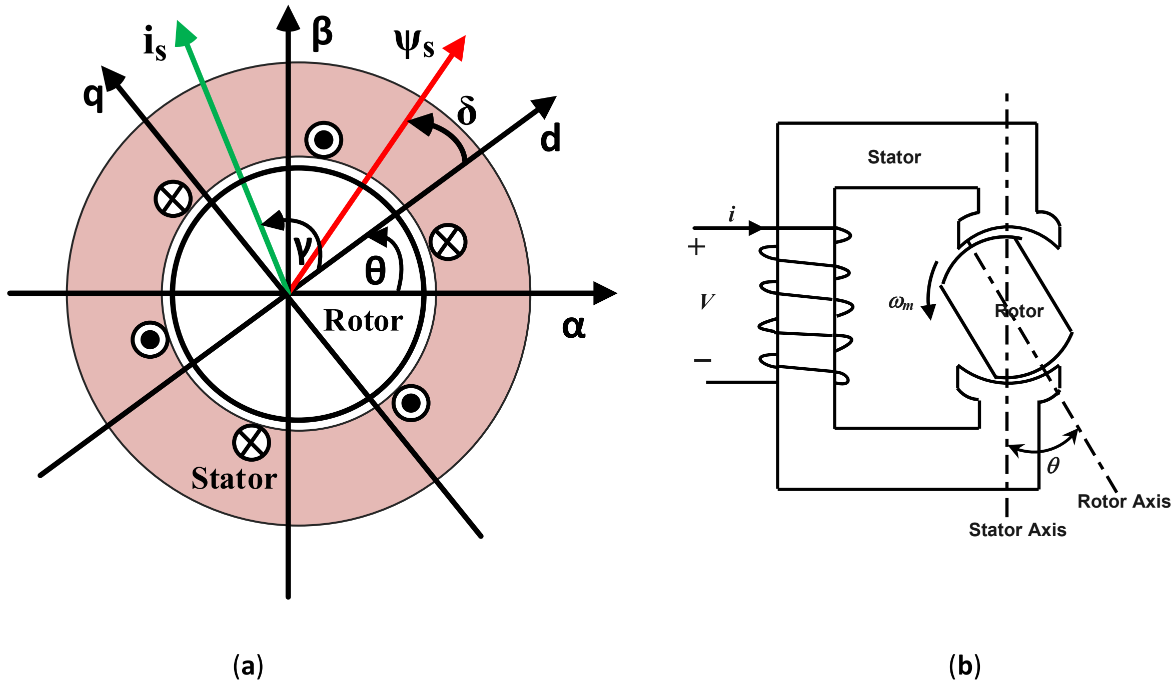

Figure.1.6. (a) Representation of the synchronous machine in the d-q and α-β reference frames ***(b)*** Schematic diagram of a reluctance machine

1.6 Electrical equations of the machine in frame αβ

With a system of two-phase currents, produced by two coils offset by $\pi/2$ in space, it can be created a rotating field identical to that created by a three-phase system (a, b, c). There are two transformations: The Clarke transformation and the Concordia transformation. The Clarke transformation preserves the amplitude of the quantities, but not the power or torque (they must be multiplied by a coefficient of 2/3). On the other hand, Concordia, which is normalised, retains the power but not the amplitudes. In the general case, this gives:

$$\begin{bmatrix} \boldsymbol{x}_a \\ \boldsymbol{x}_b \\ \boldsymbol{x}_c \end{bmatrix} = [\boldsymbol{c}_{32}] \begin{bmatrix} \boldsymbol{x}_\alpha \\ \boldsymbol{x}_\beta \\ \boldsymbol{x}_h \end{bmatrix} \quad ; \quad \begin{bmatrix} \boldsymbol{x}_\alpha \\ \boldsymbol{x}_\beta \\ \boldsymbol{x}_h \end{bmatrix} = [\boldsymbol{c}_{23}] \begin{bmatrix} \boldsymbol{x}_a \\ \boldsymbol{x}_b \\ \boldsymbol{x}_c \end{bmatrix} \tag{1.10}$$

Where:

$$[\boldsymbol{c}_{23}] = \frac{2}{3} \begin{bmatrix} 1 & -\frac{1}{2} & -\frac{1}{2} \\ 0 & \frac{\sqrt{3}}{2} & -\frac{\sqrt{3}}{2} \\ \frac{1}{2} & \frac{1}{2} & \frac{1}{2} \end{bmatrix}; \qquad [\boldsymbol{c}_{32}] = [\boldsymbol{c}_{23}]^{-1} = \begin{bmatrix} 1 & 0 & 1 \\ -\frac{1}{2} & \frac{\sqrt{3}}{2} & 1 \\ -\frac{1}{2} & -\frac{\sqrt{3}}{2} & 1 \end{bmatrix}$$

Equation 1.7 becomes:

$$\left[\mathrm{V}_{\alpha\beta h}\right] = \left[\mathrm{R}_s\right]\left[\mathrm{I}_{\alpha\beta h}\right] + \frac{\mathrm{d}}{\mathrm{dt}}\left[\Psi_{\alpha\beta h}\right] \tag{1.11}$$

Where:

$$\left[\boldsymbol{V}_{\alpha\beta h}\right] = \begin{bmatrix} \boldsymbol{v}_\alpha \\ \boldsymbol{v}_\beta \\ \boldsymbol{v}_h \end{bmatrix} \quad ; \quad \left[\boldsymbol{I}_{\alpha\beta h}\right] = \begin{bmatrix} \boldsymbol{i}_\alpha \\ \boldsymbol{i}_\beta \\ \boldsymbol{i}_h \end{bmatrix} \; ; \; \left[\boldsymbol{\Psi}_{\alpha\beta h}\right] = \begin{bmatrix} \boldsymbol{\psi}_\alpha \\ \boldsymbol{\psi}_\beta \\ \boldsymbol{\psi}_h \end{bmatrix}.$$

The flux matrix is:

$$\left[\Psi_{\alpha\beta h}\right] = \left[\mathrm{L}_{\alpha\beta h}\right]\left[\mathrm{I}_{\alpha\beta h}\right] \tag{1.12}$$

Where:

$$\left[\mathrm{L}_{\alpha\beta h}\right] = \begin{bmatrix} \mathrm{L}_1 + \frac{3}{2}\left(\mathrm{L}' + \mathrm{L}'' \cos(2\theta)\right) & \frac{3}{2}\mathrm{L}'' \sin(2\theta) & 0 \\ \frac{3}{2}\mathrm{L}'' \sin(2\theta) & \mathrm{L}_1 + \frac{3}{2}\left(\mathrm{L}' - \mathrm{L}'' \cos(2\theta)\right) & 0 \\ 0 & 0 & \mathrm{L}_1 \end{bmatrix}$$

The neutral of the machine being isolated, we have $\boldsymbol{i_h = 0}$ and we can write:

$$\begin{bmatrix} \boldsymbol{v}_\alpha \\ \boldsymbol{v}_\beta \end{bmatrix} = \boldsymbol{R}_s \begin{bmatrix} \boldsymbol{i}_\alpha \\ \boldsymbol{i}_\beta \end{bmatrix} + \frac{\boldsymbol{d}}{\boldsymbol{dt}} \begin{bmatrix} \boldsymbol{\Psi}_\alpha \\ \boldsymbol{\Psi}_\beta \end{bmatrix} \tag{1.13}$$

1.7 Electrical equations of the machine in frame dq

The park matrix is :

$$[P]=\frac{2}{3}\begin{bmatrix} \cos\theta & \cos\left(\theta-\frac{2\pi}{3}\right) & \cos\left(\theta+\frac{2\pi}{3}\right) \\ -\sin\theta & -\sin\left(\theta-\frac{2\pi}{3}\right) & -\sin\left(\theta+\frac{2\pi}{3}\right) \\ \frac{1}{2} & \frac{1}{2} & \frac{1}{2} \end{bmatrix} \tag{1.14}$$

Calculating the inverse of $[P]$ is straightforward:

$$[P]^{-1}=\begin{bmatrix} \cos\theta & -\sin\theta & 1 \\ \cos\left(\theta-\frac{2\pi}{3}\right) & -\sin\left(\theta-\frac{2\pi}{3}\right) & 1 \\ \cos\left(\theta+\frac{2\pi}{3}\right) & -\sin\left(\theta+\frac{2\pi}{3}\right) & 1 \end{bmatrix} \tag{1.15}$$

If we project all the quantities into the ***d-q*** reference frame linked to the rotor ***Figure 1.6*** using Park's transformation, we write, in the general case:

$$\begin{bmatrix} x_a \\ x_b \\ x_c \end{bmatrix}=[P]^{-1}\begin{bmatrix} x_d \\ x_q \\ x_h \end{bmatrix} \tag{1.16}$$

Equation (1.1) then becomes:

$$[P]^{-1}[V_{dqh}]=[R_s][P]^{-1}[I_{dqh}]+[P]^{-1}\frac{d[\Psi_{dqh}]}{dt}+\frac{d[P]^{-1}}{dt}[\Psi_{dqh}] \tag{1.17}$$

Where $[Xdqh]$ denotes any vector of quantities expressed in the reference frame linked to the rotor.

Multiplying the two members of (1.17) by $[P]$ gives:

$$[V_{dqh}]=[R_s][I_{dqh}]+\frac{d[\Psi_{dqh}]}{dt}+p\Omega[P]\frac{d[P]^{-1}}{d\theta}[\Psi_{dqh}] \tag{1.18}$$

With $$[P]\frac{d[P]^{-1}}{d\theta}=\begin{bmatrix} 0 & -1 & 0 \\ 1 & 0 & 0 \\ 0 & 0 & 0 \end{bmatrix}$$

We finally arrive at the following equations:

$$[V_{dqh}]=[R_s][I_{dqh}]+\begin{bmatrix} L_d & 0 & 0 \\ 0 & L_q & 0 \\ 0 & 0 & L_h \end{bmatrix}\frac{d[I_{dqh}]}{dt}+p\Omega\begin{bmatrix} 0 & -L_q & 0 \\ L_d & 0 & 0 \\ 0 & 0 & 0 \end{bmatrix}[I_{dqh}] \tag{1.19}$$

With ; $\begin{cases} L_d = L_l + \frac{3}{2}\left(L' + L''\right) \\ L_q = L_l + \frac{3}{2}\left(L' - L''\right) \\ L_h = L_l \end{cases}$

Since the neutral of the machine is isolated, which naturally implies $i_h = 0$, we can write:

$$\begin{bmatrix} v_d \\ v_q \end{bmatrix} = \begin{bmatrix} R_s & -p\Omega L_q \\ p\Omega L_d & R_s \end{bmatrix} \begin{bmatrix} i_d \\ i_q \end{bmatrix} + \begin{bmatrix} L_d & 0 \\ 0 & L_q \end{bmatrix} \frac{d}{dt} \begin{bmatrix} i_d \\ i_q \end{bmatrix} \tag{1.20}$$

p: Number of pole pairs

1.8 Vector equivalent circuit and main performance characteristics:

In the case where it is necessary to take into account the presence and influence of rotor currents. In his thesis [24] and in his publications [25], J.D.Park uses the model illustrated in ***figure 1.7*** to model a solid rotor SynRM. This model is similar to that of a MAS where the slip is always equal to unity.

Due to the sinusoidal distribution of the stator winding in a SynRM, the flux harmonics in the air gap add only an extra term to the stator leakage inductance. As a result, the SynRM's behaviour can be described using the standard equations for a wound-field synchronous machine, specifically the Park equations. However, unlike conventional machines, the SynRM lacks an excitation (field) winding, and the rotor does not have a cage. Additionally, the SynRM can be started synchronously from a standstill using suitable inverter control [26].

Where;

L_{ls} : Total winding leakage inductance.

Ψ_m : Air gap linkage flux.

ω : Reference frame electrical angular speed.

R_s : Winding resistance.

R_{cs} : Stator iron losses resistance

R_{cr} : Rotor iron losses resistance

i_m : Magnetization current

e_m : Air gap electromotive voltage (internal voltage of stator winding).

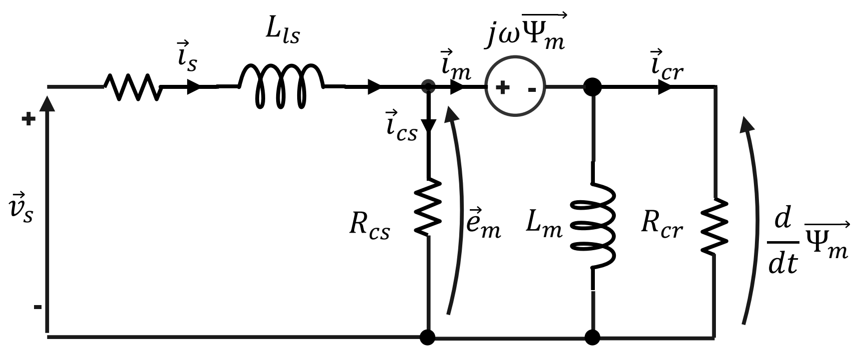

Figure 1.7. SynRM equivalent vector circuit including rotor and stator iron losses

1.9. Electromagnetic Torque

In synchronous reluctance machine the electromagnetic torque is produced by the interaction between air gap flux and its corresponding magnetizing current.

$$T_e = \frac{P_e}{\Omega} = p\left(\Psi_d i_q - \Psi_q i_d\right) = p\left(L_d - L_q\right) i_d i_q \tag{1.21}$$

The mechanical speed of rotation can be deduced from Newton's fundamental law of motion:

$$J\frac{d\Omega}{dt} + F\Omega = T_e - T_r \tag{1.22}$$

Where ; $\frac{d\theta_e}{dt} = \omega \ , \ \omega = p\Omega$

1.10. Non-linear state model

In general, to present a state model, we need to define the state vector $\boldsymbol{x}$, the input vector $\boldsymbol{u}$ and the output vector **y**. The input vector consists of the stator voltages. The state vector is made up of electrical quantities (currents) and mechanical quantities (speed and/or position***).*** [27]

1.10.1. State model in rotating frame (d - q)

In the case of torque or angular speed control, the non-linear state model state model in the rotating reference frame d-q is described by the system below:

$$\begin{bmatrix} \dot{i}_d \\ \dot{i}_q \\ \dot{\Omega} \end{bmatrix} = \begin{bmatrix} \frac{-R}{L_d} + \frac{pL_q}{L_d} i_q \Omega \\ \frac{-R}{L_q} i_q + \frac{pL_d}{L_q} i_d \Omega \\ \frac{\frac{3}{2}p\left(L_d - L_q\right)}{J} i_d i_q - \frac{F}{J}\Omega \end{bmatrix} + \begin{bmatrix} \frac{1}{L_d} & 0 & 0 \\ 0 & \frac{1}{L_q} & 0 \\ 0 & 0 & \frac{-1}{J} \end{bmatrix} \begin{bmatrix} u_d \\ u_q \\ T_r \end{bmatrix} \tag{1.23}$$

In the case of controlling the rotor position θ, this will be considered as a new state variable and the new state model is therefore written:

$$\begin{bmatrix} \dot{i}_d \\ \dot{i}_q \\ \dot{\Omega} \\ \dot{\theta} \end{bmatrix} = \begin{bmatrix} \frac{-R}{L_d} i_d + \frac{pL_q}{L_d} i_q \Omega \\ \frac{-R}{L_q} i_q - \frac{pL_d}{L_q} i_d \Omega \\ \frac{\frac{3}{2}p\left(L_d - L_q\right)}{J} i_d i_q - \frac{F}{J}\Omega \\ \Omega \end{bmatrix} + \begin{bmatrix} \frac{1}{L_d} & 0 & 0 \\ 0 & \frac{1}{L_q} & 0 \\ 0 & 0 & \frac{-1}{J} \\ 0 & 0 & 0 \end{bmatrix} \begin{bmatrix} u_d \\ u_q \\ T_r \end{bmatrix} \tag{1.24}$$

Figure.1.8 presents the SynRM model in synchronous reference frame with inputs stator voltages, and load torque. The outputs are the rotor angular velocity.

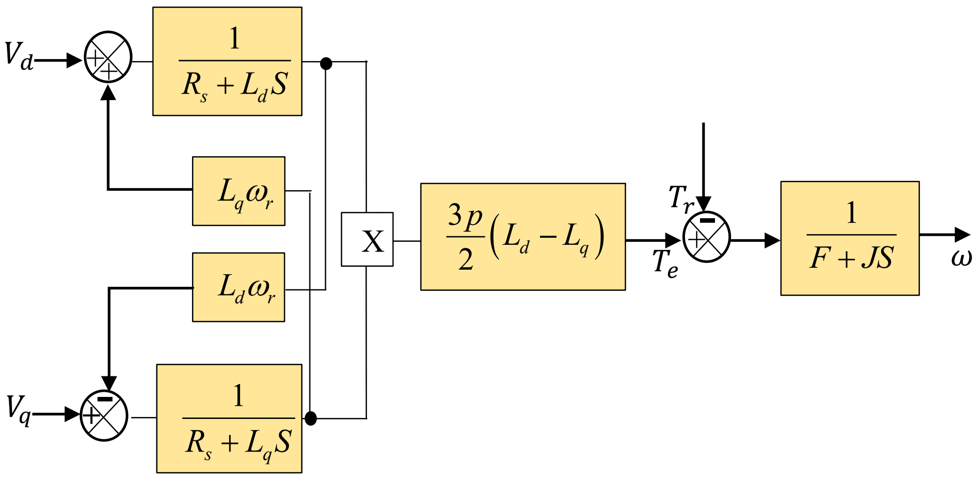

Figure 1.8. Block diagram of the SynRM system

1.11. Modelling the synchronous machine power supply

Direct current to alternating current converters, more commonly known as inverters, depending on the type of power source and the topology of the power circuit, are classified as voltage source inverters (VSI) and current source inverters (CSI). The main purpose of these topologies is to provide a three-phase voltage source, where the amplitude, phase and frequency of the voltages can be controlled. The two-level voltage inverter is made up of three arms formed by electronic switches chosen essentially according to the power and frequency of the system to be controlled, each arm comprising two IGBT power electronic components equipped with diodes mounted in anti-parallel. ***Figure 1.9*** shows a power supply diagram for a SynRM with a voltage inverter.

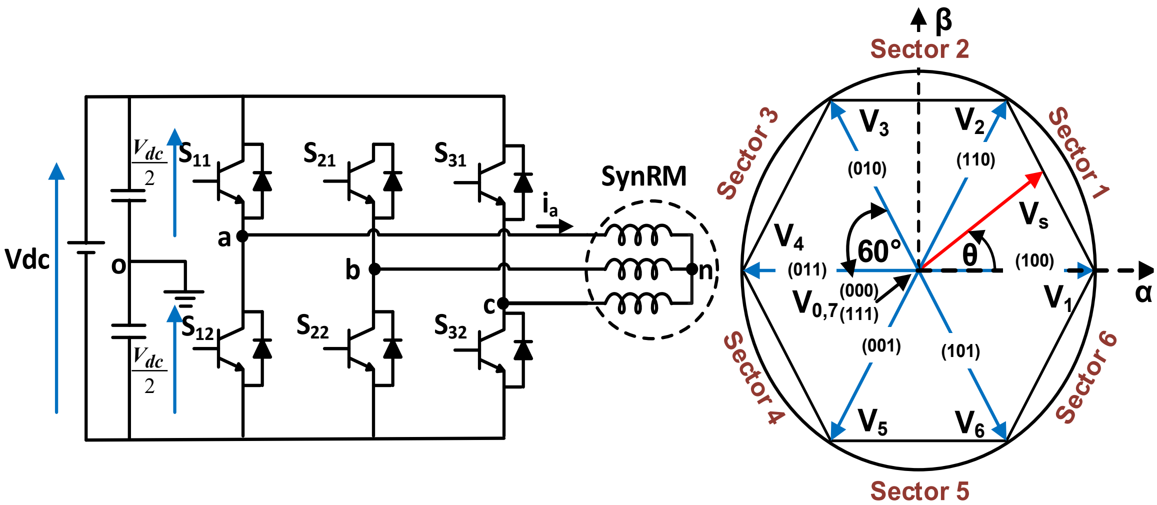

Figure 1.9 Two level voltage source inverter

S11	S21	S31	Vector Voltage
0	0	0	$V_0=0$
1	0	0	$V_1=\frac{2}{3}V_{dc}$
1	1	0	$V_2=\frac{1}{3}V_{dc}+j\frac{\sqrt{3}}{3}V_{dc}$
0	1	0	$V_3=-\frac{1}{3}V_{dc}+j\frac{\sqrt{3}}{3}V_{dc}$
0	1	1	$V_4=-\frac{2}{3}V_{dc}$
0	0	1	$V_5=-\frac{1}{3}V_{dc}-j\frac{\sqrt{3}}{3}V_{dc}$
1	0	1	$V_6=\frac{1}{3}V_{dc}-j\frac{\sqrt{3}}{3}V_{dc}$
1	1	1	$V_7=0$

TABLE 1.1. SWITCHING STATES AND VOLTAGE VECTOR

The inverter has eight switching states as shown in ***Table 1.1*** .The two switches in the same branch cannot be activated at the same time, as this would short-circuit the input voltage. Therefore, the nature of the two switches in the same leg is complementary.

$$\begin{cases} S_{11}+S_{12}=1 \\ S_{21}+S_{22}=1 \\ S_{31}+S_{32}=1 \end{cases} \tag{1.25}$$

The modulation signals are thus selected so meet some specifications, like harmonic elimination, higher fundamental component and so on. The phase voltages can be obtained from the line voltages as,

$$\begin{bmatrix} v_{ab} \\ v_{bc} \\ v_{ca} \end{bmatrix} = \begin{bmatrix} v_{an}-v_{bn} \\ v_{bn}-v_{cn} \\ v_{cn}-v_{an} \end{bmatrix} \tag{1.26}$$

As we are dealing with balanced voltages $v_{an}+v_{bn}+v_{cn}=0$, we therefore have :

$$\begin{bmatrix} v_{an} \\ v_{bn} \\ v_{cn} \end{bmatrix} = \frac{1}{3}\begin{bmatrix} v_{ab}-v_{cn} \\ v_{bc}-v_{ab} \\ v_{ca}-v_{bc} \end{bmatrix} \tag{1.27}$$

The voltages between the phases can also be written in the following form:

$$\begin{bmatrix} v_{ab} \\ v_{bc} \\ v_{ca} \end{bmatrix} = \begin{bmatrix} v_{ao} - v_{bo} \\ v_{bo} - v_{co} \\ v_{co} - v_{ao} \end{bmatrix} \tag{1.28}$$

Substituting 1.28 into 1.27 we get:

$$\begin{bmatrix} v_{an} \\ v_{bn} \\ v_{cn} \end{bmatrix} = \frac{1}{3}\begin{bmatrix} 2 & -1 & -1 \\ -1 & 2 & -1 \\ -1 & -1 & 2 \end{bmatrix}\begin{bmatrix} v_{ao} \\ v_{ao} \\ v_{ao} \end{bmatrix} \tag{1.29}$$

And note that,

$$\begin{bmatrix} v_{ao} \\ v_{bo} \\ v_{co} \end{bmatrix} = v_{dc}\begin{bmatrix} S_{11} - \frac{1}{2} \\ S_{21} - \frac{1}{2} \\ S_{31} - \frac{1}{2} \end{bmatrix} \tag{1.30}$$

Therefore,

$$\begin{bmatrix} v_{an} \\ v_{bn} \\ v_{cn} \end{bmatrix} = \frac{v_{dc}}{3}\begin{bmatrix} 2 & -1 & -1 \\ -1 & 2 & -1 \\ -1 & -1 & 2 \end{bmatrix}\begin{bmatrix} S_{11} \\ S_{21} \\ S_{31} \end{bmatrix} \tag{1.31}$$

The three-phase tensions above can be controlled based on the rotation of the spatial vector, as illustrated in ***Figure 1.10***. One can deduce from this figure that the three phase tensions are alternately represented by a rotating vector V_s. To do this, we use a fixed 2-D coordinate system, in which the horizontal α-axis is aligned in the same direction as phase A, and β is the vertical axis as usual [28]. V_s is now equivalent to the voltage vectors V_α and V_β

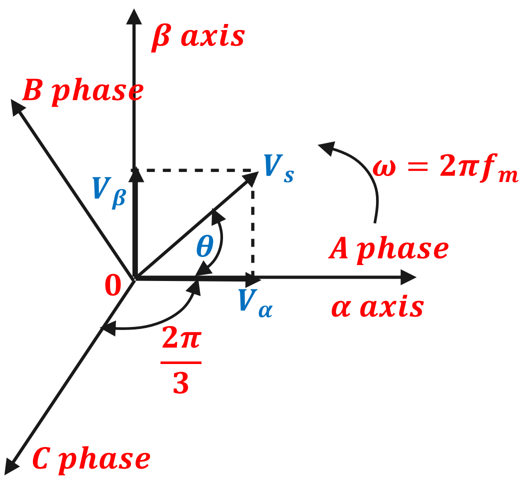

Figure 1.10. Relationship between three-phase voltage and coordinates α β

It is obvious that the three-phase voltage is completely controlled by V_α and V_β, these voltage vectors are described by a set of formulae as below.

$$\begin{bmatrix} V_\alpha \\ V_\beta \end{bmatrix} = \frac{2}{3}\begin{bmatrix} 1 & -\frac{1}{2} & -\frac{1}{2} \\ 0 & \frac{\sqrt{3}}{2} & -\frac{\sqrt{3}}{2} \end{bmatrix}\begin{bmatrix} V_{an} \\ V_{bn} \\ V_{cn} \end{bmatrix} \tag{1.32}$$

The matrix in the above equation is also expressed as:

$$\begin{cases} V_\alpha = V_{an} \\ V_\beta = \dfrac{\left(2V_{bn} + V_{an}\right)}{\sqrt{3}} \end{cases} \tag{1.33}$$

$$V_s = \sqrt{V_\alpha{}^2 + V_\beta{}^2} \tag{1.34}$$

$$\theta = arctan\left(\frac{V_\beta}{V_\alpha}\right) \tag{1.35}$$

$$\omega = 2\pi f_m \tag{1.36}$$

1.12. Control strategy principle:

The control method involves reconstructing the reference voltage at the inverter's output based on the sequence of the reference wave generation. Subsequently, the regenerated reference voltage, generated through PWM (Pulse Width Modulation) technique, is compared to a high-frequency sawtooth signal generated by the carrier generator. In the PWM control simulation depicted in ***Figure 1.11*** shows how the interaction between the reference signal and the carrier signal activates the control algorithm, which then issues commands to open or close the IGBTs (Insulated Gate Bipolar Transistors). This figure illustrates the PWM signals generated by the inverter to replicate a voltage corresponding to the reference signal.

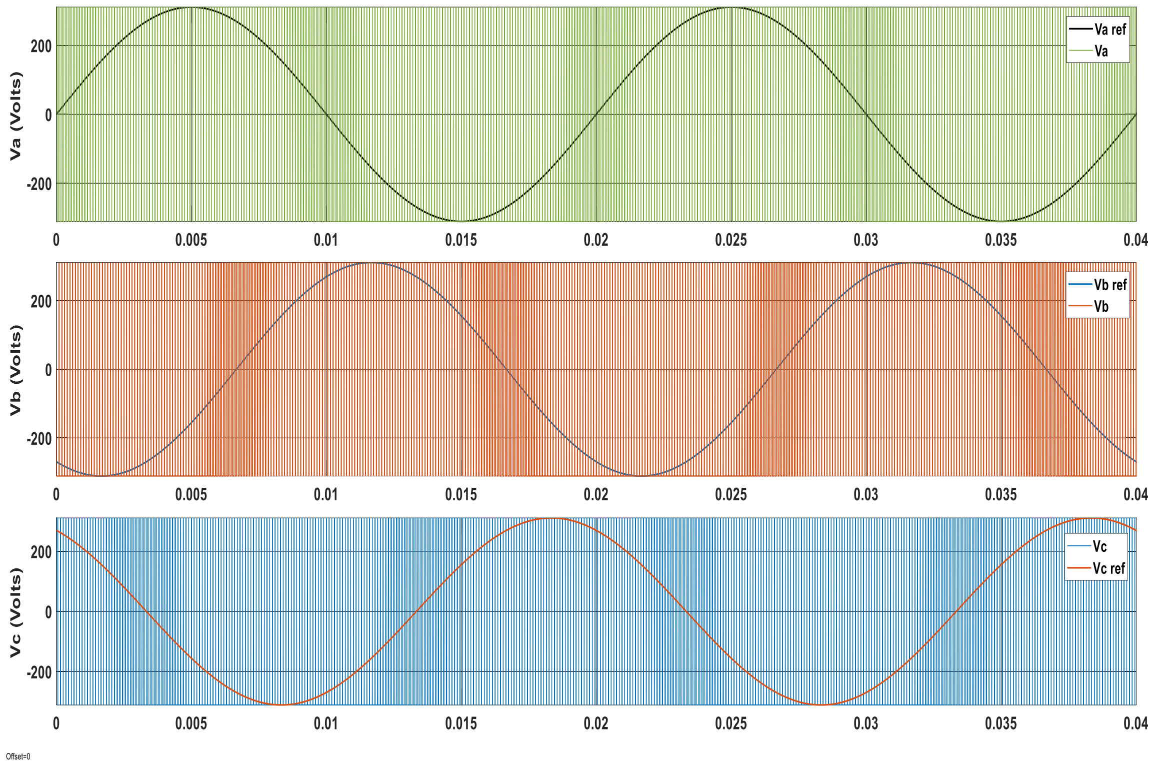

Figure 1.11. PWM voltage (Va, Vb and Vc) and their references

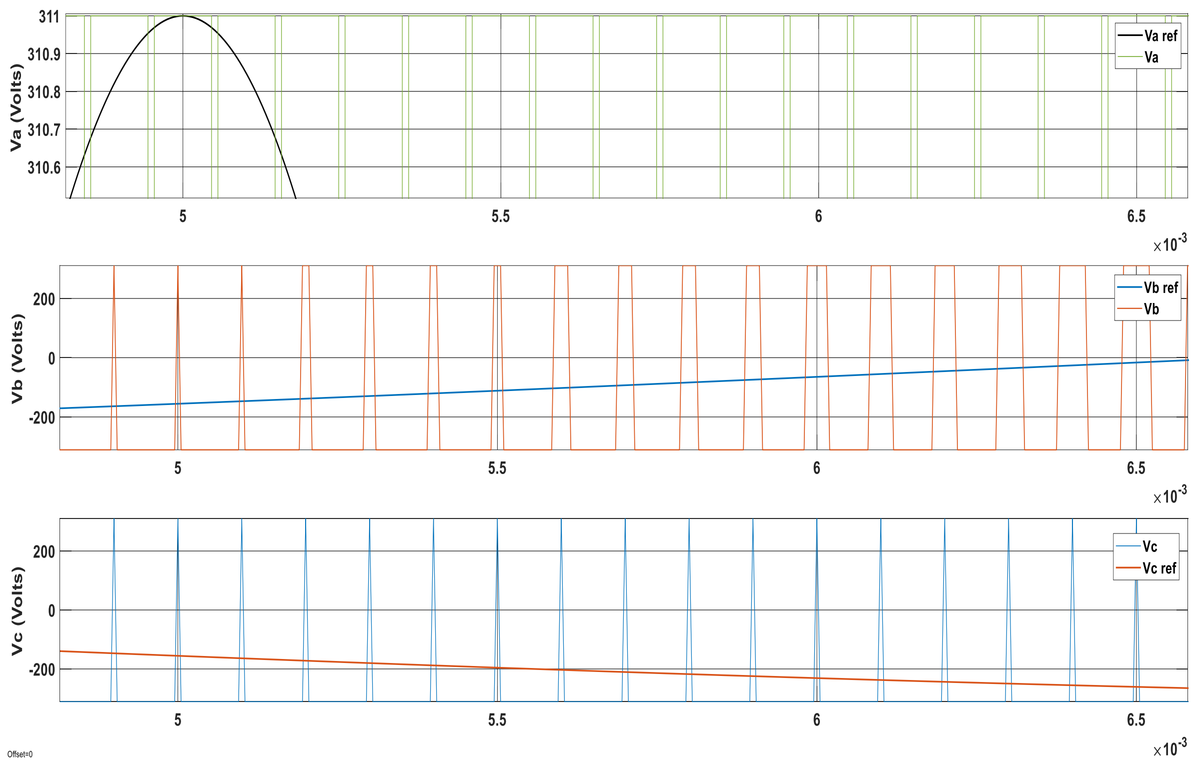

Figure 1.12. Zoom of PWM voltage (Va, Vb and Vc) and their references

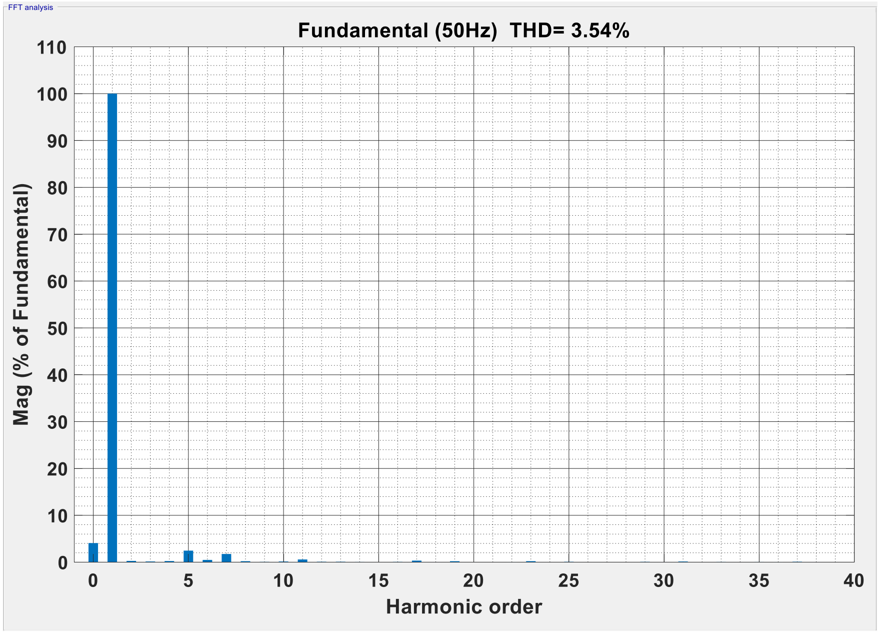

Figure 1.13. THD of the source voltage Va

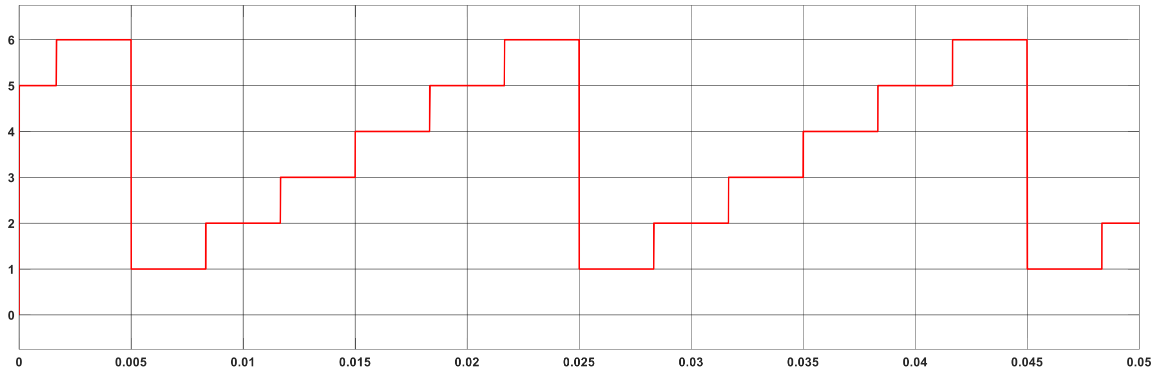

Figure 1.14. Sectors

1.13 Simulation results:

To complete the theoretical study presented above, a numerical simulation is essential. The algorithm is tested in the MATLAB environment. The SynRM parameters are shown in ***Table 1.2.***

Variable	Symbol	Value
d-axis inductance	L_d	0.1524 [H]
q-axis inductance	L_q	0.0345 [H]
Number of poles	p	2
Friction coefficient	f	0.00015 [N.m^{-1}]
Moment of inertia	J	0.00044 [Kg.m^2]
Stator resistance	R_s	8.1 [Ω]
d-time constant	T_d=L_d/R_s	0.01881 [s]
q-time constant	T_q=L_q./R_s	0.00426 [s]

TABLE 1.2. PARAMETERS OF THE MACHINE USED

1.13.1. SynRM is fed directly from the public network.

SynRM is supplied by purely sinusoidal and balanced sources, expressed as follows:

$$\begin{cases} v_a = V_m \sin(\omega t) \\ v_b = V_m \sin(\omega t - \dfrac{2\pi}{3}) \\ v_c = V_m \sin(\omega t + \dfrac{2\pi}{3}) \end{cases}$$

The following figures show the evolution of SynRM's characteristics fed directly from a balanced purely sinusoidal source, followed by the application of a mechanical load during the time interval [**1.5s,3s**].

At start-up, at no load, ***Figure 1.15*** illustrates the evolution of the SynRM's rotor speed, with ripples damping off at ***0.25 s*** heralding the onset of steady state and reaching a synchronous value of **314.16 rad/s**.

Figure 1.16 shows the evolution of the electromagnetic torque. Initially, the torque of the SynRM reaches the value of **-8.6 N.m**, then **+5.5 N.m** and exhibits oscillations which disappear after ***0.1s*** when it reaches ***3.46 N.m***, then it decreases in an almost linear fashion and stabilises at its minimum value.

Figure 1.17 shows the evolution of the stator currents along the direct and quadrature axes in a manner more or less analogous to the evolution of the speed, while slight oscillations can be seen, which disappear after ***0.1s***.

By applying a load torque equal to ***T_L= 2N.m*** at time ***t = 1.5s***, it can be seen that after small oscillations the speed returns to the synchronous speed of ***314.16 rad/s*** , the current ***I_q*** decreases slightly from ***7.92A*** to ***7.83A*** , while the current ***I_d*** increases and stabilises at ***3.84A***.

The torque reaches a value of ***3.5N.m*** and then stabilises at ***2. 02N.m*** (slightly higher than the load torque), which explains the coupling between the direct axis and the quadratic axis.

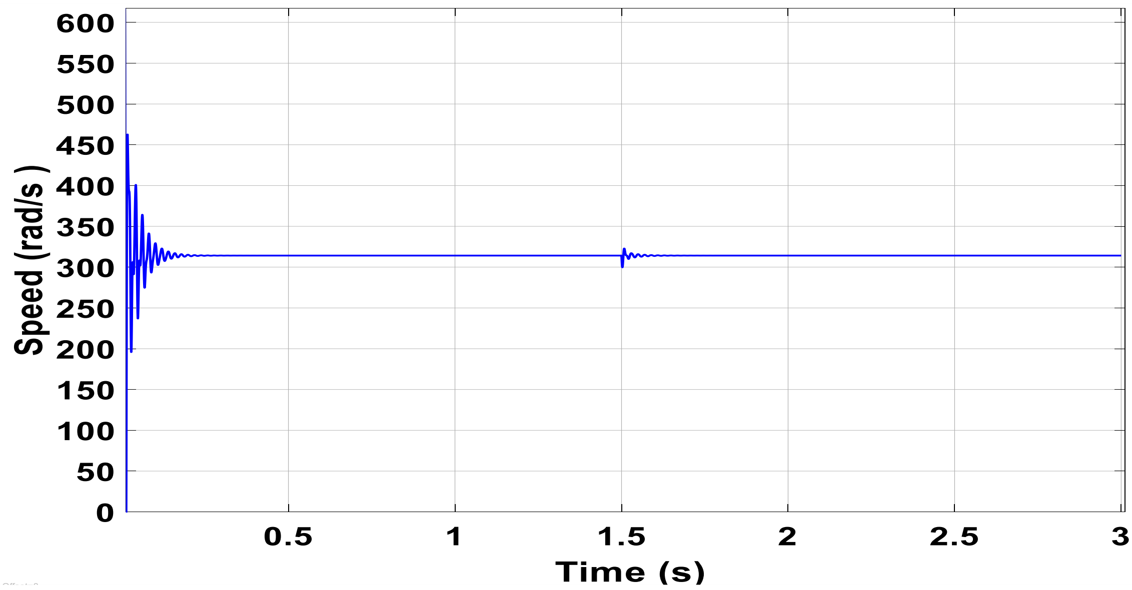

Figure 1.15. Rotational speed with no load and then under load at t = 1.5s, the machine supplied by the electrical network

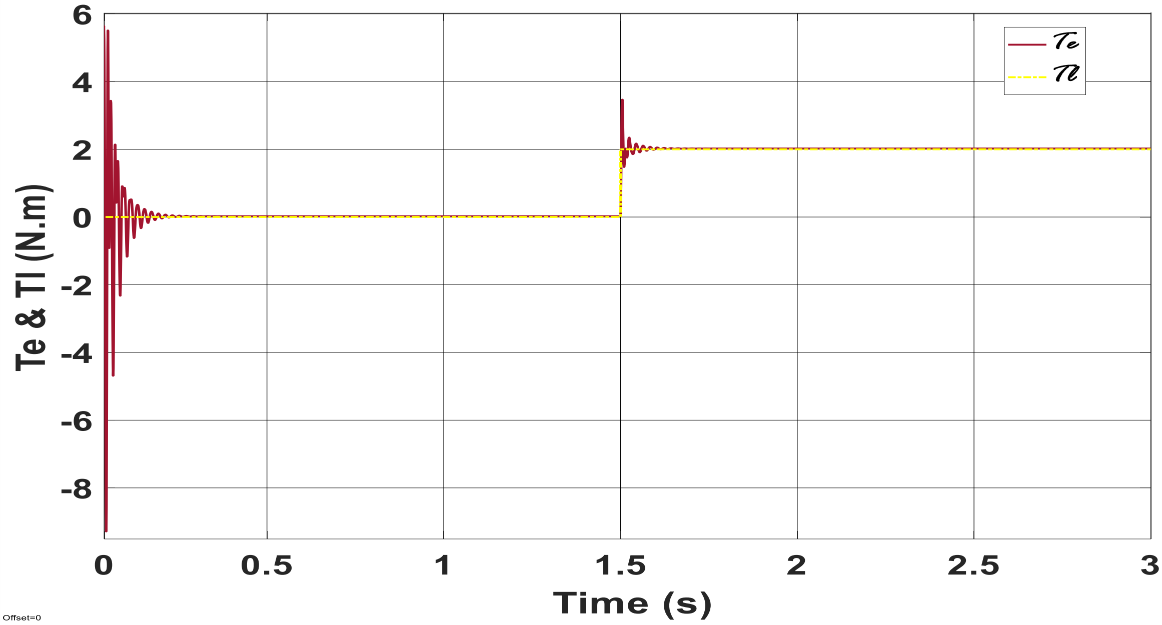

Figure 1.16. Electromagnetic torque response of the machine supplied by the electrical network

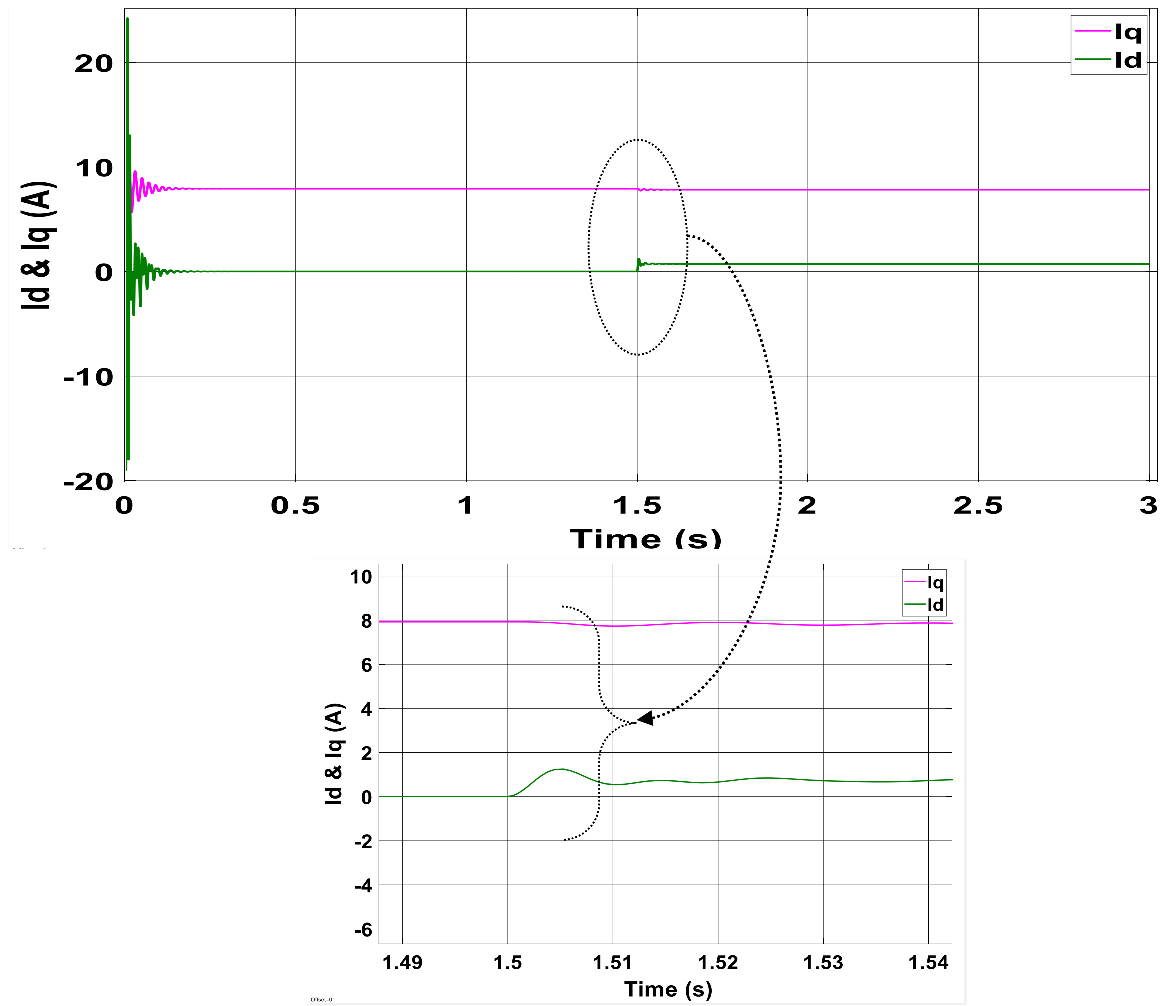

Figure 1.17. Components of the stator currents along the d and q axes of the machine supplied by the electrical network.

1.13.2. SynRM is supplied by an inverter

Figure 1.18,1.19,1.20, illustrate the progression of SynRM characteristics under the influence of ***PWM*** in the form of an ***S-Function.*** The study includes the introduction of a load T_l=2N.m within the time interval [4.5s, 9s]. The outcomes in this scenario closely resemble those achieved with a purely sinusoidal power source. Nevertheless, a closer examination of the figures, particularly those representing electromagnetic torque, stator currents, and currents in the two direct axes and in quadrature, reveals that this power supply approach induces an elevation in ripples. This increase is primarily attributed to the harmonics introduced by the inverters and PWM, exerting a notable impact on the electromagnetic torque.

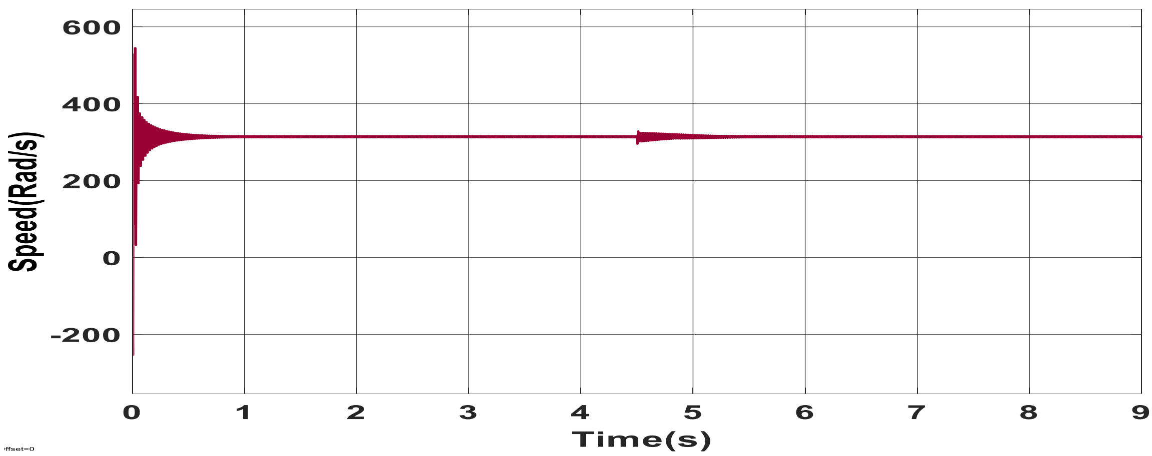

Figure 1.18. Rotation speed at no load and under load at t=4.5, the machine powered by the inverter.

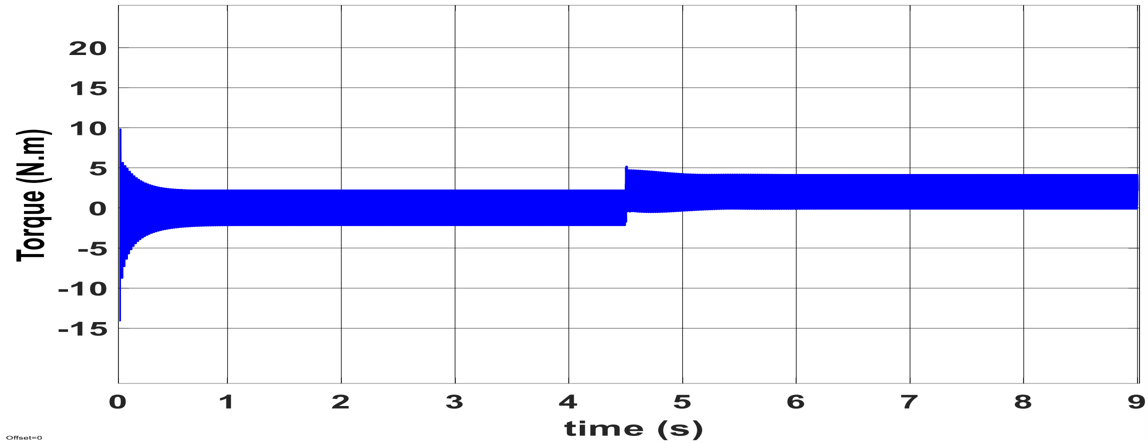

Figure 1.19. Electromagnetic torque response of the machine powered by the inverter

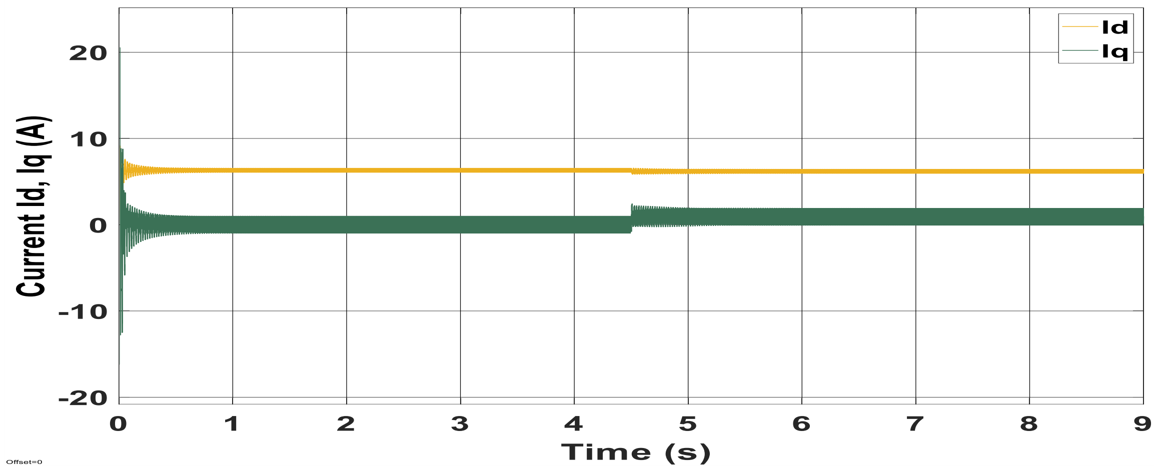

Figure 1.20. Composants du courants statoriques selon les axes et la machine alimentée par l'onduleur

1.14. Conclusion

This chapter delves into the characteristics and functionality of the SynRM, highlighting the significance of the ***Ld/Lq*** parameter in its design and optimization. A mathematical representation of the SynRM in the stationary reference frame (***α-β***) has been developed, while its behaviour in the synchronous reference frame (***d-q***) has also been analysed. This modelling is essential for applying advanced control strategies such as vector control. These representations provide a deeper insight into the electrical and magnetic properties of the machine and support the implementation of rotor flux orientation and speed regulation techniques. Furthermore, the inverter, a key element for supplying power to the SynRM, has been modelled. Simulation results, both with and without the inverter, are presented to assess its influence on the control system, particularly concerning machine performance.

Chapter 2: Control of synchronous Reluctance Machine

Chapter 2: Control of synchronous Reluctance Machine

2.1 Introduction

In this chapter, we will apply vector control by orientation of the rotor flux on the SynRM, and since the study of this type of control is linked to stability, in the sense of Lyapunov, convergence and the nature of the machine as a non-linear dynamic system, we need to devote part of the initiative to defining some concepts and definitions on the theory of stabilisation of dynamic systems.

2.2 Stability of dynamic systems

Consider the non-linear system described by:

$$\begin{cases} \dot{x}(t) = f\left(x(t), u(t)\right) \\ y(t) = g\left(x(t), u(t)\right) \end{cases} \tag{2.1}$$

In which $\boldsymbol{u}(\boldsymbol{t}) \in \Re^{n_u}$ and $\boldsymbol{y} \in \Re^{n_y}$ $\boldsymbol{x}(\boldsymbol{t}) \in \Re^{n_x}$ are the input , the output measurement and the state vectors respectively and $(\boldsymbol{f}, \boldsymbol{g}) \in \mathfrak{R}^{2n}$ are continuous non-linear functions.

Stability is defined here in terms of the behaviour of a system's trajectories close to its equilibrium points. Studying stability makes it possible to examine the evolution of the trajectory of a system when the initial state is close to a point of equilibrium.

Stability theory in Lyapunov's sense means that the solution of the equation, when initialised near an equilibrium point, remains close to that point [29] and applies to any differential equation,

Assuming that the ***nonlinear system 2.1*** under the initial condition $\boldsymbol{x}(\boldsymbol{t}_0) = \boldsymbol{x}_0$, has an equilibrium point $\bar{\boldsymbol{x}}$ then : if for each $\boldsymbol{\varepsilon} > 0$, a $\boldsymbol{\delta} > 0$ exists such that, for any initial condition $\boldsymbol{x_0}$ satisfying $|\boldsymbol{x}_0 - \bar{\boldsymbol{x}}| < \boldsymbol{\delta}$, the system 2.1 solution $\boldsymbol{x}(\boldsymbol{t})$ satisfies $|\boldsymbol{x}(\boldsymbol{t}) - \bar{\boldsymbol{x}}| < \boldsymbol{\varepsilon}$ for all $\boldsymbol{t} \geq \boldsymbol{0}$.

This means that a point $\bar{\boldsymbol{x}}$ will be a stable system equilibrium if, given a sufficiently small initial deviation from $\bar{\boldsymbol{x}}$, the solution stays arbitrarily near $\bar{\boldsymbol{x}}$ for any future time.

2.2.1. Equilibrium of the attractor

The given point $\bar{\boldsymbol{x}}$ is an attractor equilibrium of the ***2.1 system*** if for any $\varepsilon > 0$, a $\delta > 0$ exists so that for any initial condition $\bar{x}$ satisfying $|x_0 - \bar{x}| < \delta$, the resulting 2.1 solution x(t) of the ***system 2. 1*** will converge to $\bar{\boldsymbol{x}}$ as $\boldsymbol{t} \to \infty$, i.e., $\lim_{t\to\infty} |\boldsymbol{x}(\boldsymbol{t}) - \bar{\boldsymbol{x}}| = 0$.

This means that an attractor equilibrium is a stable equilibrium towards which the system's solutions converge over time, whatever the initial conditions. It behaves as an ‘attractor’ for neighbouring solutions, drawing them towards it over time. An attractor equilibrium is a more powerful concept of stability, since it implies not only that the solution stays arbitrarily close to equilibrium over all future times, but also that the solution moves closer to equilibrium as time passes.

2.2.2. Asymptotically stable equilibrium

The point $\bar{\boldsymbol{x}}$ is taken to be an asymptotically stable equilibrium for the ***system 2.1*** if is both attractive and stable . If every initial state $\boldsymbol{x}_0$ converges to the asymptotically stable equilibrium, we speak of a basin of attraction. Asymptotic stability is a practically desirable property, however, it does not specify the speed at which the trajectory $\boldsymbol{x}(\boldsymbol{t})$ converges towards equilibrium. To remedy this, the exponential stability concept is presented.

2.2.3. Exponential stability

The given point $\bar{\boldsymbol{x}}$ is an equilibrium point that is exponentially stable whenever there exist positive real numbers $\boldsymbol{\varepsilon}, \boldsymbol{\alpha}, \boldsymbol{\beta}$, and $\boldsymbol{\delta}$ with the result that for every initial value $\boldsymbol{x}_0$ that satisfies $|\boldsymbol{x}_0 - \bar{\boldsymbol{x}}| < \boldsymbol{\delta}$, the system solution satisfies $|\boldsymbol{x}(\boldsymbol{t}) - \bar{\boldsymbol{x}}| \leq \boldsymbol{\alpha}|\boldsymbol{x}_0 - \bar{\boldsymbol{x}}|\boldsymbol{e}^{-\boldsymbol{\beta t}}$ for all $\boldsymbol{t} \leq \boldsymbol{t}_0$, with $\boldsymbol{t}_0$ being a fixed time. Clearly, exponential stability involves asymptotic stability, but the converse is not necessarily true. In what follows, let's consider stability around the origin, i.e. when $\bar{\boldsymbol{x}} = 0$

2.2.4. Lyapunov first method

The first Lyapunov method, known also as the so-called indirect method, evaluates the stability of a system by investigating the system's linearization around the point of equilibrium $\bar{\boldsymbol{x}}$. This involves assessing the eigenvalues $\boldsymbol{\lambda}_i(\boldsymbol{A})$ of matrix Jacobian $\boldsymbol{A}$ at the equilibrium point , i.e

$$\boldsymbol{A} = \frac{\partial \boldsymbol{f}}{\partial \boldsymbol{x}} \bar{\boldsymbol{x}}$$

Lyapunov's indirect method is a method for finding the equilibrium point stability $\bar{\boldsymbol{x}} = 0$ with respect to a dynamical system. If every eigenvalue of the Jacobian matrix has a negative real part, i.e. their real parts are less than zero $\boldsymbol{Re}(\boldsymbol{\lambda}_i(\boldsymbol{A})) < 0$, so the equilibrium point $\bar{\boldsymbol{x}} = 0$ is regarded as exponentially stable. If one or more eigenvalues has a positive real part $\boldsymbol{Re}(\boldsymbol{\lambda}_i(\boldsymbol{A})) > 0$, then the equilibrium point $\bar{\boldsymbol{x}} = 0$ is considered unstable. If the indirect method is simple to implement, it is only a partial analysis of stability and does not provide any indication of the size of the attraction basins [29].

2.2.5. Lyapunov second method

Lyapunov's 2nd method, which is also called the direct method, implies the employment of a positive definite function (generally denoted $\boldsymbol{V}(\boldsymbol{x}(\boldsymbol{t}))$ known as the Lyapunov function) to evaluate the stability of an equilibrium point. The function should be positive within the attraction basin and decrease throughout the trajectories of the system. [29, 30].

2.2.5.1. Asymptotic stability and Local stability

To consider the ***system 2.1*** as locally stable, a differentiable and continuous function $\boldsymbol{V}(\boldsymbol{x}(\boldsymbol{t}))$, and a vicinity, $\boldsymbol{V}_0$, must exist such that :

$$\forall \boldsymbol{x} \in \boldsymbol{V}_0,\ \boldsymbol{V}(\boldsymbol{x}(\boldsymbol{t})) > 0.$$

$$\forall \boldsymbol{x} \in \boldsymbol{V}_0,\ \dot{\boldsymbol{V}}(\boldsymbol{x}(\boldsymbol{t})) = \frac{\boldsymbol{dV}(\boldsymbol{x}(\boldsymbol{t}))}{\boldsymbol{dt}} = \frac{\partial \boldsymbol{V}(\boldsymbol{x}(\boldsymbol{t}))}{\partial \boldsymbol{x}} \dot{\boldsymbol{x}}(\boldsymbol{t}) \le 0.$$

If $\boldsymbol{V}(\boldsymbol{x}(\boldsymbol{t})) > 0$ and $\dot{\boldsymbol{V}}(\boldsymbol{x}(\boldsymbol{t})) < 0$, the function $\boldsymbol{V}(\boldsymbol{x}(\boldsymbol{t}))$ is regarded as a Lyapunov function in the strict sense and the origin is regarded as asymptotically stable.

2.2.5.2. Exponential stability

The origin for the ***system 2.1*** is an exponentially stable equilibrium point provided there exists a continuous and differentiable function $\boldsymbol{V}(\boldsymbol{x}(\boldsymbol{t}))$, constants $\boldsymbol{\alpha}, \boldsymbol{\beta}, \boldsymbol{\gamma} > 0$; $\boldsymbol{\tau} \ge 0$ and there exists a neighbourhood $\boldsymbol{V}_0$ such that

$$\forall \boldsymbol{x} \in \boldsymbol{\alpha} \|\boldsymbol{x}\|^{\tau} \le \boldsymbol{V}(\boldsymbol{x}(\boldsymbol{t})) < \boldsymbol{\beta} \|\boldsymbol{x}\|^{\tau}.$$

$$\forall \boldsymbol{x} \in \boldsymbol{V}_0,\ \dot{\boldsymbol{V}}(\boldsymbol{x}(\boldsymbol{t})) < -\boldsymbol{\gamma}\, \boldsymbol{V}(\boldsymbol{x}(\boldsymbol{t})).$$

2.3 Principle of non-linear system control:

We now seek to solve a tracking problem for nonlinear multivariable systems described by the ***system 2.1.***

The main problem in controlling this type of system is to find a reference system for the state and output so that this system is a steady state, and this is only achieved under certain conditions determined by the nature of the system and the algorithm used to form the tracking error dynamics (i.e. to ensure stability conditions for the error system), so we define reference state systems as follows:

$$\begin{cases} \dot{\bar{\boldsymbol{x}}}(\boldsymbol{t}) = f(\bar{\boldsymbol{x}}(\boldsymbol{t}), \bar{\boldsymbol{u}}(\boldsymbol{t})) \\ \bar{\boldsymbol{y}}(\boldsymbol{t}) = g(\bar{\boldsymbol{x}}(\boldsymbol{t}), \bar{\boldsymbol{u}}(\boldsymbol{t})) \end{cases} \tag{2.2}$$

Where , $\bar{\boldsymbol{x}}(\boldsymbol{t}) \in \mathbb{R}^{\boldsymbol{n}}$, $\bar{\boldsymbol{u}}(\boldsymbol{t}) \in \mathbb{R}$ *and* $\bar{\boldsymbol{y}}(\boldsymbol{t}) \in \mathbb{R}$ denote respectively the reference state, the reference input and the reference output of the system (2.1), Then the problem becomes as follows :

$$\lim_{t \to \infty} \boldsymbol{e}_x(\boldsymbol{t}) = 0$$

Where

$$\boldsymbol{e}_x(\boldsymbol{t}) = \boldsymbol{x}(\boldsymbol{t}) - \bar{\boldsymbol{x}}(\boldsymbol{t})\ ;$$

$$\dot{\boldsymbol{e}}_x(\boldsymbol{t}) = \boldsymbol{f}(\boldsymbol{x}(\boldsymbol{t}), \boldsymbol{u}(\boldsymbol{t})) - \boldsymbol{f}(\bar{\boldsymbol{x}}(\boldsymbol{t}), \bar{\boldsymbol{u}}(\boldsymbol{t}))$$

$$\boldsymbol{e}_o(\boldsymbol{t}) = \boldsymbol{y}(\boldsymbol{t}) - \bar{\boldsymbol{y}}(\boldsymbol{t}) \tag{2.3}$$

2.4. Rotor flux control for variable reluctance synchronous machines

Many industrial applications require delicate control of torque, speed and/or position. Scalar control, with its limited performance, cannot meet these needs. SynRM control requires both torque and flux control. However, the electromagnetic torque formula is complex and does not resemble that of a DC machine, where the natural decoupling between flux and torque control facilitates control. Vector control, which was only introduced in the early 1970s [31-33], which requires Park transform calculations, evaluation of trigonometric functions, integration and regulation, taking advantage of technological advances in power electronics.

2.4.1 Principle of Flux Oriented Control

The controller topology shown in ***Figure 2.4*** is based on the flux-oriented control strategy in order to achieve the same decoupling between flux and torque that naturally exists in separately excited ***DC*** machines [34]. In this control strategy, the angular velocity of the reference rotor is compared with the feedback signal and the result (error) drives a ***PI*** controller to determine the quadrature component of the stator current reference to control the electromagnetic torque, while the direct component of the stator current reference is charged with controlling the magnetic state of the SynRM. The voltage commands in the reference frame ***(d-q)*** are generated by the ***PI*** regulator of the stator current control loop [35]. These will be studied in this section.

2.4.2 Control equation with oriented rotor flux

The principle of SynRM vector control using rotor flux orientation is to align the rotor flux along the ***d*** axis. The reference for current i_d is held at zero. The reference for the current i_q is determined using a Proportional Integral ***PI*** speed controller. This controller has the advantage of not introducing a zero in the closed-loop transfer function, while guaranteeing zero static error. In this control, we used non-linear decoupling to close the Park current control loop using Proportional-Integral ***PI*** controllers [62].

2.4.3 Dynamic input-output decoupling

Using the Laplace transform, we obtain the expressions for the direct and quadrature components of the stator reference voltages.

$$\begin{cases} V_d = (R_s + L_d s) i_d - \omega_r . L_q i_q \\ v_q = (R_s + L_q s) i_q + \omega_r . L_d i_d \end{cases} \tag{2.4}$$

Where ***s*** represents Laplace operator.

Analysis of these equations shows the existence of coupled terms which induce a strong interaction between the two axes. The above equations lead to two first-order linear systems with constant coefficients:

$$\begin{cases} V_d = v_d^{lin} + v_d^{dec} = \left[R_s i_d + L_d \dfrac{d}{dt} i_d \right] - \omega_r . L_q i_q \\ v_q = v_q^{lin} + v_q^{dec} = \left[R_s i_q + L_q \dfrac{d}{dt} i_q \right] + \omega_r . L_d i_d \end{cases} \tag{2.5}$$

$$V_d^{lin} = R_s i_d + L_d \frac{d}{dt} i_d \quad , \; V_q^{lin} = R_s i_q + L_q \frac{d}{dt} i_q$$

$$V_d^{dec} = -\omega_r . L_q i_q \; , \qquad v_q^{dec} = \omega_r . L_d i_d$$

We choose two new inputs v_d^{dec} and v_q^{dec} added to the decoupling terms with opposite signs. After presenting the coupling terms in the stator equations, we will investigate in the following section the regulation of direct and quadrature currents. However, the disadvantage of this solution is the use of the components of the measured currents, which can be disturbed by the harmonic content of the phase currents and measurement noise. To solve this problem, we have used the reference currents to compensate for the coupling terms.

2.5. Park current regulation study

The method of controlling the orientation of the rotor flux makes it possible to control the actual magnitudes of the currents along the direct axis and in quadrature. By comparing these values with the reference values, we obtain the reference voltages needed to control the power inverter. The direct and quadrature currents are controlled by a ***PI*** regulator whose gains are Kp_{i_d} , Kp_{i_q} Ki_{i_d} , Ki_{i_q} . To determine the parameters of the PI controller, we used the method of placing the poles of the transfer function in a closed loop. The block diagram of the i_d current control loop using a PI controller is shown in the ***figure 2.1*** below:

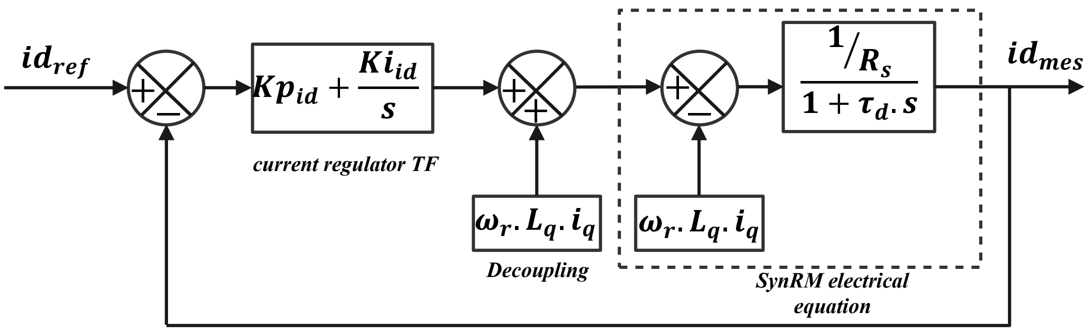

Figure 2.1. Direct axis current control loop.

The open-loop transfer function of the current along the ***d*** axis is:

$$H_{dop}(s) = Kp_{id}\left(s + \frac{Ki_{id}}{Kp_{id}}\right)\frac{1}{s}\frac{\frac{1}{L_d}}{s + \frac{R_s}{L_d}} \tag{2.6}$$

Where $\tau_d = \frac{L_d}{R_s}$, by offsetting the dominant pole, the equivalence condition is set as follows:

$$\frac{Ki_{id}}{Kp_{id}} = \frac{R_s}{L_d} \tag{2.7}$$

The transfer function in the closed-loop, after calculation and development, is:

$$H_{dcl}(s) = \frac{1}{\tau_{id}s + 1} \tag{2.8}$$

With

$$\tau_{id} = \frac{L_d}{Kp_{id}}$$

where τ_{id} = ***0.001 s*** is the current loop response time, the same controllers coefficient values are adopted for the two current loops. We can calculate the controller parameters from ***equation 2.8***, by simple identification, then we get:

$$\begin{cases} Kp_{id} = \dfrac{L_d}{\tau_{id}} \\ Ki_{id} = Kp_{id}\dfrac{R_s}{L_d} \end{cases} \tag{2.9}$$

Similarly, equations (2.5) (2.6) (2.7) can be used to construct the following block diagram:

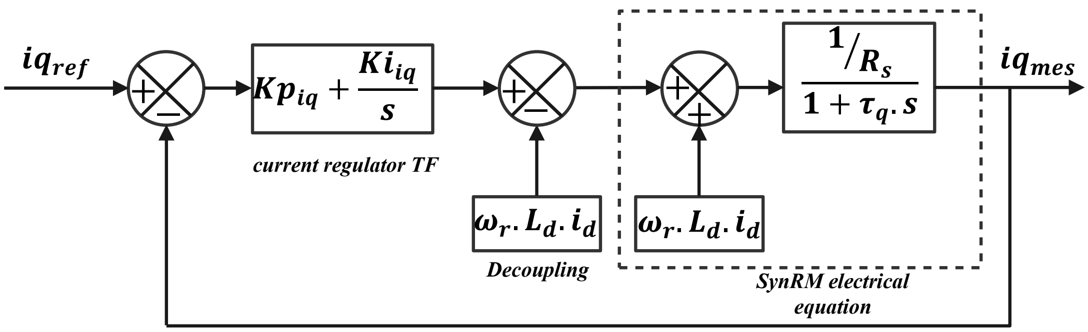

Figure 2.2. Quadrature axis current control loop.

Knowing that regulator i_d has the same form as i_q, and by offsetting the dominant pole $\frac{Ki_{iq}}{Kp_{iq}} = \frac{R_s}{L_q}$ the transfer function becomes:

$$H_{qcl}(s) = \frac{1}{\tau_{iq}s + 1} \tag{2.10}$$

With $$\tau_{iq} = \frac{L_q}{Kp_{iq}}$$

We can calculate the controller parameters from Equation (2.10), by simple identification, then we get:

$$\begin{cases} Kp_{id} = \dfrac{L_q}{\tau_{iq}} \\ Ki_{iq} = Kp_{iq}\dfrac{R_s}{L_q} \end{cases} \tag{2.11}$$

2.5.1 Speed Regulation

In order to achieve good performance for both the track (response compared to the reference) and to the speed control (response compared to the disturbance), we consider the functional diagram of the speed control loop shown schematically in ***Figure 2.3*** [36].

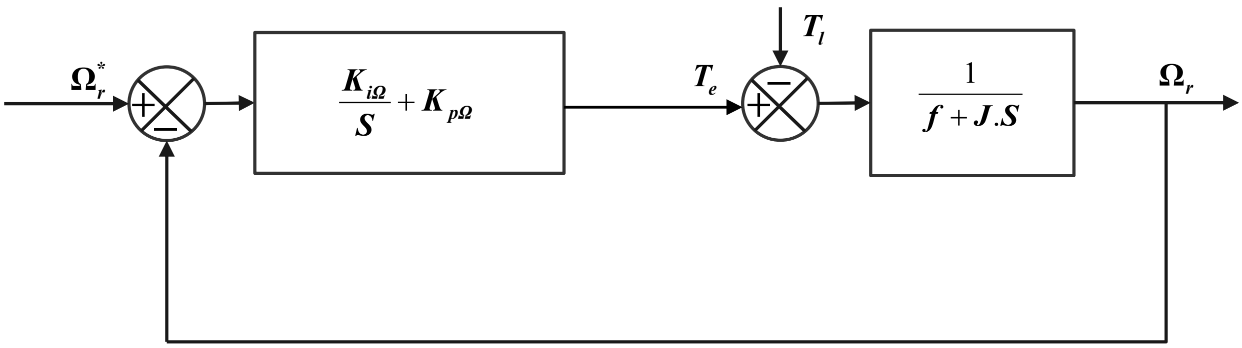

Figure 2.3. Speed regulation loop

According to the block diagram of the speed regulation, we have:

$$\Omega(s) = \frac{1}{Js + f}(T_e - T_l) \tag{2.12}$$

The transfer function of the closed-loop, after calculation, is expressed by:

$$H_{C\Omega}(s) = \frac{1}{\dfrac{J}{K_{i\Omega}K_{p\Omega}}s^2 + \dfrac{K_{p\Omega} + f}{K_{i\Omega}K_{p\Omega}}s + 1} \tag{2.13}$$

The transfer function (2.13) can be identified to a second-order system in the form:

$$G(s) = \frac{1}{\dfrac{1}{\omega_n^2}s^2 + \dfrac{2\xi}{\omega_n}s + 1} \tag{2.14}$$

This implies the identities:

$$\begin{cases} \dfrac{J}{K_{i\Omega}K_{p\Omega}} = \dfrac{1}{\omega_n^2} \\ \dfrac{K_{p\Omega} + f}{K_{i\Omega}K_{p\Omega}} = \dfrac{2\xi}{\omega_n} \end{cases} \tag{2.15}$$

If we choose $\xi = 1$ we will get a relationship between ω_n and the wanted speed response time τ_Ω, which allows us to freely set the system dynamic. This relation is written as: $\tau_\Omega \omega_n = 4.75$. (From the second-order system charts (presented in the annex)), where τ_Ω represents the system speed response time.

Having properly selected the damping coefficient $\xi = 1$ and response time $\tau_\Omega = 0.1s$ and next ω_n, we can calculate the controller parameters from ***Equation (2.14),*** by simple identification, then we get:

$$\begin{cases} K_{p\Omega} = 2J\xi\omega_n - f \\ K_{i\Omega} = J\dfrac{\omega_n^2}{K_{p\Omega}} \end{cases} \tag{2.16}$$

2.5.2. Production of electric current i_d^*

The reference current i_d^* is obtained according to the relation $i_d^* = \dfrac{1}{L_d}\phi_{rd}^*$ through the ***relation 2.17*** which defines the defluxion block.

$$\phi_{rd}^* = \begin{cases} \phi_{rn} & si\ \Omega \le \Omega_n \\ \dfrac{\Omega_n}{|\Omega|}\Omega_{rn} & si\ \ \Omega > \Omega_n \end{cases} \tag{2.17}$$

Where ϕ_{rn} and Ω_n are the nominal rotor flux and the nominal speed respectively.

2.5.3. Production of electric current i_q^*

The i_q^* reference current is obtained from the electromagnetic torque produced by the speed regulator as follows

$$i_q^* = \frac{Te}{K_f} \tag{2.18}$$

Where
$$K_f = \frac{1}{\frac{3}{2}p\left(L_d - L_q\right)i_d^*}$$

2.6. Simulation results

This section presents the simulation results of vector control applied to a voltage-fed SynRM. ***Equation 1.24*** were used to model the machine. ***Figure 2.6*** shows the simulation results for the speed control. It can be seen that the controlled speed follows its reference with a tracking error of ***5 rad/s***. As shown in ***Figure 2.7***, the largest value reached by the error is when the torque is applied. It can also be seen that at points where there is a change in the nature of the motion, the error is small. ***Figure 2.8*** shows the evolution of the electromagnetic torque, where it embodies the principle of fundamental motion, we note the proportionality between the electromagnetic torque and the stator current $\boldsymbol{i_q}$, as shown in ***Figure 2.9*** with a little ripple in the torque and stator currents, the response of the two components of the stator current clearly shows the decoupling introduced by the vector control of the machine from the electromagnetic torque, which depends only on the $\boldsymbol{i_q}$ component.

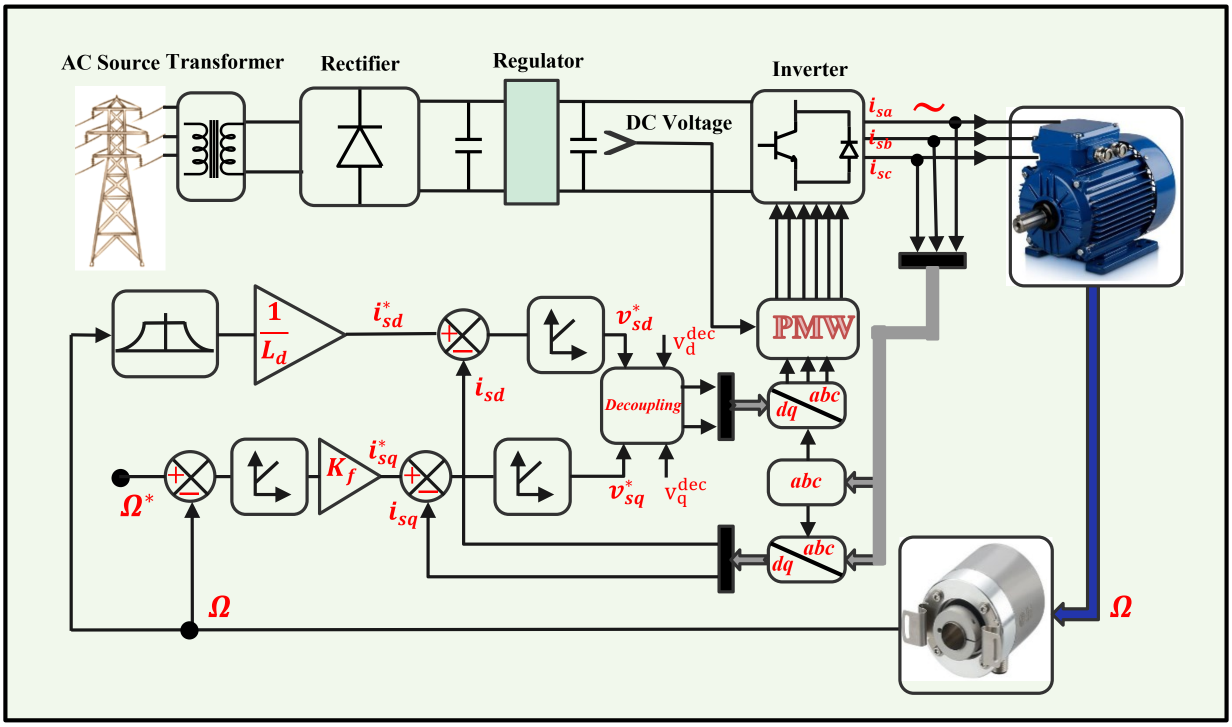

Figure 2.4. Block diagram of vector control with an inverter

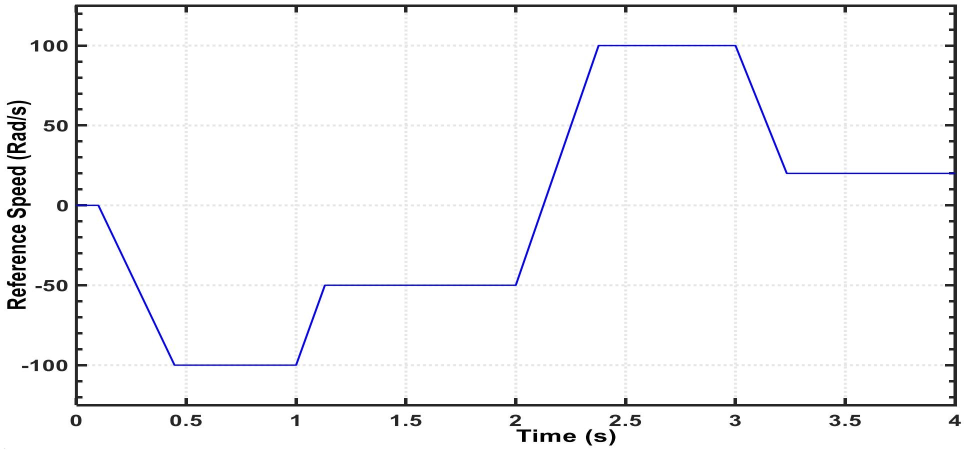

(a)

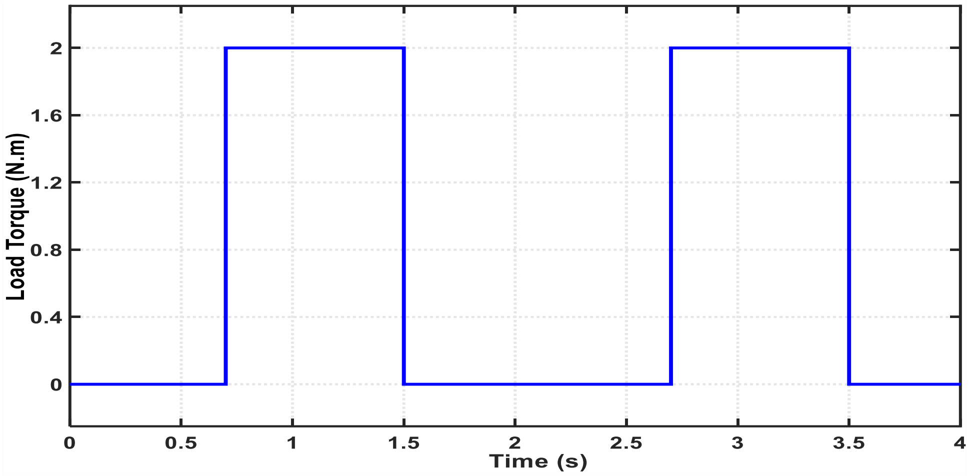

(b)

Figure 2.5. Benchmark command trajectory: (a) Reference speed, (b) Load torque PI" controlled rotation speed.

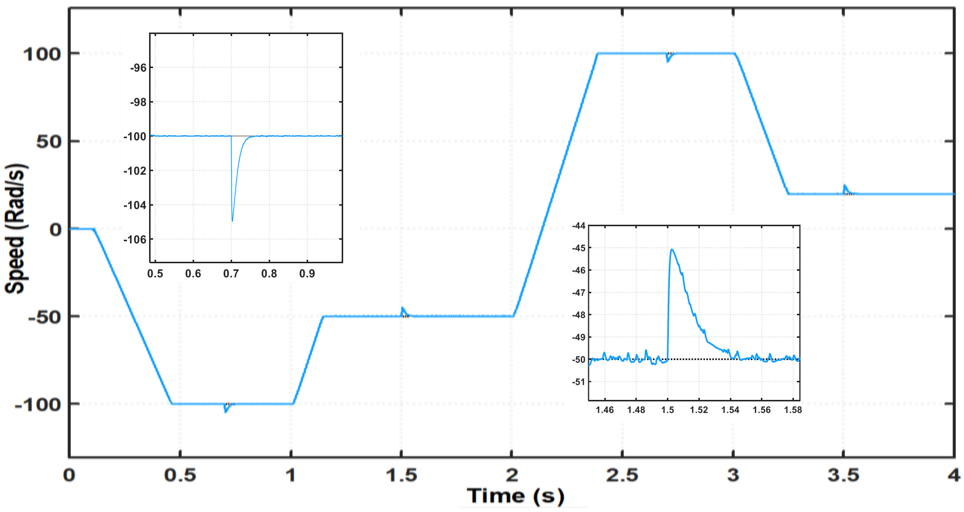

Figure 2.6. PI controlled rotation speed.

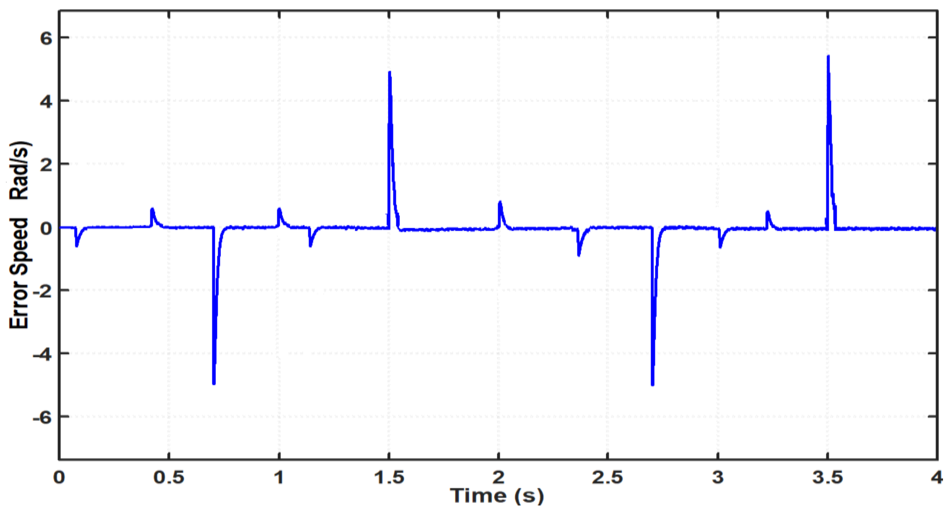

Figure 2.7. Error between the reference speed and the measured speed PI

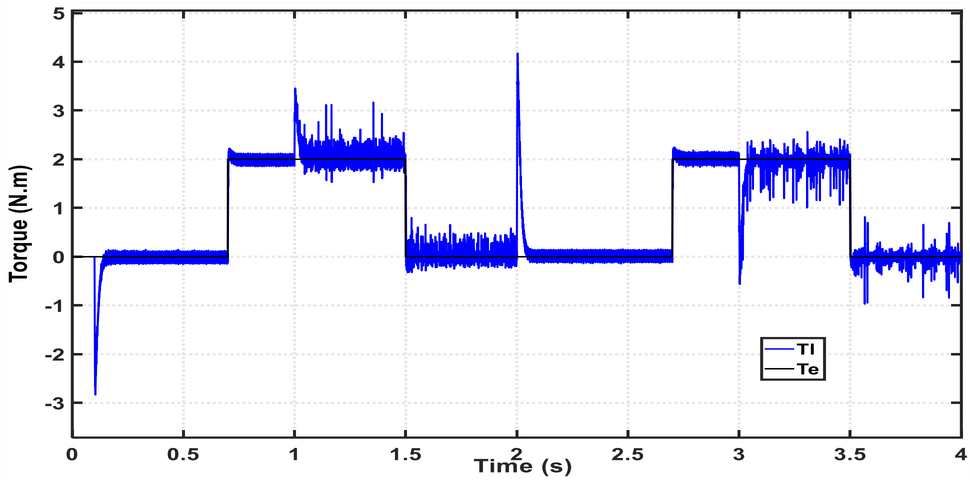

Figure 2.8. PI electromagnetic torque response

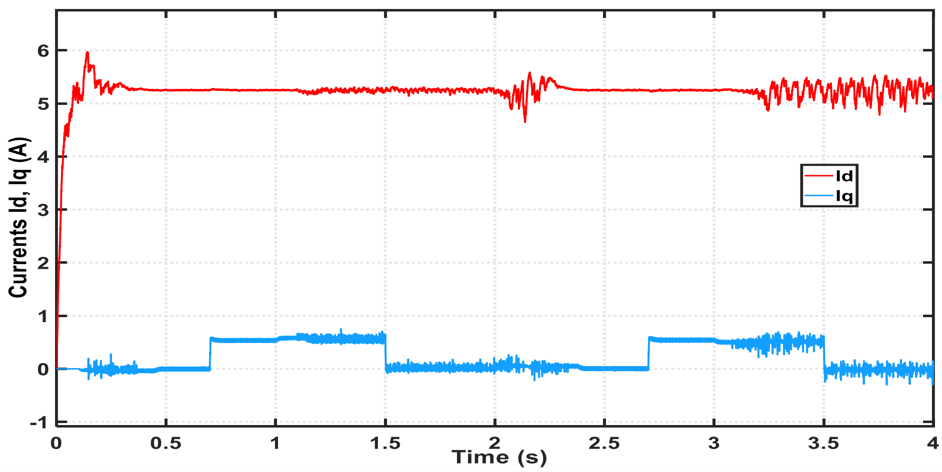

Figure 2.9. Stator current components along the *d* and *q* axes of the "PI" controller

The results of the vector control were evaluated by means of a no-load start-up simulation, followed by a series of cyclic variations in the load torque applied to the variable reluctance synchronous machine (***SynRM***). These tests were designed to evaluate the performance of the control system in a variety of machine operating scenarios.

The simulation starts with a reference speed applied over a defined period, and then load torque changes are introduced at specific times. The results of the simulation show that the PI controller works well, but it is not perfectly resistant to load variations, resulting in a slight drop in speed.

In addition, the response of electromagnetic torque and stator flux is analysed to assess the decoupling between these quantities and their behaviour in response to load variations. These results confirm the effectiveness of vector control in maintaining stable performance despite changes in operating conditions.

This chapter presents the simulation results of vector control applied to the Synchronous Variable Reluctance Machine (***SynRM***). The simulations are carried out on a ***SynRM*** machine connected directly to the mains and controlled by a direct vector control (DVC) by orientation of the stator flux, with the specific SynRM parameters specified in ***Table 1.2*.**

A no-load start-up simulation is carried out to assess the robustness of the control. A reference speed of ***100 rad/s*** is maintained for a period of time, followed by a change in load torque applied at instants (0.2s,1.5s,2.7s,3.5s). The results show that the ***PI*** controller is resistant to load variations and torque overshoot when load is applied.

In addition, the simulations illustrate the decoupling between the electromagnetic torque and the stator flux. These results confirm the effectiveness of the vector control applied to the ***SynRM*** and its ability to maintain stable performance despite load variations.

2.7. Conclusion

In this Chapter, we presented the modelling and identification of a Synchronous Reluctance Machine and the study of its vector control using the Park Transform. The machine was controlled through a PWM mechanism, and the modelling of the SynRM facilitated the implementation of vector control, achieving dynamic behaviour comparable to that of a continuously operating machine.

MATLAB simulations demonstrated this strategy, particularly at low speeds, for managing speed and electromagnetic torque.

Various strategies can be employed to enhance the machine's operational performance, providing robust dynamics depending on the desired objectives. In the third chapter, we outline the implementation of predictive control with mechanical sensors by testing the robustness of the machine.

Chapter 3: General Predictive Control

Chapter 3: General Predictive Control

3.1. Introduction

With the rapid advancements in digital computing, it's now nearly impossible to find an area of human activity unaffected by this technology. Computers have enabled the integration of complex and sophisticated techniques into control processes, facilitating the development of efficient strategies that are both cost-effective and practical—something previously unattainable with earlier devices and mechanisms. Techniques such as nonlinear control, multivariable control, robust control, and predictive control are prime examples. Predictive control, in particular, arose from a genuine need in the industrial sector for control systems that could surpass the performance of traditional controllers like ***PID***, all while addressing increasingly stringent operational and production constraints [37].

As an advanced control method in automation, predictive control is designed to manage complex industrial systems. Its core principle involves using a dynamic model of the process within the controller in real-time to forecast future system behaviour. Unlike other control techniques, predictive control must be computed online, optimizing system performance based on inputs and outputs (such as state, torque, etc.) to predict future behaviour over a set time frame known as the prediction horizon. The optimization process produces a control vector, with the first value of the optimal sequence applied to the system, after which the process is repeated with updated data in the next time interval.

Predictive control is particularly effective for managing systems with multiple inputs and outputs where a simple PID controller falls short. It is especially useful in scenarios involving significant delays, inverse responses, and numerous disturbances.

3.2 Principle of model predictive control

Predictive control is the repeated resolution at each time step of an optimal control problem: "how to go from the current state to an objective in an optimal way while satisfying constraints". To achieve this, the state of the system must be known at each iteration using a numerical solver [38]. The block diagram for generalised predictive control is shown in ***figure 3.1***, where we observe the commands ***u(k)*** to be applied to the system to obtain rallying around the setpoint ***w(k)***. The numerical model is obtained by a discretisation (***z-transform***) of the continuous transfer function of the model, which makes it possible to calculate the predicted output over a finite horizon.

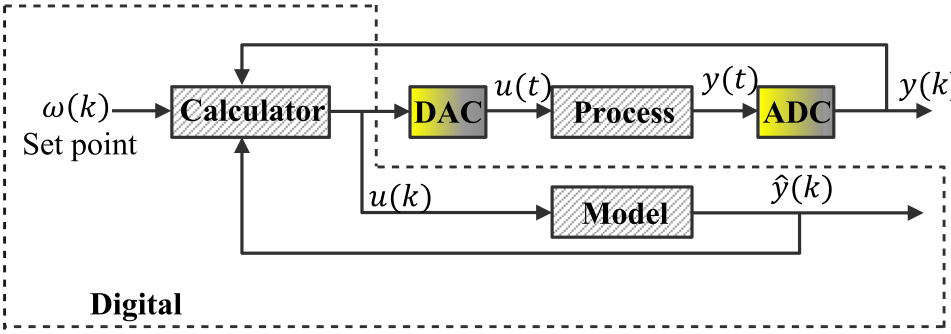

Figure 3.1. Block diagram for generalised predictive control.

3.3. General predictive control strategy

If the process output is to coincide with a set point or reference trajectory in the future, it is necessary:

- Predict the future output of the process over a defined time horizon using the numerical model of the system. We denote the predicted outputs by $\boldsymbol{y}(\boldsymbol{t}+\boldsymbol{k} \mid \boldsymbol{t})$, $\boldsymbol{k}=0..\boldsymbol{n}$ and the prediction horizon by ***N***. These outputs depend on the output and input values of the process to be controlled, which are known up to time ***t***.
  ($\boldsymbol{k} \mid \boldsymbol{t}$) indicates the value of the variable at the instant t+k calculated at the instant t
- Calculate the sequence of control signals, denoted by $\boldsymbol{u}(\boldsymbol{t}+\boldsymbol{k} \mid \boldsymbol{t})$, $\boldsymbol{k}=0..\boldsymbol{n}-1$, minimising a performance criterion in order to lead the process output to a reference output. We denote by $\boldsymbol{\omega}(\boldsymbol{t}+\boldsymbol{k} \mid \boldsymbol{t})$, $\boldsymbol{k}=0..\boldsymbol{n}$, usually the performance criterion to be minimised is a compromise between a quadratic function of the errors between $\boldsymbol{y}(\boldsymbol{t}+\boldsymbol{k} \mid \boldsymbol{t})$ and $\boldsymbol{\omega}(\boldsymbol{t}+\boldsymbol{k} \mid \boldsymbol{t})$ a control effort cost. Furthermore, the minimisation of such a function may be subject to constraints on the state and, more generally, on the control.
- The control signal $\boldsymbol{u}(\boldsymbol{t}+\boldsymbol{k} \mid \boldsymbol{t})$ is sent to the process while the other control signals are ignored. At time $\boldsymbol{t}+1$ the real output $\boldsymbol{y}(\boldsymbol{t}+\boldsymbol{k} \mid \boldsymbol{t})$ is acquired and the process starts again at the first [39-42].***figure3.1***

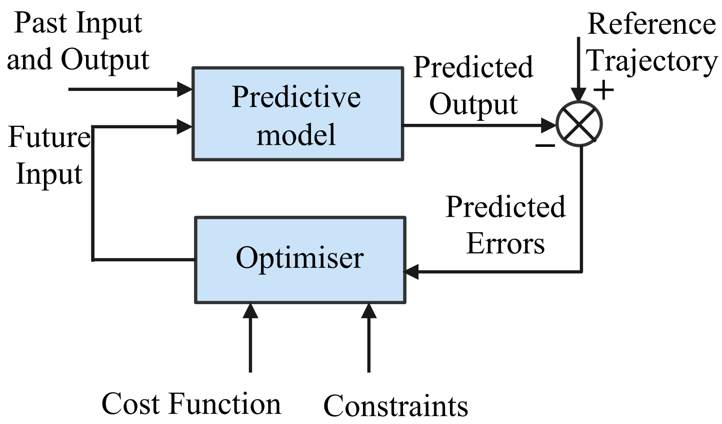

Figure 3.2. Block diagram of the basic structure of MPC algorithms.

Figure 3.3 illustrates this methodology and its implementation uses the basic structure shown in ***Figure 3.2***. The two fundamental loops to note in this figure are the model and the optimiser. The model must be able to capture the dynamics of the process, predict future outputs accurately and be easy to implement, with the optimiser providing the control actions. In the presence of constraints, the solution is obtained using iterative algorithms, which obviously take longer to compute [43].

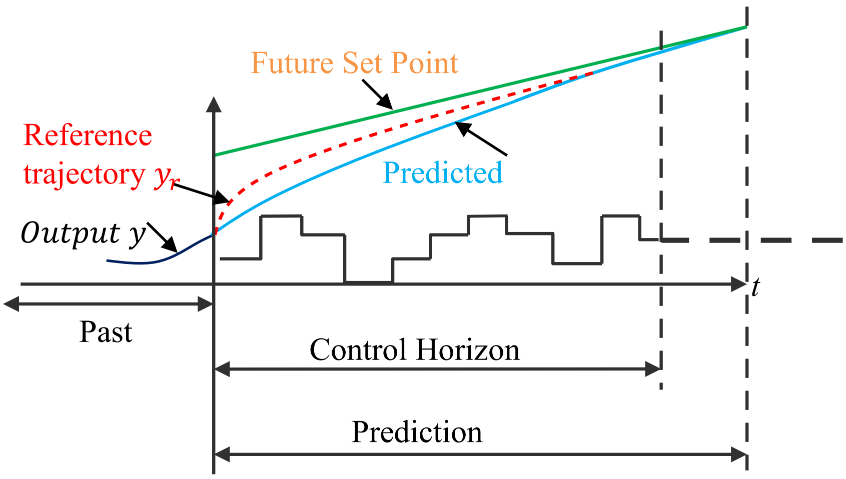

Figure 3.3. Principle of model predictive control.

3.4 Model formulation

The philosophy of Generalised Predictive Control is based on four main ideas which reproduce the basic decision-making mechanisms of human behaviour: creation of an anticipatory effect by exploiting the trajectory to be followed in the future, definition of a numerical prediction model, minimisation of a quadratic criterion with a finite horizon, and the principle of the receding horizon. We then consider the following points:

The process model can be represented in various ways (by transfer function, by state variables, impulse response, etc…), but the structure adopted here is the ***CARMA*** form:

$$A\left(z^{-1}\right)y\left(t\right)=z^{-d}B\left(z^{-1}\right)u\left(t-1\right)+e\left(t\right) \tag{3.1}$$

Where $u\left(t\right)$ and $y\left(t\right)$ are the control input and measured output variable respectively and $e\left(t\right)$ is a variable average signal. ***d*** is the number of samples contained in the delay.

A and ***B*** are polynomials in terms of the back-offset operator (z^{-1}) such that :

$$A\left(z^{-1}\right)=1+a_1z^{-1}+a_2z^{-2}+\ldots+a_{na}z^{-na} \tag{3.2}$$

$$B\left(z^{-1}\right)=b_0+b_1z^{-1}+b_2z^{-2}+\ldots+a_{nb}z^{-nb} \tag{3.3}$$

Where

n_a: Represents the degree of the polynomial ***A***.

n_b: Represents the degree of the polynomial ***B***.

The model described by ***equation 3.1*** represents the ***CARMA*** (**C**ontrol **A**uto **R**egressive on **M**oving **A**verage) model; several self-tuning theories are based on this model.

However, it seems to be unsuitable for some industrial applications in which the disturbances are non-stationary.

Practically two main types of disturbances are considered:

- Random step disturbance in random time which occurs in the case of a change in the material, or the quality of the material.
- Brown's disturbance, which occurs in the case of an energy imbalance.

For these two types of disturbance, the appropriate model is:

$$e\left(t\right)=C\left(z^{-1}\right)\frac{\xi\left(t\right)}{\Delta} \tag{3.4}$$

With

$$C\left(z^{-1}\right)=1+c_1z^{-1}+c_2z^{-2}+\ldots+a_{nc}z^{-nc} \tag{3.5}$$

$C\left(z^{-1}\right)$: is a stable polynomial of order n_c.

$\xi\left(t\right)$: is an uncorrelated random sequence representing white noise with mean zero.

$$\Delta=1-z^{-1} \tag{3.6}$$

Where Δ is a differentiation operator.

Combining equation (3.1) with (3.5) gives:

$$A\left(z^{-1}\right)y\left(t\right)=B\left(z^{-1}\right)z^{-d}u\left(t-1\right)+C(z^{-1})\frac{\xi\left(t\right)}{\Delta} \tag{3.7}$$

This represents the ***CARMA*** model. The use of this model (with the introduction of an integrator in the control system) provides two essential advantages:

- Improved quality of identification of the process model parameters to be controlled.
- The effect of eliminating the influence of unwanted disturbance oscillations (free offset).

3.5 Predictor development

For simplicity during development $c(z^{-1})$ is chosen to be equal to 1 ,we obtain the model [19]:

$$\left[A\left(z^{-1}\right)y\left(t\right)=B\left(z^{-1}\right)z^{-d}u\left(t-1\right)+\frac{e\left(t\right)}{\Delta}\right].\Delta E\left(z^{-1}\right)z^{j} \tag{3.8}$$

To derive the j-step-ahead predictor, consider the identity

$$1=E_j\left(z^{-1}\right)\tilde{A}\left(z^{-1}\right)+z^{-j}F(z^{-1}) \tag{3.9}$$

With

$$\tilde{A}\left(z^{-1}\right)=\Delta A(z^{-1}) \tag{3.10}$$

$E_j\left(z^{-1}\right)$: is a polynomial of order *(j -1)*

$F\left(z^{-1}\right)$: is a polynomial of order $\boldsymbol{n_a}$

Multiplying equation (3.8) by the term $\Delta E(z^{-1})z^{j}$ gives :

$$\tilde{A}\left(z^{-1}\right)E_j\left(z^{-1}\right)y\left(t+j\right)=E_j(z^{-1})B(z^{-1})\Delta u\left(t+j-d-1\right)+E_j(z^{-1})e\left(t+j\right) \tag{3.11}$$

Using the Diophantine identity (3.9) we obtain:

$$\left(1-z^{-1}F_j(z^{-1})\right)y\left(t+j\right)=E_j(z^{-1})e\left(t+j\right)B(z^{-1})\ \Delta u\left(t+j-d-1\right)+E_j(z^{-1})e\left(t+j\right) \tag{3.12}$$

This gives the output equation $y\left(t+1\right)$

$$y\left(t+j\right)=F_j(z^{-1})y\left(t\right)+E_j(z^{-1})B(z^{-1})\Delta u\left(t+j-d-1\right)+E_j(z^{-1})e\left(t+j\right) \tag{3.13}$$

As $E_j(z^{-1})$ is of degree ***(j-1)***, the product $E_j(z^{-1})e\left(t\right)$ is zero, which proves the robustness of the algorithm whose noise components are all zero in the future, which makes this type of editor optimal and robust, hence the predictive model is as follows [44]:

$$\tilde{y}(t+j\,|\,t)=G_j(z^{-1})\Delta u(t+j-d-1)+f_j(t+j) \tag{3.14}$$

With:

$$\Delta u(t+j-d-1)=u(t+j-d-1)-u(t+j-d-2) \quad \text{for} \quad 1\le j\le N_u \tag{3.15}$$

$$G_j(z^{-1})=E_j(z^{-1})B(z^{-1}) \tag{3.16}$$

$$f_j(t+j)=F_j(z^{-1})y(t) \quad \text{for} \quad j=1..N_2 \tag{3.17}$$

$$F_j(z^{-1})=f_{j,0}+f_{j,1}z^{-1}+..+f_{j,na}z^{-na} \tag{3.18}$$

$$E_j(z^{-1})=e_{j,0}+e_{j,1}z^{-1}+..+e_{j,(j-1)}z^{-(j-1)} \tag{3.19}$$

Long-horizon prediction is therefore achieved by recursive calculation of the polynomial $G_j(z^{-1})$ and the function $f_j(t+j)$.

To calculate $G_{j+1}(z^{-1})=E_j(z^{-1})_{j+1}B(z^{-1})$ and $f_{j+1}(t+j)=F_{j+1}(z^{-1})y(t)$

we proceed from the recursion of the Diophantine equation used previously.

3.6. Solving Diophantine equations

Equations $E_{j+1}(z^{-1})$ and $F_{j+1}(t+1)$ can be obtained from equation $E_j(z^{-1})$ and $F_j(z^{-1})$ and so on [41].

$$(1=E_{j+1}(z^{-1})\tilde{A}(z^{-1})+z^{-j-1}F_{j+1}(z^{-1}) \tag{3.20}$$

Subtracting (3.9) from (3.20) gives:

$$\left(E_{j+1}(z^{-1})-E_j(z^{-1})\right)\ \tilde{A}(z^{-1})+z^{-j}\left(z^{-1}F_{j+1}(z^{-1})-F_j(z^{-1})\right)=0 \tag{3.21}$$

Given that the polynomials $A(z^{-1})$ and z^{-1} are prime, we can write

$$E_{j+1}(z^{-1})-E_j(z^{-1})=r_j z^{-1} \tag{3.22}$$

Replacing in expression (3.21) gives:

$$z^{-j}\left(z^{-1}F_{j+1}(z^{-1})-F_j(z^{-1})+r_j\tilde{A}(z^{-1})\right)=0 \tag{3.23}$$

$$F_{j+1}(z^{-1})=z\left(F_j(z^{-1})-r_j\tilde{A}(z^{-1})\right) \tag{3.24}$$

Where; $$F_{j+1}\left(z^{-1}\right)=f_{j+1,0}+f_{j+1,1}z^{-1}+..+f_{j+1,na}z^{-na} \tag{3.25}$$

$$\tilde{A}\left(z^{-1}\right)=\alpha_0+\alpha_1 z^{-1}+\alpha_2 z^{-2}+..+\alpha_{na+1}z^{-(na+1)} \tag{3.26}$$

With $$\alpha_0=1$$

$$\alpha_i=\alpha_i-\alpha_{i-1}$$

$$\alpha_{na+1}=-a_{na} \qquad \text{with } i=0,1,..,n_a$$

After identification in (3.23), we obtain the following recurrent relations:

$$r_j z^{-1}=f_{j,0} \tag{3.27}$$

$$f_{j+1,i}=f_{j+1,i}-\alpha_{i+1}r_j \tag{3.28}$$

with $i=0,1,..,n_a$.

$$f_{j+1,na}=-\alpha_{na+1}r_j$$

These relations determine the polynomial $F_{j+1}\left(z^{-1}\right)$ and from (3.22) we get

$$E_{j+1}\left(z^{-1}\right)=E_j\left(z^{-1}\right)+r_j z^{-1} \tag{3.29}$$

The calculation iterations are initialized assuming that for j=1 , $E_1=1$. We consider a number of predictions for which j varies from a minimum value to a maximum value, which introduces the notion of the receding prediction horizon which will be limited by N_2 as indicated above and which represents the maximum limit of the prediction horizon or $N_u \le j \le N_2$, and N_u must be greater than or equal to the process delay time, to ensure that the output is affected by the first control sequence $u(t)$, with the assumption that the controls are performed in an open loop where the noise components are ignored when calculating the predictions $\tilde{y}(t+1)$. For simplicity, we take $N_1=1$ and $N_2=N$

Equation (3.14) gives:

$$\begin{cases} \tilde{Y}(t+d+1|t) = G_{d+1}\Delta u(t) + F_{d+1}y(t) \\ \tilde{y}(t+d+1|t) = G_{d+2}\Delta u(t+1) + F_{d+2}y(t) \\ . \\ . \\ . \\ \tilde{y}(t+d+1|t) = G_{d+N}\Delta u(t+N-1) + F_{d+N}y(t) \end{cases} \tag{3.30}$$

The resulting predictive model is expressed in vector form as follows

$$\tilde{Y} = G\Delta u + f \tag{3.31}$$

With

$$\tilde{Y} = [\tilde{y}(t+1)\,\tilde{y}(t+2)..\ \tilde{y}(t+N_2)]^T$$

$$\Delta u = [\Delta u(t)\ \Delta u(t+1)..\ \Delta u(t+N_2-1)]^T$$

$$F = [f(t+1)\,f(t+2)..\ f(t+N_2)]^T$$

The matrix G is lower triangular NxN

$$G = \begin{bmatrix} g_0 & 0 & . & . & . & . & 0 \\ . & g_0 & . & . & . & . & 0 \\ . & . & . & . & . & . & . \\ . & . & . & . & . & . & . \\ g_{N-1} & g_{N-2} & . & . & . & . & g_0 \end{bmatrix}$$

$$G_{ij} = g_j \quad \text{for} \quad j = 0,1,.. \le i$$

$$G_{ij} = 0 \quad \text{for} \quad j > i$$

3.7. Optimisation criteria

Once the predictions have been made, we need to find the future control sequence to be applied to the system to achieve the desired setpoint by following the reference trajectory. To do this, we minimise a cost function that differs from method to method, but generally contains the squared errors between the reference trajectory and the predictions over the prediction horizon, as well as the variation in control [45].

This cost function is as follows:

$$J(N_1, N_2, N_u) = \sum_{j=N_1}^{N_2}[\tilde{y}(t+j\,|\,t) - w(t+j)]^2 + \sum_{j=1}^{N_u}\lambda(j)[\Delta u(t+j-1)]^2 \tag{3.32}$$

With

$\Delta u(t+j) = 0$ for $j \geq N_u$

$\tilde{y}(t+j\,|\,t)$: Predicted output at $(t+j)$.

$w(t+j)$: Reference setpoint or trajectory at time $(t+j)$.

$\Delta u(t+j+1)$: Control increment at time $(t+j-1)$.

$\lambda(j)$: Control signal weighting coefficient.

N_1 : Minimum prediction horizon.

N_2 : Maximum prediction horizon.

N_u : Control prediction horizon.

The analytical minimisation of this function provides the sequence of future commands, only the first of which will actually be applied to the system. The procedure is iterated again at the next sampling period using the sliding horizon principle.

The expression of the criterion calls for several remarks:

- If we actually have the setpoint values in the future, we use all this information between horizons N_1 and N_2 to make the predicted output converge towards this setpoint.
- The incremental aspect of the system can be found by considering Δu in the criterion
- The coefficient λ is used to give more or less weight to the control in relation to the output, in order to ensure convergence when the initial system presents a risk of instability [42].

The criterion previously introduced in analytical form (3.32) can also be written in matrix form as:

$$J = (Gu + f - w)^T\ (Gu + f - w) + \lambda u^T u \tag{3.33}$$

With

$$W = [w(t+1)\ \ w(t+2)\ldots\ w(t+N)]^T$$

The optimal solution is then obtained by deriving (3.33) with respect to the vector of control increments:

$$J = \lfloor\ \tilde{u}^T G^T + (f - w)^T \rfloor \lfloor\ (G\tilde{u} + (f - w)\rfloor + \lambda\tilde{u}^T\tilde{u} \tag{3.34}$$

$$J = \tilde{u}^T \left[G^T G + \lambda I \right] \tilde{u} + \tilde{u}^T G^T \left(f - w \right) + \left(f - w \right)^T G\tilde{u} + \left(f - w \right)^T \left(f - w \right) \tag{3.35}$$

$$\frac{\partial J}{\partial \tilde{u}} = 2[G^T G + \lambda I\ )\ \tilde{u} + 2G^T \left(f - w \right) \tag{3.36}$$

Let this be the optimal solution:

$$\Delta u_{opt} = (G^T G + \lambda I)^{-1} G^T \left(f - w \right) \tag{3.37}$$

Thus only G and f are needed to determine the vector of optimal control increments to be applied, including $\Delta u_{opt}(t)$ which represents the first element of the vector which will be confirmed to be applied to the input of the controlled process;

$$\Delta u_{opt}\left(t \right) = K_1 \left(w - f \right) \tag{3.38}$$

Where K_1 represents the first row of the dynamic control matrix K

$$K_1 = (G^T G + \lambda I)^{-1} G^T \tag{3.39}$$

The predicted future control sequence will be:

$$\tilde{U}\left(t \right) = u\left(t - 1 \right) + K_1 \left(w - f \right) \tag{3.40}$$

3.8. Control parameters for the GPC

- Minimum output horizon

If the dead time d of the process is known exactly, N_1 takes this value. But when d is unknown or variable, N_1 takes the value 1.

- Maximum output horizon

A higher value of N_2 is suggested corresponding to the rise time of the process

- The control horizon

This is an important design and tuning parameter, a variable of N_u =1 gives generally acceptable control for simple and stable open loop processes.

Increasing N_u makes the control and corresponding output more active until a step is reached where any further increase in N_u has no influence [46].

For an unstable system, good control is achieved when N_u is at least equal to the number of unstable poles. For high performance, a higher value of N_u is desirable.

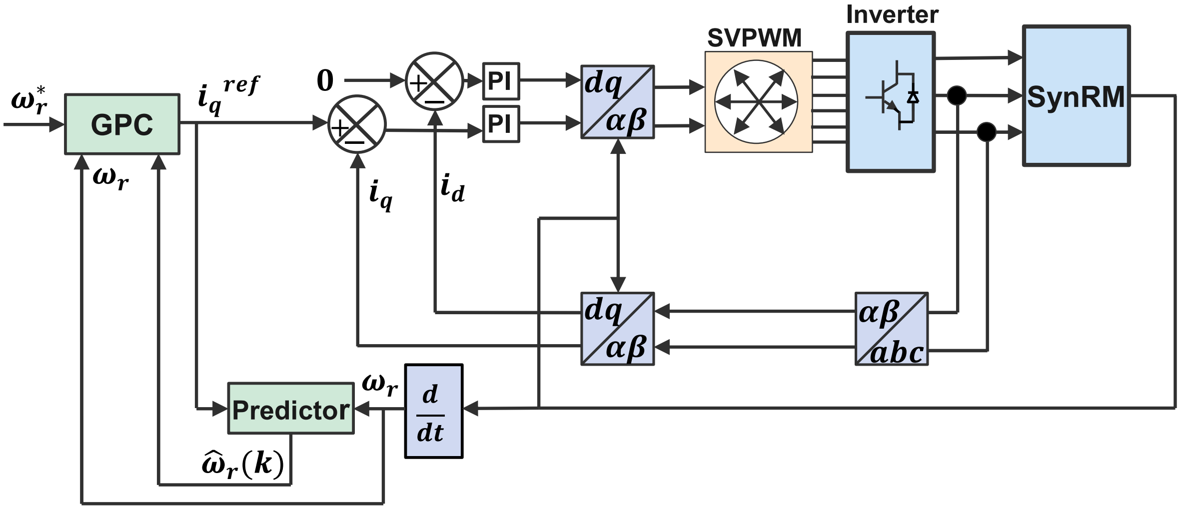

Figure 3.4. Block diagram of SynRM control via GPC.

The use of N_u < N_2 is more significant, making it possible to reduce the size of the matrix ($G^T G + \lambda I$) which will be of size N_u x N_u instead of N_y x N_y which leads to minimising the power required for the prediction and order computation procedure.

- Weighting factor

Dumur's findings show that it makes sense to choose this factor in the vicinity of $\lambda_{opt} = tr\left(G^T G\right)$.

G being the matrix formed by the coefficients of the index response.

3.9. Simulation results

Figure 3.4 shows the block diagram for speed control of the ***SynRM*** by a ***GPC*** type controller, and the currents by ***PI*** type controllers.

To illustrate the performance of the Predictive Control applied to adjusting the speed of the SynRM, a no-load start-up was simulated with the ***2 N.m*** load applied at ***t=0.4s***, then the machine was subjected to a change of speed setpoint from ***100 rad/s*** to ***-100 rad/s***. We tested the robustness and the influence of the weighting factor on the ***SynRM*** quantities.

The simulation results obtained with the following setting parameters:

$N_1 = 1$; $N_2 = 10$; $N_u = 3$; $\lambda = 0.8$; $T_s = 30\mu s$

T_s is the sampling period

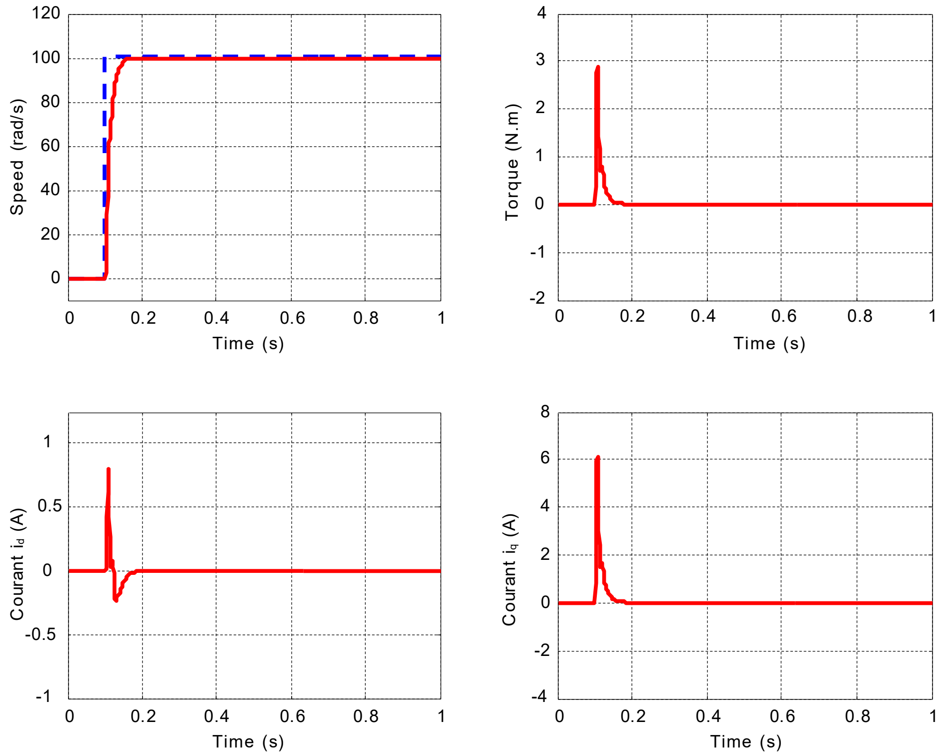

Figure 3.5. Simulation results for a no-load start-up with a speed setpoint of 100 rad/s

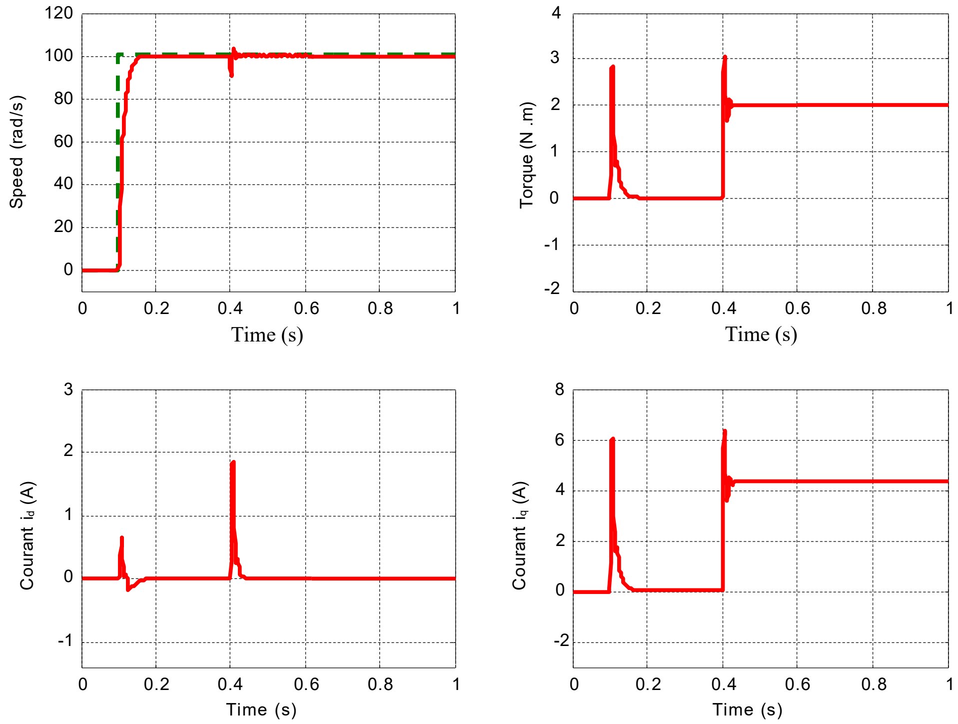

Figure 3.6. Simulation results for a start-up under load at t=0.4s for a speed of 100 rad/s

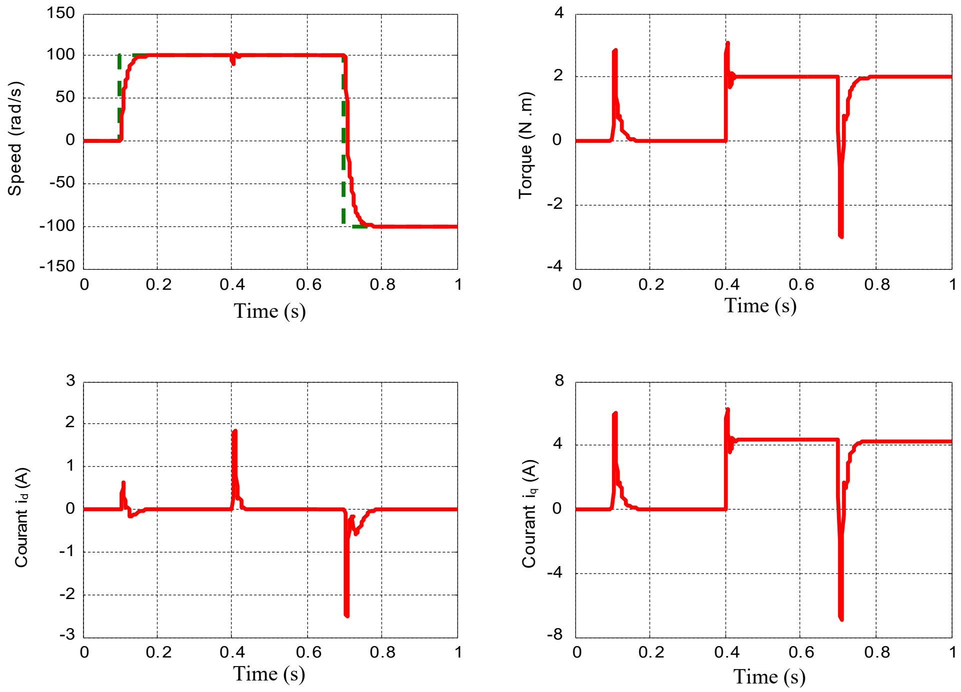

Figure 3.7. Simulation results for a

load start at t=0.4s for a speed of 100rd/s with setpoint inversion (-100rd/s)

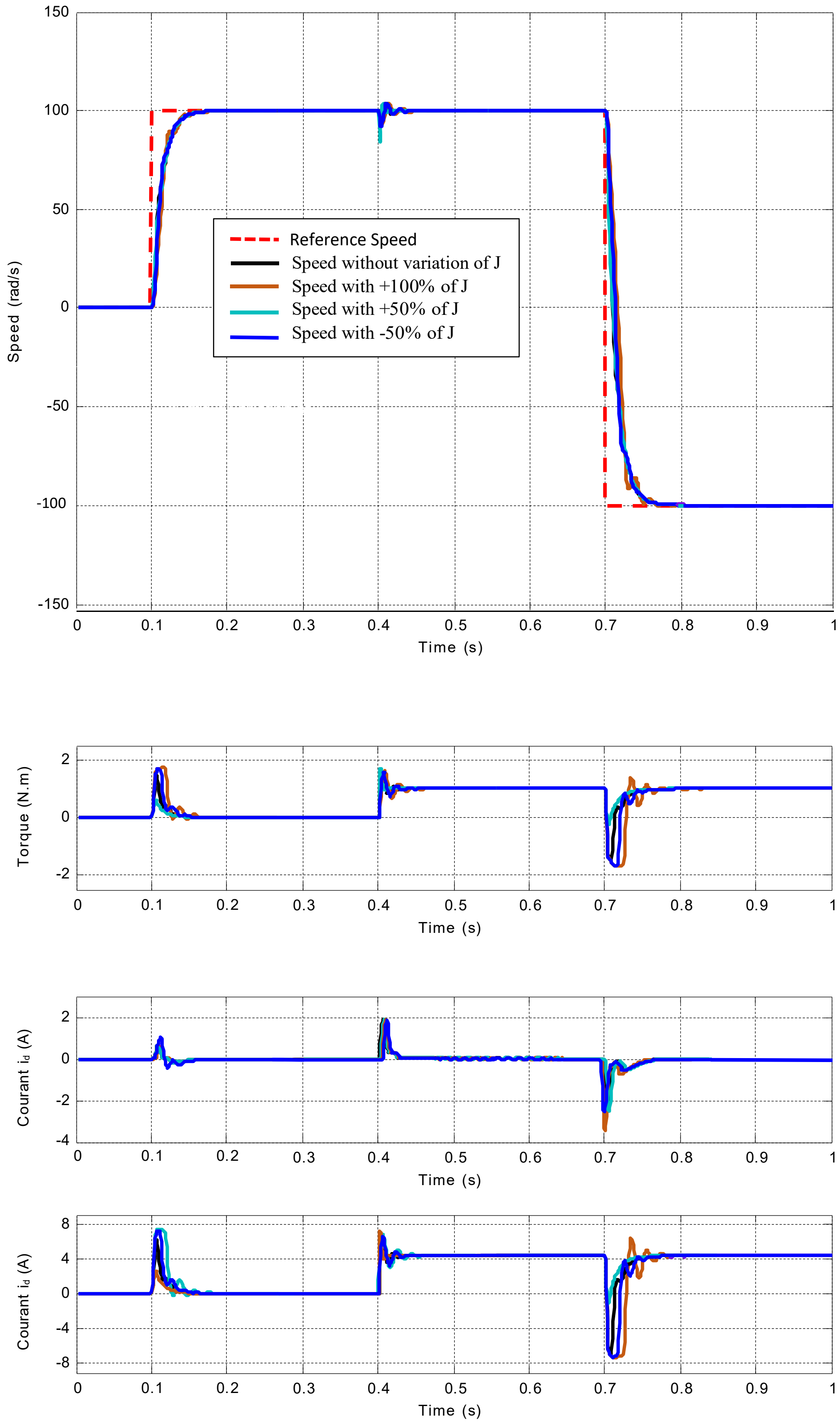

Figure 3.8. Simulation results for variations in inertia J

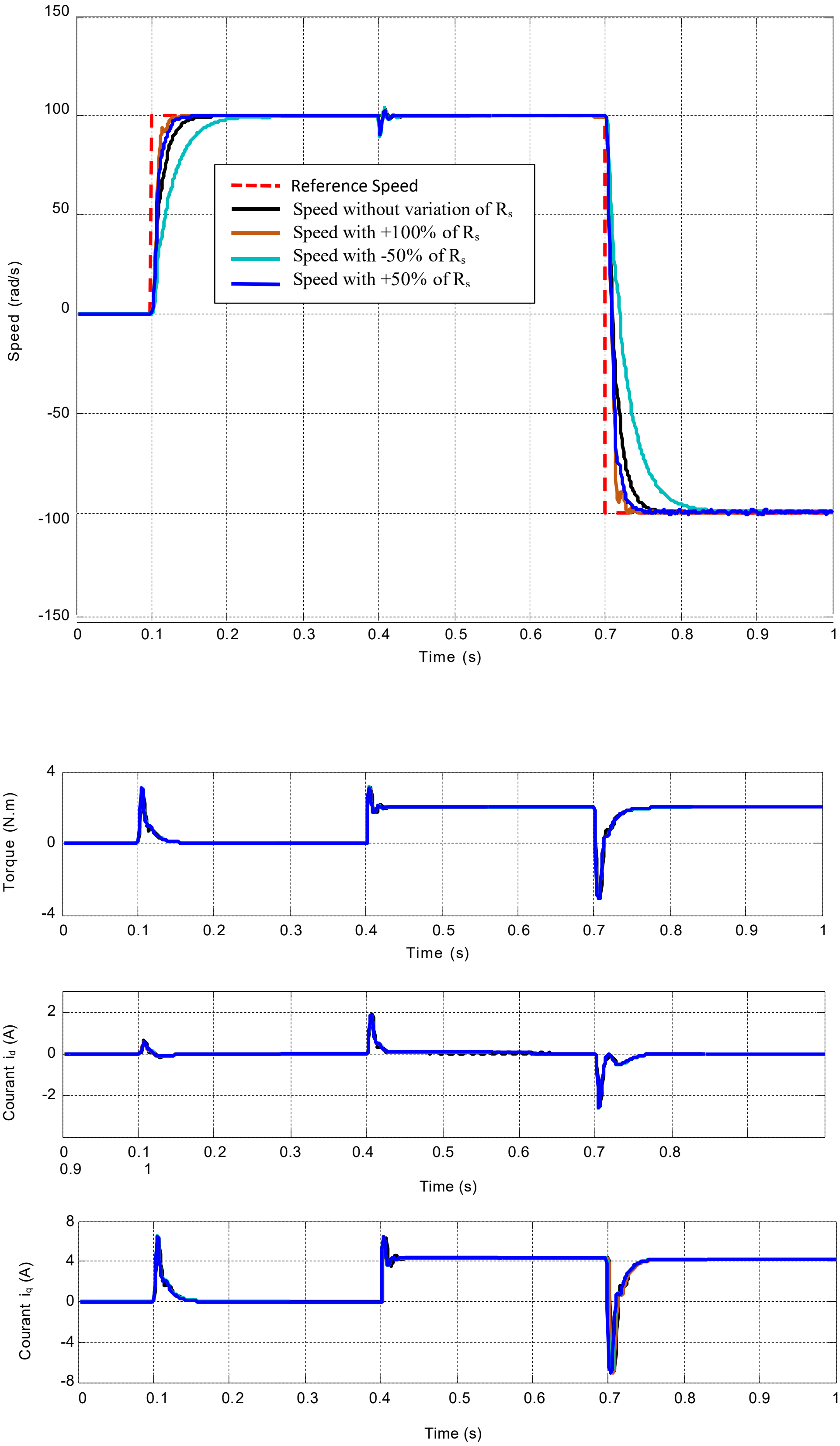

Figure 3.9. Simulation results for variations in R_s resistance

3.10. Simulation results and interpretation

Figure 3.5 shows the characteristics at no-load start-up of the ***SynRM*** for a reference speed of ***100 rad/s***. It can be seen that the speed profile follows its setpoint well without overshooting, with a very short response time. On start-up, the electromagnetic torque is equal to the maximum of the machine's capacity ***3 N.m***, after which it stabilises at virtually zero in steady state. It can also be seen that the stator current i_d is zero and the stator current i_q is the image of the electromagnetic torque, indicating the decoupling introduced by the ***SynRM*** vector control.

Figure 3.6 shows the application of the load torque $T_l = 2\ N.m$ at ***t=0.4s***, this load causes a slight loss of speed which is quickly restored, the electromagnetic torque compensates for the load torque.

Figure 3.7 shows the inversion of the speed set point from ***100 rad/s*** to ***-100 rad/s***, in response to this change the electromagnetic torque takes on the value (-3 N.m) then rises to the value of the resistive torque ***2 N.m*** and the speed still follows its reference.

Figure 3.8 shows the variation in inertia, and it can be seen that this variation does not affect the robustness of the control.

Figure 3.9 shows the influence of the variation in stator resistance. It can be seen that the speed dynamics is slightly delayed, but the disturbance rejection remains effective.

3.11. Conclusion

In this chapter we have studied predictive control, which is a combination of prediction of future process behaviour and feedback control, applied to ***SynRM***.

The simulation results obtained show that the PC performs very satisfactorily with both setpoint variation and disturbance variation. Various tests were carried out, and the simulation results show that the PC is robust to parametric variations.

From the results obtained, we can see that the PC provides remarkable performance, particularly with regard to the tracking of the position at its imposed set point and the rejection of the disturbance in relation to the PI regulator studied in the previous chapter. The PC is also robust to variations in electrical parameters. These parameters therefore have a decisive influence on the system's behaviour. But it is not always easy to find optimum values for these parameter.

Chapter 4: Sensorless Control of SynRM Using Model Reference Adaptive System with Predictive Control

Chapter 4: Sensorless Control of SynRM Using Model Reference Adaptive System with Predictive Control

4.1. Introduction

The utilization of position or speed sensors in synchronous reluctance machine drives, including tachometer-based speed sensors, optical incremental sensors, or electromechanical resolvers, presents numerous practical challenges. These encompass hardware complexity, difficulties in adapting to hostile environments, heightened costs, diminished reliability due to cable and sensor issues, challenges in mechanically attaching sensors to the electric machine, increased machine length, and susceptibility to electromagnetic noise interference. To address these issues, various sensorless control schemes have been devised for variable speed ***SynRM*** drives. Sensorless drives obviate the need for traditional speed or position monitoring devices, instead relying on monitored voltages, currents, and mathematical models to infer speed and/or position signals [47]. Among these schemes, Model Reference Adaptive System ***MRAS*** is favoured for its simplicity in operation. Also the Model Predictive Control ***MPC*** emerges as a promising alternative to ***PI*** controllers in speed loops, offering advantages such as order reduction, disturbance rejection, robustness, and straightforward implementation via power converters. MPC operates within a Variable Structure System (***VSS***), employing a switching logic with high-frequency discontinuous control actions based on system state, disturbances, and reference inputs.

This chapter presents the flexible sensor of an integrated ***MRAS-MPC*** as an advanced solution for sensorless control in two approaches. Using this framework, a simulation model for a sensorless ***FOC*** synchronous reluctance machine drive is developed and validated using detailed simulation results. Its performance is compared with that of the ***PI*** controller.

4.2. Model Reference Adaptive System

4.2.1. MRAS Overview

The model reference approach leverages two distinct machine models: a reference model and an adjustable model, both tasked with estimating the same state variable. By comparing the outputs of these models, the estimation error serves as a basis for adapting the speed. This difference between the estimated vectors drives a ***PI*** controller. The controller's output fine-tunes the adjustable model, subsequently affecting rotor speed. However, ***PI*** controllers can experience performance degradation due to continuous fluctuations in machine parameters, operating conditions, and nonlinearities introduced by the inverter [47].

4.2.2. MRAS Design

The adaptation algorithm in the Model Reference Adaptive System ***MRAS*** ensures system stability and strives to achieve convergence of the estimated speed to the desired value, while maintaining favourable dynamic performance. The ***MRAS*** observer's adaptive scheme can be designed using

Popov's criteria, which is associated with the hyperstability of a class of feedback systems. Generally, a model reference adaptive speed observer can be described as an equivalent nonlinear feedback system, comprising a time-invariant linear feedforward subsystem and a time-varying nonlinear feedback subsystem. In ***Figure 4.1***, the input to the linear time-invariant system, denoted as $\boldsymbol{u}$, consists of the stator voltage and currents, while the output $\boldsymbol{y}$ is the speed-tuning signal. The output of the nonlinear time-varying system is $\boldsymbol{\omega}$, with $\boldsymbol{u} = -\boldsymbol{\omega}$.

The algorithm for rotor speed estimation, or adaptation mechanism, is selected based on ***Popov's theory of hyperstability***. This theory requires the transfer function of the linear time-invariant system to have a strictly real positive matrix, while the non-linear time-varying feedback system meets ***Popov's integral inequality***. ***Figure 4.1*** illustrates the standard non-linear time-varying feedback system, which is considered asymptotically stable if it meets two conditions:

- The error must converge asymptotically.
- The transfer function of the time-invariant linear feed-forward block must be strictly real positive.
- The non-linear time-varying block must satisfy Popov's integral inequality:

$$\boldsymbol{n} = \int_0^t \boldsymbol{y}^T \boldsymbol{\omega} dt \geq -\lambda^2 \tag{4.1}$$

Where λ^2 : Finite positive constant

$\boldsymbol{\omega}$: Output vector of the feedback block

$\boldsymbol{y}$: Input vector

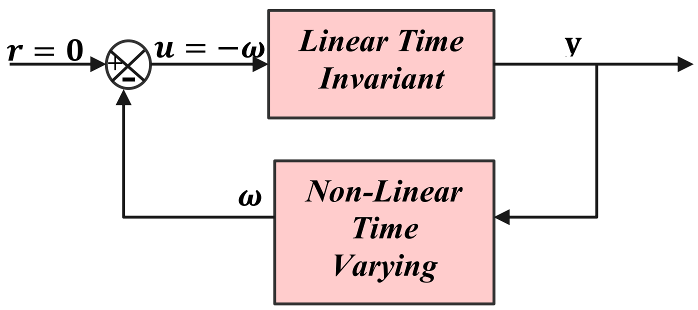

Figure 4.1. Standard Non-Linear Time varying feedback system

4.2.3. MRAS Based Speed Estimation

The stator current-based MRAS is used for SynRM speed estimation. The ***SynRM*** itself is used as the reference model and the q-axis and d-axis equations of the stator current model are used as the adjustable model. An essential concern in ***MRAS*** is the conception of adaptive laws. The Lyapunov stability and the Popov hyper stability theory have been used as the default design methods to obtain a secure stable adaptive system.The ***SynRM*** dynamic model can be further adjusted from the model state ***equation 1.18*** and the adjustable ***SynRM*** model can be written:

$$\frac{d}{dt}\begin{bmatrix} \hat{i}_{ds} \\ \hat{i}_{qs} \end{bmatrix} = \begin{bmatrix} -\frac{R}{L_d} & \hat{\omega}_r \\ -\hat{\omega}_r & -\frac{R}{L_q} \end{bmatrix}\begin{bmatrix} \hat{i}_{ds} \\ \hat{i}_{qs} \end{bmatrix} + \begin{bmatrix} \frac{1}{L_d} & 0 \\ 0 & \frac{1}{L_q} \end{bmatrix}\begin{bmatrix} v_{ds} \\ v_{qs} \end{bmatrix} \tag{4.2}$$

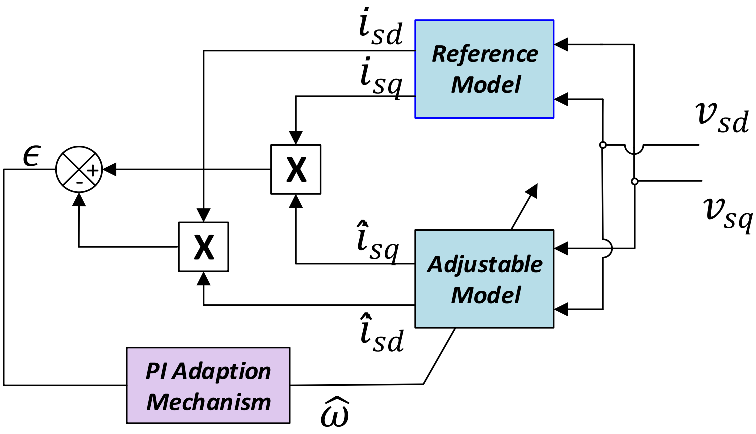

Figure 4.2. Structure of MRAS Based Speed Observer

The following state error equations are obtained by subtracting (1.18) which applies to the adjustable model from the reference model equations:

$$\frac{d}{dt}\begin{bmatrix} e_d \\ e_q \end{bmatrix} = \begin{bmatrix} -\frac{Rs}{L_{ds}} & \omega_r \\ -\omega_r & -\frac{R_s}{L_{qs}} \end{bmatrix}\begin{bmatrix} e_d \\ e_q \end{bmatrix} - J\left(\omega_r - \hat{\omega}_r\right)\begin{bmatrix} \hat{i}_{ds} \\ \hat{i}_{qs} \end{bmatrix} \tag{4.3}$$

Where : $e_d = i_{ds} - \hat{i}_{ds}$, $e_q = i_{qs} - \hat{i}_{qs}$, $J = \begin{bmatrix} 0 & -1 \\ 1 & 0 \end{bmatrix}$

Equation (4.3) can be represented as;

$$\left[\dot{e}\right] = \left[A\right]\left[e\right] - \left[\omega\right] \tag{4.4}$$

Where ; $\left[\omega\right] = \left(\omega - \hat{\omega}\right)\begin{bmatrix} -\hat{i}_{qs} \\ \hat{i}_{ds} \end{bmatrix}$ is the feedback block.

On the forward block, ***figure 4.3*-a**, the term $\left[\omega\right]$ is the input and $\left[e_\omega\right]$ is the output.

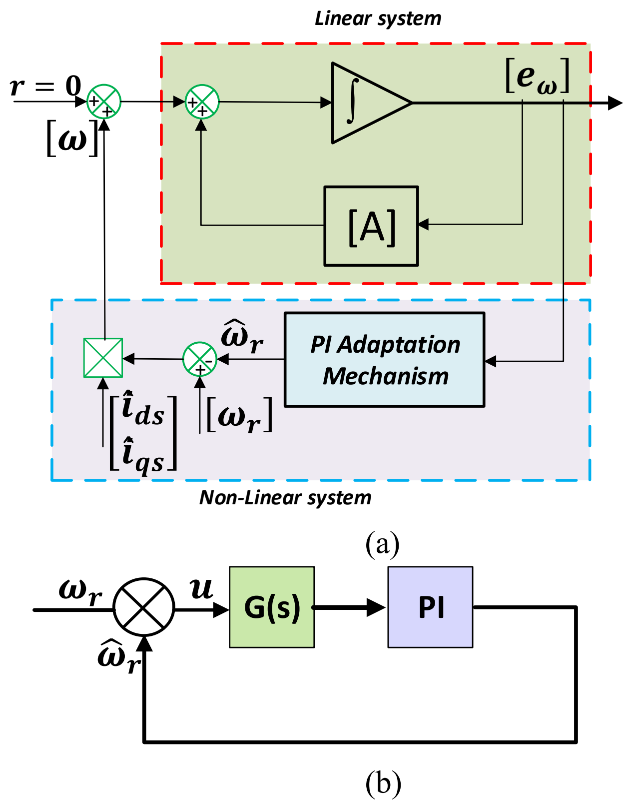

Figure 4.3. MRAS simplified structure diagram

With the simplified boundary condition $\left[e(\infty)\right]T = 0$ for any initialisation [48],[49], the asymptotic behaviour of the adaptation mechanism is realised. Therefore, the system is hyperstable when the transfer matrix of the direct path is written as follows:

$$G(S) = (SI - A)^{-1} \tag{4.5}$$

can be verified which is strictly positive real.In the nonlinear feedback block, the input and output satisfy the Popov criterion [49]:

$$\int_0^{t_1} [e]^T [\omega] \mathrm{d}t \geq -\gamma^2 \tag{4.6}$$

With

$$[e]^T [\omega] \mathrm{d}t = \left(e_d \hat{i}_{qs} - e_q \hat{i}_{ds}\right)(\omega_r - \hat{\omega}_r) \tag{4.7}$$

Where γ is positive real constant.

Shauder [49] suggests that the Popov criterion is respected by the adaptation law. It is expressed by the equation:

$$\hat{\omega}_r = \left[\partial_2(e) + \int_0^t \partial_1(e) \mathrm{d}t \right] \tag{4.8}$$

Substituting [e] and [ω] values, equation 4.7 becomes:

$$\int \left\{ \left[e_d \hat{i}_{qs} - e_q \hat{i}_{ds} \right] \left[\left(\omega_r - \partial_2(e) \right) - \int_0^t \partial_1(e) \mathrm{d}t \right] \right\} \mathrm{d}t \geq -\gamma^2 \tag{4.9}$$

This inequality can be solved using the following well-known relation:

$$\int_0^{t_1} k(\dot{f}(t) f(t) dt \geq -\frac{1}{2} k f(0)^2, k > 0 \tag{4.10}$$

With this expression, Popov's inequality can be demonstrated by the functions below:

$$\partial_1 = k_i \left(e_q \hat{i}_{ds} - e_d \hat{i}_{qs} \right) = k_i \left(i_{qs} \hat{i}_{ds} - i_{ds} \hat{i}_{qs} \right) \tag{4.11}$$

$$\partial_2 = k_p \left(e_q \hat{i}_{ds} - e_d \hat{i}_{qs} \right) = k_p \left(i_{qs} \hat{i}_{ds} - i_{ds} \hat{i}_{qs} \right) \tag{4.12}$$

With

$$\varepsilon = i_{qs} \hat{i}_{ds} - i_{ds} \hat{i}_{qs} \tag{4.13}$$

The estimated rotor speed is used to generate an adaptation design for the ***MRAS*** speed observers. We can obtain the adaptive law of the observer by reorganized the ***MRAS*** structure diagram in ***Figure 4.3***.The state expression is represented as follow :

$$\begin{cases} \dot{e} = Ae + Bu \\ y = B^T e \end{cases} \tag{4.14}$$

From ***Figure 4.3.a***, it can be seen that the adaptation mechanism is related to the state error , the transfer function of forward channel can be deduced according to the state space expression ***equation 4.5*** , $\frac{y(s)}{u(s)}$ as $G(s)$,

$$G(s) = \frac{\left(s + \frac{R_s}{L} \right) \left(i^2_{ds} + i^2_{qs} \right)}{s^2 + 2\frac{R_s}{L} s + \left(\frac{R_s}{L} \right)^2 + \hat{\omega}^2} \tag{4.15}$$

So, its simplified structure diagram can be represented as two blocks of ***G(s)*** and ***PI*** in series where $\hat{\omega}_r$ is the output and ω_r is the input as in ***Figure 4.3-b*** and because the value of $\left(i^2_{ds} + i^2_{qs} \right) = 1$ for maximum torque per Ampere control strategy. This can get the transfer function of system, $G_c(s)$:

$$G_c(s) = \frac{k \left(s + \frac{R_s}{L} \right) (s + z)}{s^3 + 2\frac{R_s}{L} s^2 + \left(\left(\frac{R_s}{L} \right)^2 + \omega_r^2 \right) s} \tag{4.16}$$

Where $k = K_p$ and $z = \frac{k_i}{k_p}$

This can therefore be employed to tune the ***PI*** controller parameters with the method of root locus analysis as simplified as the structure diagram in ***Figure 4.4***, making the system reach the intended result. The design of K_p and k_i is introduced to achieve ***MRAS*** stability, tracking errors, and more robust operation Adaptive ***PI*** controller design criteria is achieved with the use of the root locus method by taking the transfer function of the plant and setting the time domain constraint ***Figure 4.4***

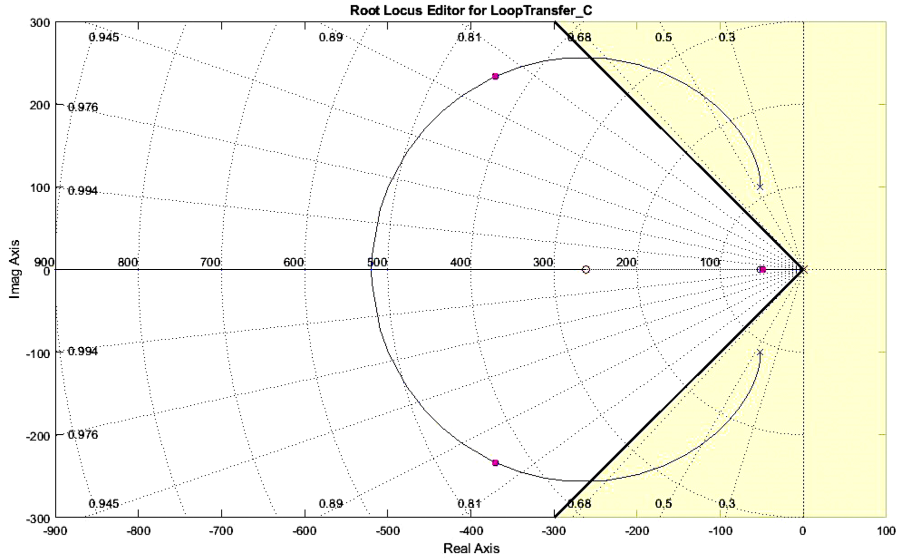

Figure 4.4. Root locus of closed loop adaptive control system

The constraint taken into account in this design is the percentage overshoot, the settling time and the rise time which are respectively less than ***2.09%***, ***0.0582*** seconds and ***0.00503*** seconds. Therefore, ***z*** is taken of ***165*** and from the root locus diagram of $G_c(s)$ in ***Figure 4.4*** and ***Figure 4.5*** the maximum possible gain of ***k*** should be obtained from the specifications of settling time, maximum overshoot and rise times of the specification. In this case K_i= **47258** then the value of K_p should become **286.41**.

As shown in ***Figure 4.5***, the stator current-based ***MRAS*** speed observer's closed-loop transfer function has all its poles in the left half of the s-plane and therefore, the system has been stable in the operating point.

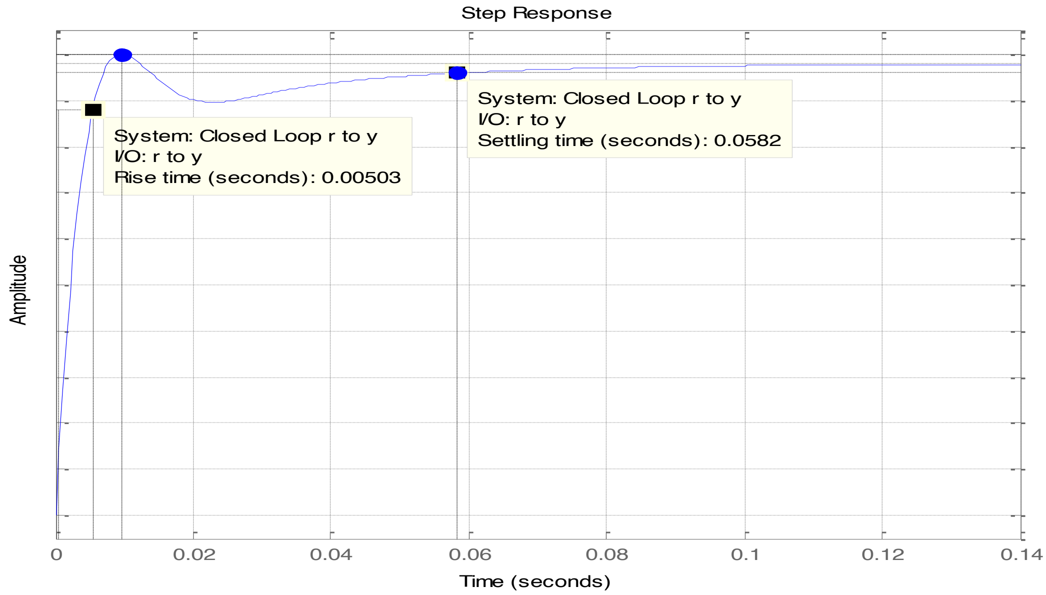

Figure 4.5. Root locus of closed loop Step Response

Figure 4.6 shows the SynRM block diagram based on the ***FOC*** (Field Oriented Control) scheme employed in this work

The principal idea by which the ***FOC*** is implemented is the employment of a suitable coordinate system that permits decoupled control of the electrical torque $\boldsymbol{T_e}$ and the rotor flux magnitude $|\phi_r|$.

This is realized through aligning the coordinate system to the rotor flux [50],[51].

The machine model is first transformed into ***d-q*** components through the ***α-β*** to ***d-q*** transformation. This transformation requires the rotor speed angle which is estimated as shown in the block of ***MRAS*** speed observer [51].

In addition, the ***MRAS*** scheme operates as a feedback sensor similar to the shaft position/speed sensor. It can calculate the angular speed of the rotor and generate the angular position of the rotor integrating the angular speed [52]. The estimated machine speed is differentiating with the desired speed. Then it is sent to ***PI*** controller. Its purpose is to generate torque reference based on the speed differences, where $\boldsymbol{i_{qs}(ref)}$ is the reference current derived from the torque control loop and $\boldsymbol{i_{ds}(ref)}$ is derived from the rotor flux control loop. The components $\boldsymbol{i_{sd}}$ and $\boldsymbol{i_{sq}}$ are in comparison with the references $\boldsymbol{i_{ds}(ref)}$ and $\boldsymbol{i_{qs}(ref)}$. The current controller outputs are $\boldsymbol{v_{ds}(ref)}$ and $\boldsymbol{v_{qs}(ref)}$, furthermore applied to an inverse Park transformation and used to produce $\boldsymbol{v_{\alpha s}(ref)}$ and $\boldsymbol{v_{\beta s}(ref)}$ based on the position of the rotor speed, which are stator vector voltage components in the stationary orthogonal reference frame. They represent the inputs to the space vector ***PWM***.

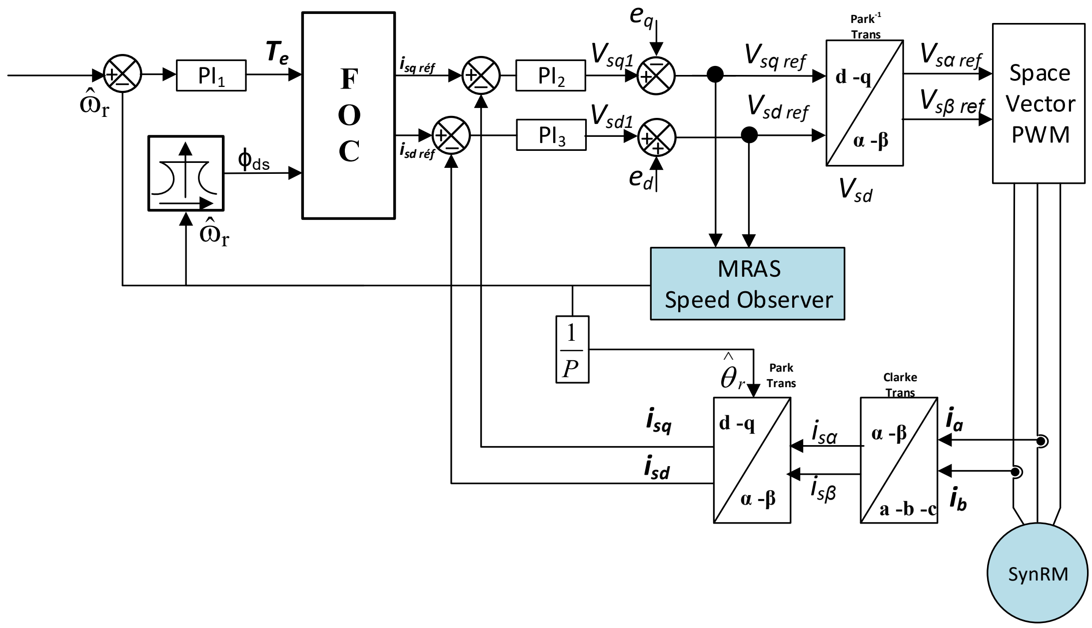

Figure 4.6. Sensorless vector control of SynRM based MRAS Speed Observer

This block's outputs are the signals that control the three-phase inverter's power circuit, which turns electrical energy from direct current (***DC***) into alternating current (***AC***) [53], [54]. In this case, the voltage that keeps the current error to a minimum is set to ***110 volts*** and the appropriate switching status signals are produced at ***t=0.1ms***.

The ***PWM*** signals which is finally fed into a controlled inverter to provide required three phase voltage to power the machine under different operating conditions.

The use of Clarke transformation is to convert the 3-Phase stator currents measured into a two phase. This projection's outputs are denoted by $i_{\alpha s}$ and $i_{\beta s}$, when the Park's transformation rotates $\alpha - \beta$ axis to $d - q$ currents (i_{ds} and i_{qs}) with the reference frequency.

4.3. Predictive Speed Control

One of the main advantages of the ***MPC*** is the ability to control several different variables using a single cost function. This makes it possible to implement predictive speed control while maintaining stator currents at given conditions. It is desirable to consider limiting the amplitude of the currents and optimising the torque in relation to the amperes.

This application of ***MPC*** introduces some difficulties, such as the non-linear model of the system, the large differences between the dynamics of the speed (mechanical dynamics) and the dynamics of the stator currents (electrical dynamics), and the quantification noise in the speed measurement [55].

4.3.1. Machine model discretisation

The resolution of the optimisation problem is a control vector with the first input of the optimal sequence being sent to the system. The problem is once again solved over the next time interval using the updated system data.

For a sampling time T_s and using the Euler approximation [56] of the stator current derivatives, the predictive machine of ***model 1.24*** will be discretised, this means that:

$$\frac{\mathrm{d}\boldsymbol{i}}{\mathrm{d}\boldsymbol{t}} \approx \frac{\boldsymbol{i}(\boldsymbol{k}+1)-\boldsymbol{i}(\boldsymbol{k})}{\boldsymbol{T}_s} \tag{4.17}$$

where T_s corresponds to the sampling period, and $i_{(k+1)}$ and $i_{(k)}$ are the ***(k+1)*** th and ***(k)***th measured stator currents, respectively.

To predict the current at sampling time ***k+1*** with the measured position, speed and currents at sampling time ***k***, a discrete model of the machine is needed. ***Equation 4.18*** is a rearranging of ***Equation 2.4***, where the derivative of the current has been isolated on the left side of the equal sign.

$$\begin{cases} \dfrac{di_d(t)}{dt} = \dfrac{1}{L_d}u_d(t) - \dfrac{R}{L_d}i_d(t) + \dfrac{\omega(t)L_q}{L_d}i_q(t) \\ \dfrac{di_q(t)}{dt} = \dfrac{1}{L_q}u_q(t) - \dfrac{R}{L_q}i_q(t) - \dfrac{\omega(t)L_d}{L_q}i_d(t) \end{cases} \tag{4.18}$$

The derivative can also be expressed with Newton's difference quotient as shown in Equation 4.19 if the time steps are approaching zero. In this case the time step Δt will be the sampling time of the controller. If the sampling time is small, this will be a valid approximation for the derivative.

$$\frac{df(t)}{dt} = \lim_{\Delta t \to 0} \frac{f(t+\Delta t) - f(t)}{\Delta t} \tag{4.19}$$

A Taylor series like Equation 4.20 can also be applied instead of Equation 4.19. If only a first order Taylor series is used; it gives the same result as with Equation 4.19

$$f(t+\Delta t) = f(t) + \Delta t\, f'(t) + \frac{1}{2!}\Delta t^2 f''(t) + .. \tag{4.20}$$

Equation 4.18 or the first order Taylor expansion from Equation 4.19 is substituting the current derivative which gives Equation 4.21

$$\begin{cases} \dfrac{i_d(t+\Delta t)-i_d(t)}{\Delta t} = \dfrac{1}{L_d}u_d(t) - \dfrac{R}{L_d}i_d(t) + \dfrac{\omega(t)L_q}{L_d}i_q(t) \\ \dfrac{i_q(t+\Delta t)-i_q(t)}{\Delta t} = \dfrac{1}{L_q}u_q(t) - \dfrac{R}{L_q}i_q(t) - \dfrac{\omega(t)L_d}{L_q}i_d(t) \end{cases} \tag{4.21}$$

If Δt is equal to a fixed sampling period T_s which is small enough to neglect the changes of angular velocity $\omega(k)$, then the otherwise non-linear back-EMF terms, can be considered as constants [57]. This means that Equation 4.20 can be discretised as shown in Equation 4.22.

$$\begin{cases} i_d(k+1) = \dfrac{T_s}{L_d}u_d(k) + \left(1-\dfrac{RT_s}{L_d}\right)i_d(k) + \dfrac{\omega(k)L_qT_s}{L_d}i_q(k) \\ i_q(k+1) = \dfrac{T_s}{L_q}u_q(k) + (1-\dfrac{RT_s}{L_q})i_q(k) - \dfrac{\omega(k)L_dT_s}{L_q}i_d(k) \end{cases} \tag{4.22}$$

Here in Equation 4.22 the predicted $i_{dq}{}^{p}(k+1)$ current is presented in matrix form.

$$\begin{bmatrix} i_d(k+1) \\ i_q(k+1) \end{bmatrix} = \begin{bmatrix} 1-\dfrac{RT_s}{L_d} & \dfrac{\omega(k)L_qT_s}{L_d} \\ -\dfrac{\omega(k)L_dT_s}{L_q} & 1-\dfrac{RT_s}{L_q} \end{bmatrix} \begin{bmatrix} i_q(k) \\ i_d(k) \end{bmatrix} + \begin{bmatrix} \dfrac{T_s}{L_d} & 0 \\ 0 & \dfrac{T_s}{L_q} \end{bmatrix} \begin{bmatrix} u_d(k) \\ u_q(k) \end{bmatrix} \tag{4.23}$$

$$\begin{bmatrix} i_d(k+1) \\ i_q(k+1) \end{bmatrix} = A(k) \begin{bmatrix} i_q(k) \\ i_d(k) \end{bmatrix} + B(k) \begin{bmatrix} u_d(k) \\ u_q(k) \end{bmatrix} + C(k)$$

$$C(k) = 0\,,$$

$$i_{dq}{}^{p}(k+1) = A(k)i_{dq}{}^{p}(k) + Bu_{dq}{}^{p}(k) \tag{4.24}$$

Now a general discretisation of the machine model is obtained. This can be applied to a model predictive controller.

These equations are used to calculate the stator current predictions for the eight different switching states, denoted by ***V0*** **-** ***V7***, and their associated voltage vectors in the stationary reference frame ***αβ*** using a **DC** voltage V_{dc}, with the six inverter switches named ***Sa*** ... $\bar{S}c$ produced by the well-known three-phase inverter with two voltage sources which is connected to the SynRM. After that, the Park transformation is introduced to transform the stator voltages into the ***dq*** rotation frame as in [58].

4.3.2. Cost function and weighting factor selection

Model Predictive Control uses the system model in order to predict the future behaviour of the controlled variables. In order to obtain the desired actuation, the controller uses the model information in a cost function. The choosing of this cost function is the main effort once an accurate model is obtained. The control structure of model predictive control is shown in ***Figure 4.7.***

The current is measured at sampling time $\boldsymbol{k}$ and the predictive current controller calculates the seven possible current vectors at sampling instant ***k+1***, $\boldsymbol{i}_{dq}{}^{p}(\boldsymbol{k}+1)$, corresponding to the six active and the zero vector voltage using ***Equation 4.23*** from the machine discrete model. These current vectors are evaluated by a cost function, that will find the optimum voltage vector that minimises the current error. The simplest cost function for this purpose could be the one presented in ***equation 4.25.***

$$\boldsymbol{g}=\left(\boldsymbol{i}_d^p(\boldsymbol{k}+1)\right)^2+\left(\boldsymbol{i}_q^*-\boldsymbol{i}_q^p(\boldsymbol{k}+1)\right)^2+\begin{cases}\infty if\left|\boldsymbol{i}_d^p\right|>\boldsymbol{i}_{max}\ or\left|\boldsymbol{i}_q^p\right|>\boldsymbol{i}_{max}\\ 0\,if\left|\boldsymbol{i}_d^p\right|\le\boldsymbol{i}_{max}\ and\left|\boldsymbol{i}_q^p\right|\le\boldsymbol{i}_{max}\end{cases} \tag{4.25}$$

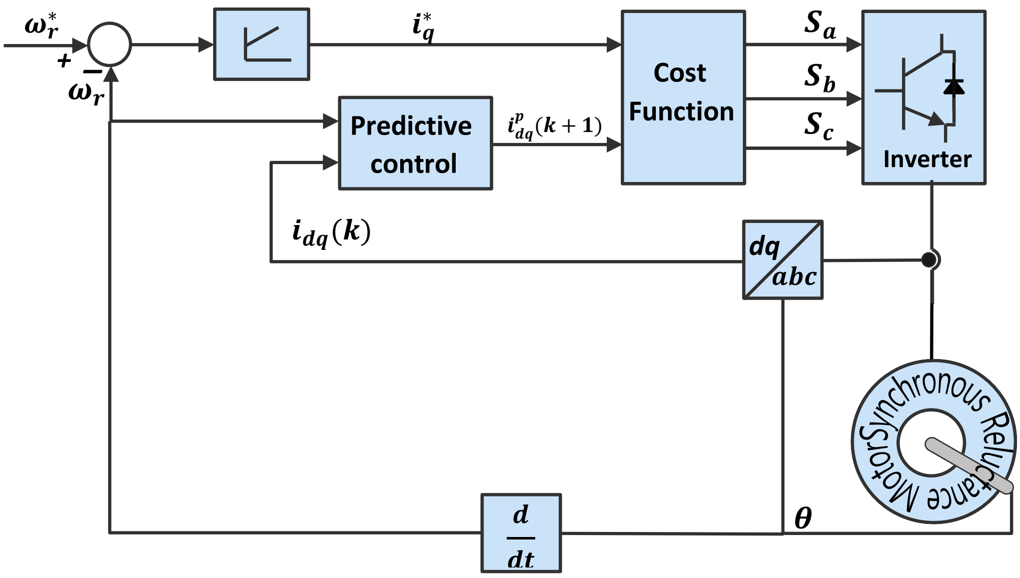

Figure 4.7. Predictive control structure.

where the first term represents the minimization of the reactive power, allowing the torque by ampere optimization, the second term is defined for tracking the torque-producing current, and the last term is a nonlinear function for limiting the amplitude of the stator currents. $\boldsymbol{i}_{max}$ is the value of the maximum allowed stator current magnitude. In this way, if a given voltage vector generates predicted currents with a magnitude higher than $\boldsymbol{i}_{max}$ then the cost function will be $\boldsymbol{g}=\infty$, and , in consequence, this voltage vector will not be selected. On the other hand, if the predicted stator currents are below the limits, the cost function will be composed of the first two terms only and the voltage vector that minimizes the current error will be selected.

4.4. Control Scheme

Two approaches are proposed to improve ***SynRM*** control:

1-First approach is to estimate the rotor speed by the ***MRAS*** observer and then submit this estimate to the Model predictive control.

2- Second approach consists of replacing the conventional ***PI*** current controller rotor speed with that based on model predictive control ***MPC*** using the adaptive model reference observer ***MRAS*** upstream.

4.4.1. First approach

In order to feed the predictive control model and reach the optimal speed, it is necessary to subject it to the model reference adaptive system, which employs the state observer model with current error feedback and the rotor current model as two models for current estimation. Thus, to extract the estimated speed, the difference between the outputs of the state observer model and the rotor current model is used to obtain a zero error.

Vector control provides good performance in transient condition in addition to steady state condition [59], [60].

Figure.4.8. shows the field-oriented control of a ***SynRM*** utilizing predictive control and ***MRAS*** current control. In addition, a ***PI*** controller is employed for controlling the speed and generating the reference for the torque output current $i_{sq_{ref}}$ provided by the ***MRAS*** speed observer. A predictive current controller is employed to follow this current. In the predictive circuit diagram, the discrete-time model of the machine is used to forecast the components of the stator current for each of the seven different voltage vectors produced by the inverter. The voltage vector that keeps a cost function to a minimum is chosen and implemented for a full sampling interval.

The aim of the system of current control is to keep the error between the reference and the measured currents values to a minimum. This objective, in the case of SynRM speed control, can be defined as

a cost function ***equation 4.24*** that meets certain requirements such as monitoring the reference speed, torque by ampere optimization and limiting the current intensity.

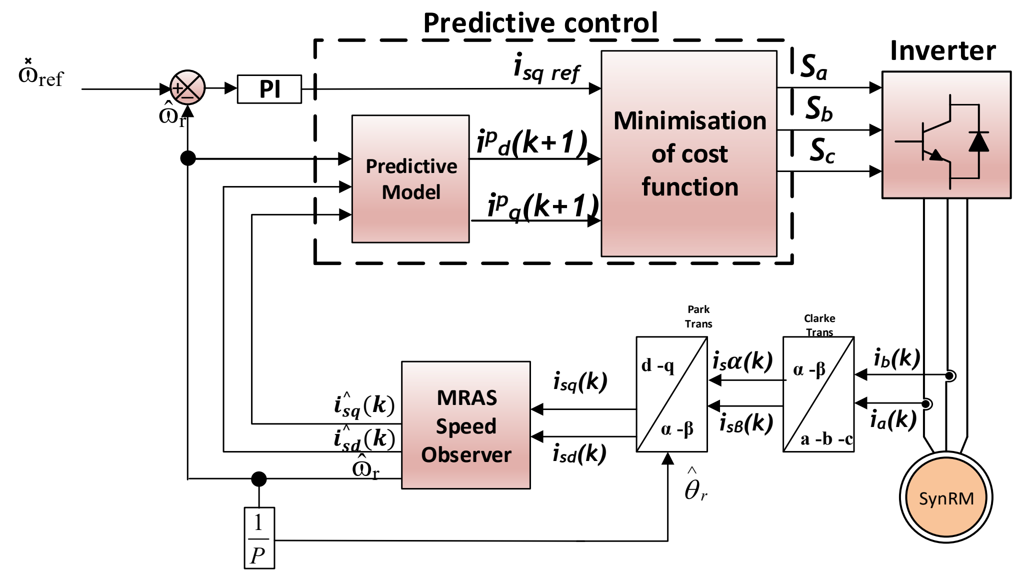

Figure 4.8. Foc of a SynRM using predictive and MRAS current control

4.4.1.1. Simulation Results

Results using the first approach scheme are shown in ***Figure 4.9***, in this figure a speed reference step change is performed at time the beginning, then a speed reversal at time $\boldsymbol{t = 0.15\ s}$. It can be seen from these results that all the objectives of the control are achieved during the tests. Fast tracking of the torque-producing current $\boldsymbol{i_{sq}}$ is achieved while the $\boldsymbol{i_{sd}}$ current is near zero. During transients the magnitude of the currents is limited and both components are decoupled.

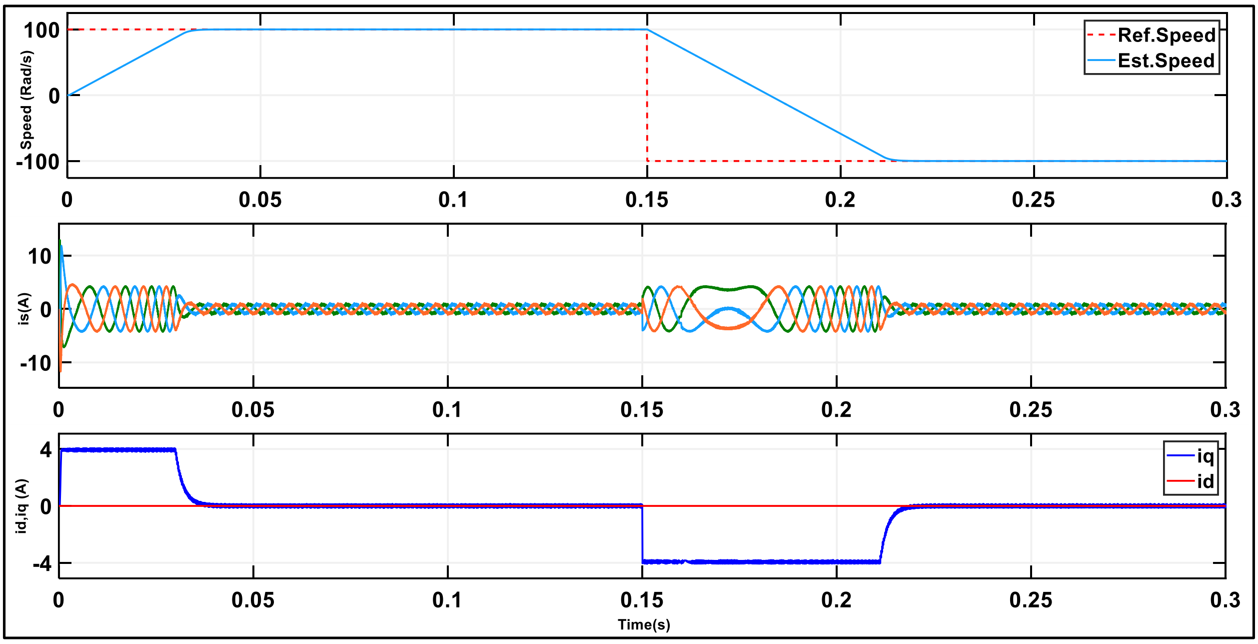

Figure 4.9. SynRM Mras-Mpc behaviour, rotor speed and stator currents

The behaviour of this approach for a speed reversal is shown in ***Figure 4.9***. During this transient the maximum allowed i_{sq} current is applied, which is effectively limited by the last term of the cost function equation 4.24. The i_{sd} current component is near zero even during the transients.

4.4.2. Second approach

The remarkable efficiency and price/performance ratio that ***PID*** controllers enjoy is still difficult to match. However, this type of controller does not cover all needs and their performance suffers in a certain field of applications such as non-linear, instability, non-stationary, and pure high delay. These limitations have favoured the emergence of predictive control based on digital models. These digital controllers are more capable of algorithmic processing, integrating calculation and logic, than purely analogue controllers.

Following the same principle as the first approach, the stator current and speed are estimated using the ***MRAS*** technique, then fed into the ***MPC*** block, but with the ***PI*** regulator replaced by this ***MPC*** block in order to calculate the reference voltage vector ***RVV***.

This new approach which takes into account all the mechanical and electrical variables in a control law via a new cost function allows to obtain the signals switched to the power converter.

4.4.2.1. Setting MPC block

The ***MPC*** block is an interactive tool for designing ***MPC*** controller. It is implemented as part of the Model Predictive Control Toolkit. An ***MPC*** problem is formulated as a quadratic programming ***QP*** problem that attempts to minimize a quadratic cost function. ***MPC*** computations become more complex as the number of states, constraints, order length and prediction horizons increase. To reduce the complexity and computational time of the ***MPC*** in order to run it faster, we apply model order reduction techniques that are used to discard states that do not contribute to the dynamics of the system and use a shorter control and prediction horizon.

All ***MPC*** does online is finding the region in which the current state lies and evaluate the linear function to create the current control action. Reducing the iterative optimisation process to the evaluation of the linear function greatly simplifies the runtime calculations. To ensure that a solution is found within the sampling time and that there is even some extra time left for other tasks that need to be executed on the computer. To address this, we determine a maximum value for the number of optimisation iterations.

MPC uses a plant model to make predictions and an optimizer to find the optimal control action, we can specify ***MPC*** design parameters for the prediction and control horizons, and then we see how the system behaviour changes for a larger prediction horizon, then we will play with the control horizon by increasing it to 3 to get better control, after setting all these parameters we can fine tune our controller using the slider, we will drag it to the right for more aggressive control and once the response looks good, we export the controller which updates the ***MPC*** controller block and runs the simulation.

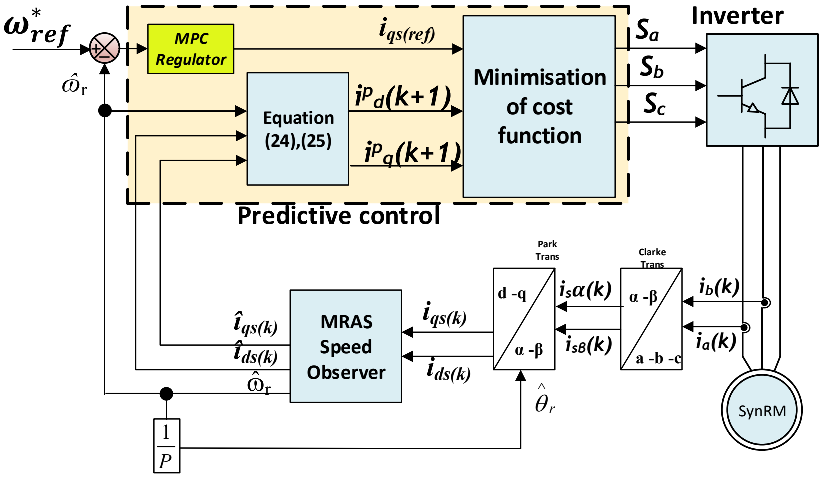

Figure 4.10. The proposed MRAS-MPC controller

Figure 4.10. shows the proposed ***MRAS-MPC*** for ***SynRM***; the ***PI*** speed controller to generate the torque producing reference current $\boldsymbol{i_{qs}}$ to be injected with the currents $\boldsymbol{i_{ds}}$ and $\boldsymbol{i_{qs}}$ which are subject to predictive control is replaced by the bloc ***MPC***, the currents estimated by the ***MRAS*** technique are used in the prediction model to improve the robustness of the proposed method. These current vectors are evaluated by a cost function, that will find the optimum voltage vector that minimises the current error.

The vector voltage can be calculated using ***equation 2.4***

$$\begin{cases} V_{ds,ref}(k) = R_s\hat{i}_{ds}(k) + L_{ds}\left(\dfrac{i_{ds,ref}(k+1) - \hat{i}_{ds}(k)}{T_s}\right) - \hat{\omega}_r(k)L_{qs}\hat{i}_{qs}(k) \\ V_{qs,ref}(k) = R_s\hat{i}_{qs}(k) + L_{qs}\left(\dfrac{i_{qs,ref}(k+1) - \hat{i}_{qs}(k)}{T_s}\right) + \hat{\omega}_r(k)L_{ds}\hat{i}_{ds}(k) \end{cases} \tag{4.25}$$

The expression of the cost function can be defined as follows:

$$g = \left|i_{ds,ref}(k+1) - i_{ds}(k+1)\right| + \left|i_{qs,ref}(k+1) - i_{qs}(k+1)\right| + \begin{Bmatrix} 0\,if\,\sqrt{i_{ds}(k+1)^2 + i_{qs}(k+1)^2} \leq i_{s,max} \\ \infty if\,\sqrt{i_{ds}(k+1)^2 + i_{qs}(k+1)^2} > i_{s,max} \end{Bmatrix} \tag{4.26}$$

4.4.2.2. Simulation results and discussion

The parameters of the cost function (rate weight of manipulated variable =0.1) and the horizons (prediction horizon =3, control horizon =1) are determined such that the Hessian matrix of the ***PQ*** is positively defined. The following ***table 4.1*** lists the controller's minimum ***MPC*** parameter along prediction horizon for each manipulated variable (***MV***) and output variable (***OV***).

MV(Reference Torque) Weights Rate	OV (Speed) Weights
0.00742736	13.4637

TABLE 4.1. PENALTY WEIGHTS ON MANIPULATED VARIABLE(MV) RATES AND OUTPUT VARIABLES(OV)

In what follows, for ***SynRM*** machine featuring a two-level inverter for which the parameters and ratings are given in ***Table 1.2*** steady-state performance of the ***MRAS-MPC*** is compared with that of the standard ***MRAS-PI***. The comparison is made in terms of speed response time, disturbance rejection, torque ripple and stator current.

Looking at ***Figures 4.12*** and ***4.14*** it can be assumed that the proposed ***MRAS-MPC*** has similar performance to that of a conventional ***MRAS-PI*** controller. In order to clear up possible misunderstandings, the performance of a ***MRAS-MPC*** controller was tested under similar conditions.

The advantages of this new approach are its superior disturbance rejection capability (**97. 5%**), ***Figures 4.13.c*** and ***4.16*** , perfect speed ripple reduction, except for a slight response due to adjusting the state estimation in the ***MPC*** toolbox to a slower mode in order to keep the ripple low, also excellent ripple reduction regarding torque ***Figure 4.13.a***, perfect load torque reaction compared to the ***PI*** controller, and the stator current components behave correctly with perfect ripple reduction as shown in ***Figure 4.13.b***, and to illustrate the performance of this new controller, a summary ***Table 4.2***. is provided below to justify the proposed controller, in addition a speed error is performed as shown in ***Figure 4.15.***

Controllers	Speed	Torque	Stator currents
PI controller	Slow tracking with disturbance rejection capability (94 %)	increased picks and more ripples	More picks
New controller	Good tracking with superior disturbance rejection capability (97. 5%) and perfect speed ripple reduction	Decreased picks and Less ripples	Decreased picks

TABLE 4.2. COMPARISON RESULTS BETWEEN THE DIFFERENT CONTROLLERS

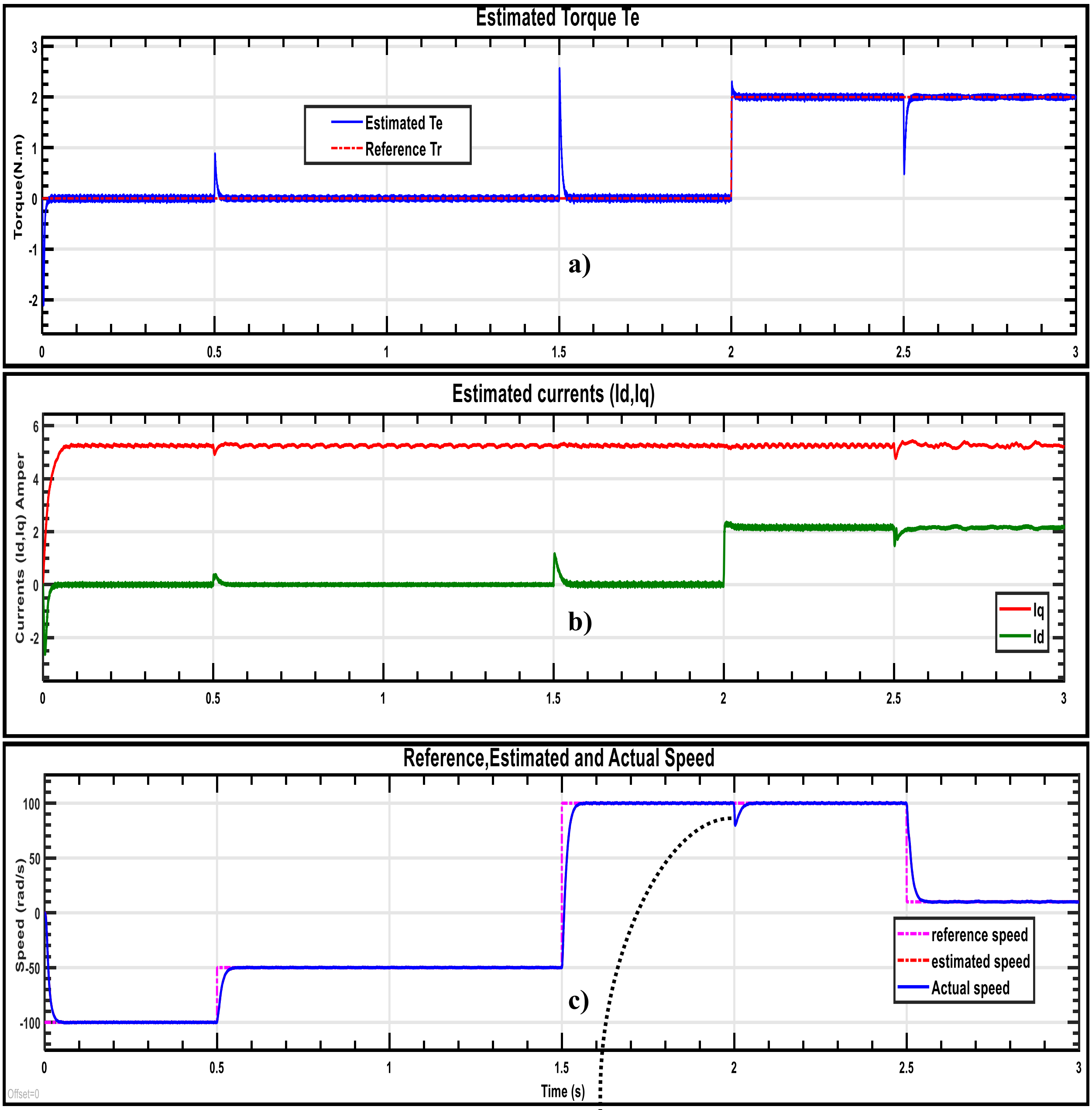

Figure 4.11. Behaviour of PI controller for SynRM. Torque, Stator Currents and Rotor speed

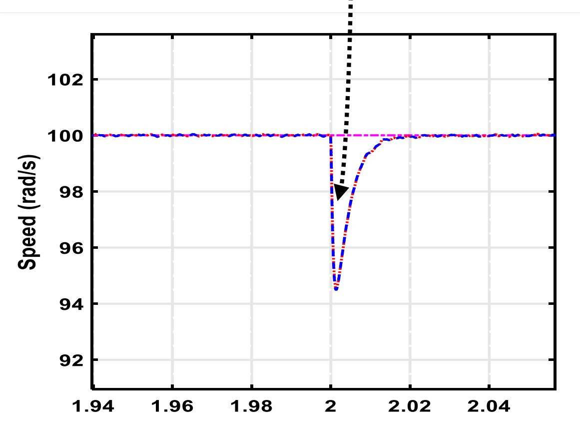

Figure 4.12. Zoom Speed PI Controller

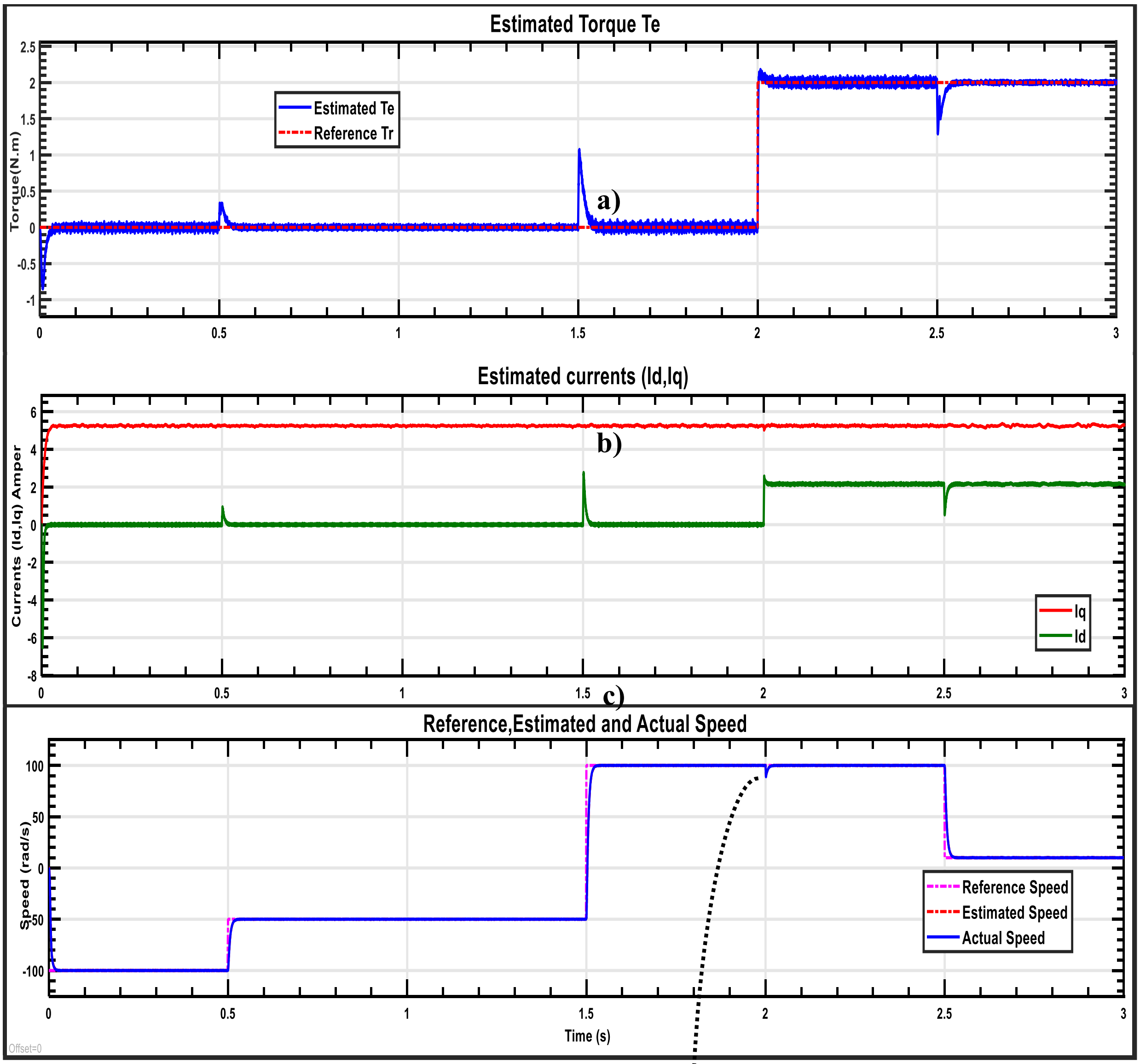

Figure 4.13. Behaviour of the proposed MRAS-MPC controller for the SynRM. Torque, Stator Currents and Rotor speed

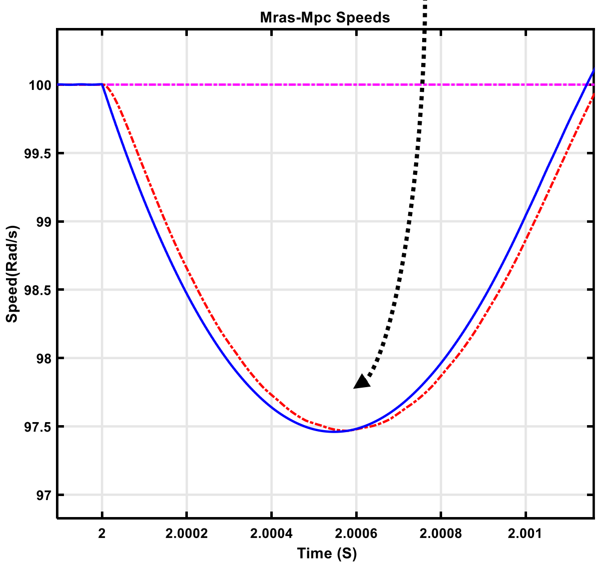

Figure 4.14. Zoom Speed MRAS- MPC Controller

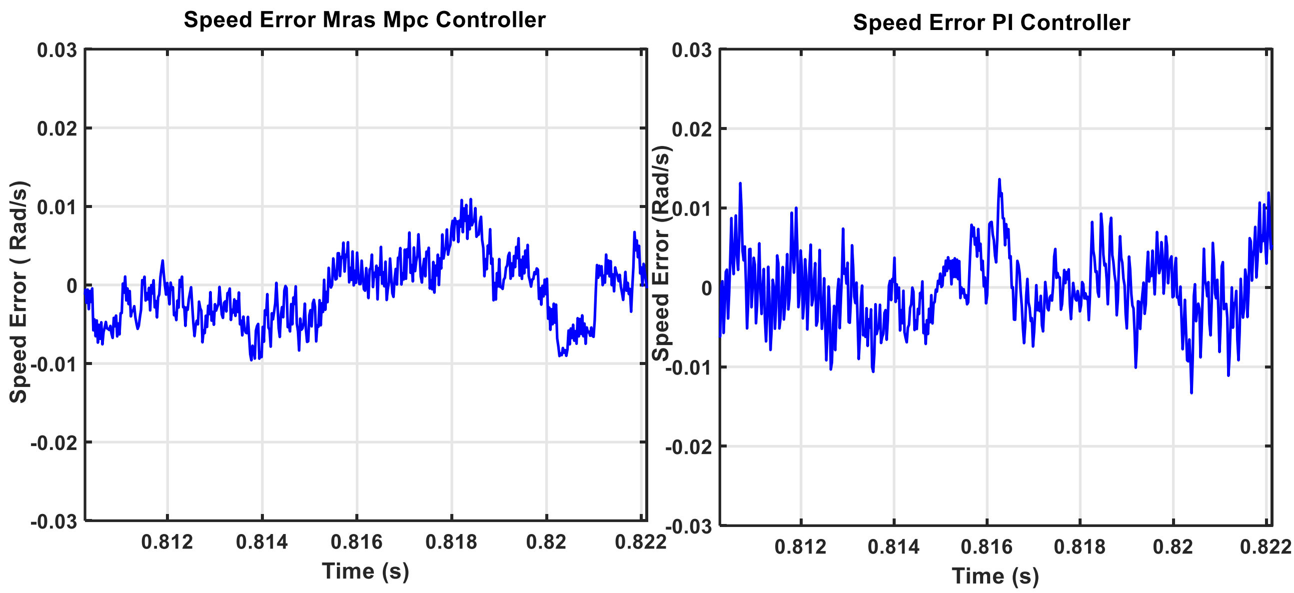

Figure 4.15. Zoom in on speed error

4.5.Conclusion

The predictive control associated with MRAS technique was implemented as a new approach with simulation at a constant speed of 100 rad/s, and an inverter switching of 13.56 MHz, the disturbance rejection capability is greatly improved and the perfect reduction of speed, torque and stator current ripple, an instantaneous reaction of electromagnetic torque to changes in speed and load torque which keeps the system in the right function with respect to that of PI controller.

- The new controller can produce the appropriate voltage to reach the reference speed.

- The simulation results highlighted the performance improvements introduced by this approach.

SynRM's sensorless accuracy estimation performs poorly when the speed is close to zero and the machine parameters need to be studied in more detail, due to voltage measurement noise and integrator drift, although significant progress has been made recently in these areas. Further research is underway in the next study to implement low-pass filters (LPFs) at the input of the MRAS block to reduce torque ripple and pure voltage integration so that they can be implemented in the real world.

General Conclusion

In this thesis, we addressed the problem of sensorless control of the SynRM. Our objective was to propose a non-linear control law without mechanical sensors (using a Speed Observer).

The sensorless control law we have proposed is a vector control based on 'PI' controllers and 'MPC' type controllers combined with an MRAS for regulation.

In this context , Model Reference Adaptive System (MRAS) is favoured for its simplicity in operation. Model Predictive Control (MPC) emerges as a promising alternative to PI controllers in speed loops, offering advantages such as order reduction, disturbance rejection, robustness, and straightforward implementation via power converters. MPC operates within a Variable Structure System (VSS), employing a switching logic with high-frequency discontinuous control actions based on system state, disturbances, and reference inputs.

Mras – Mpc controller is the proposed and newest strategy, it combines all the cascaded structure in one control law to obtain the switching vector by minimizing the predefined cost function. Its advantages are very fast dynamic response without overshooting, while its disadvantages are the variable switching frequency and high current/torque ripples. FOC is the most popular control with cascaded PI controllers (current and speed), its advantages are constant switching frequency and low torque ripples, while its weakness is the slow dynamic response.

The mathematical model of the system is presented first, followed by the analysis of Lyapunov stability, which has been detailed specifically in the Mras observer. This is followed by the design methodology of the proposed observer with a Mras - Mpc cascade on the one hand, and the replacement of the PI controller by the Mpc controller on the other, while retaining the Mras - Mpc cascade approach.

Simulation verification tests have been carried out on industrial trajectories and the results obtained demonstrate the effectiveness and robustness of the proposed observer.

To further improve the performance and robustness of the proposed observer, future research will involve the generalisation of the proposed algorithm to make it suitable for dealing with large uncertainties in induction machine parameters under critical working conditions due to heating, saturation and other physical effects. In addition, further developments of the proposed algorithm would also make it suitable for applications where an adaptive strategy is required to overcome the observational uncertainty of the system.

With all these good results presented by the observer, there are still some points to be rectified in future work, since we noted in the first chapter that the machine model is created after taking into account simplifying assumptions and since private research into the modelling of synchronous machines is interested in minimising these assumptions, it is necessary to join in and try to train the observer within the framework of the new models, which are more complex than their predecessors to some extent, future work will also focus on the diagnostic aspect and on studying the performance of the observer under other machine operating conditions, such as fault conditions, and we are also proposing it for synchronous machines or other systems because the scope for its use is wider than others.

Further research is underway in the next study to implement low-pass filters (LPFs) at the input of the MRAS block to reduce torque ripple and pure voltage integration so that they can be implemented in the real world.

Annex

Current regulator

$$\left(Kp_{id}+\frac{Ki_{id}}{s}\right)=\left(\frac{Kp_{id}.s+Ki_{id}}{s}\right)=Kp_{id}\left(\frac{s+\frac{Ki_{id}}{Kp_{id}}}{s}\right)=Kp_{id}\left(s+\frac{Ki_{id}}{Kp_{id}}\right).\frac{1}{s}$$

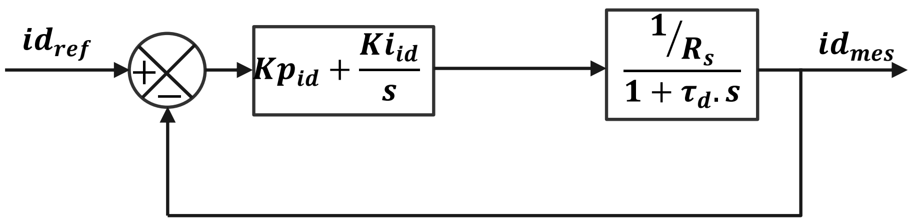

The open loop of this circuit is as follows:

$$H_{op}(s)=[Kp_{id}\left(s+\frac{Ki_{id}}{Kp_{id}}\right).\frac{1}{s}].[\frac{\frac{1}{R_s}}{1+\frac{L_d}{R_s}.s}] \qquad \text{With} \quad \tau_d=\frac{L_d}{R_s}$$

$$\frac{\frac{1}{R_s}}{1+\frac{L_d}{R_s}.s}=\frac{1}{R_s+L_d.s}=\frac{\frac{1}{L_d}}{s+\frac{R_s}{L_d}}$$

$$H_{op}(s)=[Kp_{id}\left(s+\frac{Ki_{id}}{Kp_{id}}\right).\frac{1}{s}].\frac{\frac{1}{L_d}}{s+\frac{R_s}{L_d}}\equiv \quad \text{........ Equation 2.6}$$

By offsetting the dominant pole , $\frac{Ki_{id}}{Kp_{id}}=\frac{R_s}{L_d}$ we get :

$H_{op}(s)=Kp_{id}.\frac{1}{L_d}.\frac{1}{s}$ …….. The closed loop with feedback equal to one is:

$$\frac{Output}{input}=\frac{id_{mes}}{id_{ref}}=\frac{Kp_{id}.\frac{1}{L_d}.\frac{1}{s}}{1+Kp_{id}.\frac{1}{L_d}.\frac{1}{s}}=\frac{Kp_{id}}{Kp_{id}+L_d.s}=\frac{1}{1+\frac{L_d}{Kp_{id}}.s}$$

With $\tau_{id}=\frac{L_d}{Kp_{id}}$

$$H_{dc}(s)=\frac{1}{1+\tau_{id}.s}\equiv \quad \text{........ Equation 2.8}$$

Block diagram of vector control figure 2.4:

$$Te = \frac{3}{2}p\left(L_d - L_q\right)i_d i_q$$

i_d constant $\Rightarrow$ ($i_d = \dfrac{\Psi_d}{L_d}$) therefore $T_e = K\, i_q$ linear function

$$K = \frac{3}{2}p\left(L_d - L_q\right)i_d \;\Rightarrow \left\{ \begin{array}{c} i_q^* = \dfrac{T_e}{\frac{3}{2}p\left(L_d - L_q\right)i_d^*} \\ i_d = \dfrac{\Psi_d}{L_d} \end{array} \right\}$$

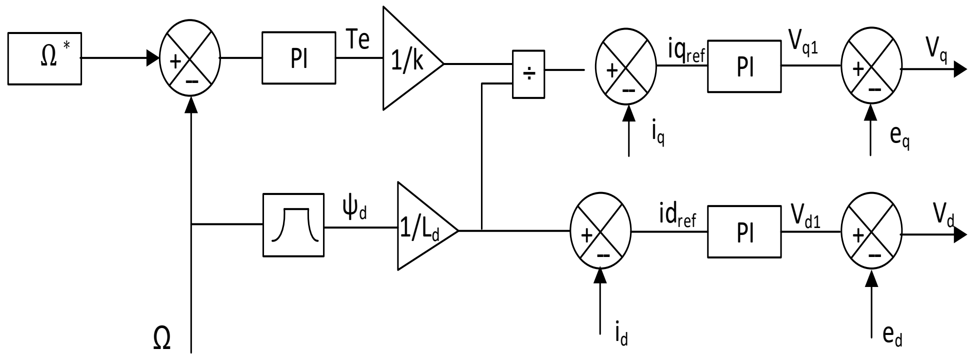

Control study:
For different damping coefficients ξ we can find a relationship between (ξ and $\tau_\Omega \omega_n$). The following table shows this relationship:

ξ	$\tau_\Omega \omega_n$
0.4	7.7
0.5	5.3
0.6	5.2
0.7	3
1	4.75

Bibliography

[1] Mcallister, Pat et Nase, Ilir. The impact of Minimum Energy Efficiency Standards: Some evidence from the London office market. Energy Policy, 2019, vol. 132, p. 714-722.

[2] De Almeida, Anibal T, Fong, Joao, Falkner, Hugh, et al. Policy options to promote energy efficient electric machines and drives in the EU. Renewable and Sustainable Energy Reviews, 2017, vol. 74, p. 1275-1286.

[3] E. Bostanci, M. Moallem, A. Parsapour and B. Fahimi, "Opportunities and Challenges of Switched Reluctance Machine Drives for Electric Propulsion: A Comparative Study," IEEE Transactions on Transportation Electrification, vol. 3, no. 1, pp. 58-75, March 2017

[4] T.J.E. Miller, A. Hutton, C. Cossar, and D.A. Staton. Design of a synchronous reluctance machine drive. IEEE Transactions on Industry Applications, 27(4):741–749, July/Aug. 1991

[5] Li, C., Wang, G., Zhang, G., Zhao, N., & Xu, D. (2020). Adaptive pseudorandom high-frequency square-wave voltage injection based sensorless control for SynRM drives. IEEE Transactions on Power Electronics, 36(3), 3200-3210.

[6] C. Li, G. Wang, G. Zhang and D. Xu, "High Frequency Torque Ripple Suppression for High Frequency Signal Injection Based Sensorless Control of SynRMs", 2019 IEEE Applied Power Electronics Conference and Exposition (APEC), pp. 2544-2548, 2019..

[7] Park, J. D. (2007). Modeling and control of a high-speed solid-rotor synchronous reluctance flywheel machine/generator. The Pennsylvania State University.

[8] Boztas, G., & Aydogmus, O. (2022). Implementation of sensorless speed control of synchronous reluctance machine using extended Kalman filter. Engineering Science and Technology, an International Journal, 31, 101066.

[9] S. Bolognani, M. Zigliotto and M. Zordan, "Extended-range PMSM sensorless speed drive based on stochastic filtering", IEEE Trans. Power Electron., vol. 16, no. 1, pp. 110-117, Jan. 2001.

[10] T. Senjyu, K. Kinjo, N. Urasaki and K. Uezato, "High efficiency control of synchronous reluctance machines using extended Kalman filter", IEEE Trans. Ind. Electron., vol. 50, no. 4, pp. 726-732, Aug. 2003

[11] Soltani, J., & Zarchi, H. A. (2003, November). Robust optimal speed tracking control of a current sensorless synchronous reluctance machine drive using a new sliding mode controller. In The Fifth International Conference on Power Electronics and Drive Systems, 2003. PEDS 2003. (Vol. 1, pp. 474-479). IEEE24.

[12] F. P. Scalcon, C. J. Volpato, T. Lazzari, T. S. Gabbi, R. P. Vieira and H. A. Gründling, "Sensorless Control of a SynRM Drive Based on a Luenberger Observer with an Extended EMF Model," IECON 2019 - 45th Annual Conference of the IEEE Industrial Electronics Society, Lisbon, Portugal, 2019, pp. 1333-1338, doi: 10.1109/IECON.2019.8927192.

[13] Control System Design Guide Using Your Computer to Understand and Diagnose Feedback Controllers Book • Fourth Edition • 2012.

[14] Sun, P., Zhang, D., Bai, Z., Xiao, Q., Chen, B., & Yu, Z. (2019, August). Comparison study of Mras and emf-based sensorless control for synchronous reluctance machine. In 2019 22nd International Conference on Electrical Machines and Systems (ICEMS) (pp. 1-5). IEEE.

[15] Zhang, K., Yang, X., & Xu, X. (2020, November). Sensorless Control of Synchronous Reluctance Machine over Full Speed Range. In 2020 23rd International Conference on Electrical Machines and Systems (ICEMS) (pp. 1663-1667). IEEE.

[16] Ferdoud, S M., Garcia, Pablo, Oninda., Mohammad Abdul Moin, al, MTPA and field weakening control of synchronous reluctance machine, 9th International Conference on Electrical and Computer Engineering (ICECE), (2016). p. 598-601.

[17] Ghaderi A., Hanamoto T., Wide-Speed-Range Sensorless Vector Control of Synchronous Reluctance Machines Based on Extended Programmable Cascaded Low-Pass Filters, IEEE Transactions on Industrial Electronics, vol. 58, no. 6, (2011), pp. 2322-2333.

[18] S. Racewicz, D. Riu, N. Retière, P. Chzran, Non-linear half-order modeling of synchronous machine, in: International Electrical Machines and Drives Conference IEMDC, Miami, United States, 2009.

[19] S. Maiti, C. Chakraborty, S. Sengupta, Simulation studies on model reference adaptive controller based speed estimation technique for the vector controlled permanent magnet synchronous machine drive, Simulation Modelling Practice and Theory 17 (2009) 585–596.

[20] Nikmaram, B., Davari, S. A., Naderi, P., Garcia, C., & Rodriguez, J. (2021). Sensorless simplified finite control set model predictive control of SynRM using finite position set algorithm. IEEE Access, 9, 47184-47193.

[21] Mohand Ouramdane Hamiti. Réduction des ondulations de couple d'une machine synchrone à réluctance variable. P151, Thése de Doctorat de l'université Henri Poincaré Nancy-I, 2009. (pages 21, 33).

[22] Robert E Betz, Rolf Lagerquist, Milutin Jovanovic, Timothy JE Miller, and Richard H Middleton. Control of synchronous reluctance machines. IEEE Transactions on Industry applications, 29(6) :1110–1122, 1993. (Page 23).

[23] Thierry Lubin. Modélisation et commande de la machine synchrone à réluctance variable : prise en compte de la saturation magnétique. PhD thesis, Université Henri Poincaré; Nancy I, 2003.

[24] J.-D. Park, "Modeling and Control of a High-Speed Solid-Rotor Synchronous Reluctance Flywheel Machine/Generator," The Pennsylvania State University, 2007.

[25] Park, Jae-Do, KALEV, Claude, et Hohmann, Heath. Modeling and control of solid-rotor synchronous reluctance machines based on rotor flux dynamics. IEEE transactions on magnetics, 2008, vol. 44, no 12, p. 4639-4647

[26] T. A. Lipo, T. J. E. Miller, A. Vagati, I. Boldea, L. Malesani, and T. Fukao, "Synchronous reluctance drives" tutorial presented at IEEE-IAS Annual Meeting, Denver, CO, Oct.1994.

[27] A. Aghmadi, H. Hussein and O. A. Mohammed, "Enhancing Energy Management System for a Hybrid Wind Solar Battery Based Standalone Microgrid," 2023 IEEE International Conference on Environment and Electrical Engineering and 2023 IEEE Industrial and Commercial Power Systems Europe (EEEIC / I&CPS Europe), Madrid, Spain, 2023, pp. 1-6, doi: 10.1109/EEEIC/ICPSEurope57605.2023.10194769.

[28] D Arun Dominic, Thanga Raj Chelliah, Analysis of field-oriented controlled induction machine drives under sensor faults and an overview of sensorless schemes, ISA Transactions, Volume 53, Issue 5,2014, Pages 1680-1694.

[29] Mohamed Zerrougui. Observation et commande des systemes singuliers non linéaires. PhD thesis, Université Henri Poincaré-Nancy I, 2011. (Pages 57, 59, 68).

[30] Mohammed Chadli. Stabilité et commande de systèmes décrits par des multimodèles. PhD thesis, Vandoeuvre-les-Nancy, INPL, 2002. (pages 59, 60,61, 64).

[31] M. Oueder, M. Farza, R. Ben Abdennour, M. M'Saad, A high gain observer with updated gain for a class of MIMO nontriangular systems, Systems & Control Letters 61 (2012) 298–308 02/01/ 2012.

[32] M. Ghanes, J. De Leon and A. Glumineau, Observability Study and Observer-Based Interconnected Form for Sensorless Induction Machine, Proceedings of the 45th IEEE Conference on Decision & Control San Diego, CA, USA, December 13-15, 2006.

[33] Ramzi Trabelsi, Adel Khedher, Mouhamed Faouzi Mimouni, Faouzi M'sahli, Backstepping control for an induction machine using an adaptive sliding rotor-flux observer, Electric Power Systems Research 93 (2012) 1– 15

[34] Dramane Traore. COMMANDE NON LINEAIRE SANS CAPTEUR DE LA MACHINE ASYNCHRONE. Automatique /Robotique. Thèse de doctorat Ecole Centrale de Nantes (ECN), 2008.

[35] Daniel Depernet. Optimisation de la commande d'un onduleur MLI a trois niveau de tension pour machine asynchrone. Energie électrique. Thèse de doctorat Université de Reims - Champagne Ardenne,1995

[36] Zahraoui, Y., Moutchou, M., Tayane, S., Elbadaoui, S. (2022). Investigation of Different Speed Controllers to Improve the Performance of Vector-Controlled Synchronous Reluctance Machine. In: Hamlich, M., Bellatreche, L., Siadat, A., Ventura, S. (eds) Smart Applications and Data Analysis. SADASC 2022.

[37] Ponce de León Puig, Nubia Ilia. Design of a hysteresis predictive control strategy with engineering application cases. Doctoral Thesis, Universitat politècnica de catalunya (UPC) ,2021.(pages 67,68)

[38] Ben brahim amal "Commande Prédictive Généralisée d'une Machine Synchrone à Aimants Permanents"thèse de magistère en électrotechnique, université de batna 2009

[39] E. G. Migliore, " Commande Prédictive à Base de Programmation Semi Définie", thèse de doctorat, l'Institut National des Sciences Appliquées de Toulouse, 2004.

[40] Lozada, M. C. (2003). Sur les modeles flous adaptatifs dynamiques (Doctoral dissertation, INSA de Toulouse).

[41] E.F. Camacho, C. Bordons, "Model Predictive Control", Springer-Verlag London, 2nd edition, 2003.

[42] Patrick Boucher, Didier Dumur, "la commande prédictive", collection méthodes et pratiques de l'ingénieur, école centrale de Lille, 1996.

[43] A. Desbiens et al., "Global predictive control: A unified control structure for decoupling setpoint tracking, feedforward compensation and disturbance rejection dynamics," IEEE Proc. Control Theory and Application, 2000.

[44] O. Asvadi-Kermani et al., "Energy Optimization of Air Handling Units Using Constrained Predictive Controllers Based on Dynamic Neural Networks," in IEEE Access, vol. 10, pp. 56578-56590, 2022, doi: 10.1109/ACCESS.2022.3177660.

[45] Ramdani, Ammar et Grouni, Said. Dynamic matrix control and generalized predictive control, comparison study with IMC-PID. International Journal of Hydrogen Energy, 2017, vol. 42, no 28, p. 17561-17570.

[46] Clarke, David W., Mohtadi, Coorous, et Tuffs, P. Simon. Generalized predictive control—Part I. The basic algorithm. Automatica, 1987, vol. 23, no 2, p. 137-148.

[47] Kumar, Rahul, DAS, Sukanta, et Bhaumik, Adrish. Speed sensorless model predictive current control of doubly-fed induction machine drive using model reference adaptive system. ISA transactions, 2019, vol. 86, p. 215-226.

[48] Nguyen A T., Rafaq M S., Choi H H., Jung J W., A Model Reference Adaptive Control Based Speed Controller for a Surface-Mounted Permanent Magnet Synchronous Machine

Drive, IEEE Transactions on Industrial Electronics, vol. 65, no. 12, (2018), pp. 9399-9409

[49] Schauder C., Adaptive speed identification for vector control of induction machines without rotational transducers, IEEE Transactions on Industry Applications, vol. 28, no. 5, (1992), pp. 1054-1061.

[50] Boztas, Gullu., Aydogmus, Omur., Implementation of sensorless speed control of synchronous reluctance machine using extended Kalman filter, Engineering Science and Technology, an International Journal, (2022), vol. 31, p. 101066.

[51] Yousefi Talouki A., Pescetto P., Pellegrino G., Sensorless Direct Flux Vector Control of Synchronous Reluctance Machines Including Standstill, MTPA, and Flux Weakening, IEEE Transactions on Industry Applications, vol. 53, no. 4, (2017) , pp. 3598-3608

[52] Rodriguez Jose., Patricio Cortes., Predictive control of power converters and electrical drives, John Wiley – Sons Book Company (2012)

[53] Farhan A., Abdelrahem M., Saleh A., Shaltout A., Kennel R., Simplified Sensorless Current Predictive Control of Synchronous Reluctance Machine Using Online Parameter Estimation, Energies, vol. 13, (2020), no. 2, p. 492.

[54] Carlet, Paolo Gherardo., Tinazzi, Fabio., Bolognani, Silverio., al., An effective model-free predictive current control for synchronous reluctance machine drives, IEEE Transactions on Industry Applications, vol. 55, no 4, (2019), p. 3781-3790.

[55] E. Fuentes, C. Silva, D. Quevedo, and E. Silva, "Predictive speed control of a synchronous permanent magnet machine," in IEEE International Conference on Industrial Technology, ICIT 2009, 2009, pp. 1–6

[56] Clarke G M,. Burden R L,. Faires J D,. Numerical Analysis, Cengage Learning, (2012).

[57] Morel, Lin-Shi, Retif, Allard, and Buttay, 2009. F. Morel, Xuefang Lin-Shi, J.-M. Retif, B. Allard, and C. Buttay. A Comparative Study of Predictive Current Control Schemes for a Permanent-Magnet Synchronous Machine Drive. Industrial Electronics, IEEE Transactions on, 56(7), 2715-2728, 2009. ISSN 0278-0046. doi:10.1109/TIE.2009.2018429.4.

[58] Gao X., Abdelrahem M., Hackl C M., Zhang Z., Kennel R., Direct Predictive Speed Control With a Sliding Manifold Term for PMSM Drives, IEEE Journal of Emerging and Selected Topics in Power Electronics, vol. 8, no. 2, (2020) ,pp. 1258-1267.

[59] J.A. Satisteban, R.M. Stephen, “Vector control methods for induction machines: An Overview,” IEEE Transactions on Education, Vol.44, No.2, pp.170.

[60] Farhan, Ahmed, Mohamed Abdelrahem, Adel Shaltout, Ralph Kennel, and Amr Saleh. "Encoderless Current Predictive Control of Synchronous Reluctance Machine by Extended Kalman Filter based State Estimation." In PCIM Europe digital days 2020; International Exhibition and Conference for Power Electronics, Intelligent Motion, Renewable Energy and Energy Management, pp. 1-8. VDE

[61] Chatelain, Machines électriques, Traité d'Electricité, Volume X, Presses Polytechniques Romandes, Lausanne, 1983, 628p

[62] Khlaief, A. (2012). Contribution à la commande vectorielle sans capteur mécanique des machines synchrones à aimants permanents (MSAP) (Doctoral dissertation, AixMarseille Université).p 83.

[63] R.R. Moghaddam, Synchronous Reluctance Machine Design, Thesis Master in Power Electrical Engineering, Royal Institute of Technology (KTH), Sweden, April, 2007.

[64] Jae-Do Park. Modeling and control of high-speed solid rotor synchronous reluctance flywheel machine/generator. doctoral thesis. etda.libraries.psu.edu,2007, (page 13).

Abstract

This thesis focuses on variable speed synchronous machine drives, highlighting their advantages such as robustness and high reliability. Previous research has explored variable speed control of these drives, particularly for applications such as rail traction and marine propulsion.

Many problems require the estimation of the state of a system using an observer. However, modelling and synthesising the observer becomes a difficult task for non-linear systems.

Synchronous Variable Reluctance Machines (SynRMs) have advantages, but their control can be complex due to model non-linearity and parameter fluctuations.

The research presented in this thesis focuses on the state estimation of non-linear systems represented by an Mras-Mpc controller which is proposed as the newest strategy, it combines all cascade structures into one control law to obtain the switching vector by minimising the predefined cost function.

After an introduction to predictive control (MPC) and the optimisation criterion, the Mras is presented in detail while developing its stability in order to propose two approaches with two different cost functions combining the two observers into a single one to consolidate the quantities to be estimated. The first approach consists of feeding the input quantities of the predictive control model with the output quantities of the model's reference adaptive system, in order to achieve the optimum speed.

In the second approach, we propose a controller that estimates the speed by replacing traditional PI controllers with a predictive control model that calculates a new speed estimate based on the MRAS scheme using only stator current and voltage measurements and then optimises the vector voltage that minimises the current error.

Key words: Sensorless Control, Synchronous reluctance machine, Model Reference Adaptive System, model predictive control, Direct Vector Control, Pulse Width Modulation, predictive, Lyapunov stability.

ملخص

تركز هذه الأطروحة على محركات الماكينات المتغيرة السرعة المتزامنة مع تسليط الضوء على مزاياها مثل المتانة والموثوقية العالية وقد تناولت الأبحاث السابقة التحكم في السرعة المتغيرة لهذه المحركات خاصةً في تطبيقات مثل الجر بالسكك الحديدية وعملية الدفع البحرى .

تتطلب العديد من المسايل تقدير حالة النظام باستخدام مراقب ومع ذلك تصبح نمذجة المراقب وتوليفه مهمة صعبة بالنسبة للأنظمة غير الخطية.

تتمتع آلات الممانعة المتغيرة المتزامنة (SynRMs) بمزايا ولكن يمكن أن يكون التحكم فيها معقدًا بسبب عدم خطية النموذج وتذبذب المتغيرات.

يركز البحث المقدم في هذه الأطروحة على تقدير حالة الأنظمة غير الخطية المتمثلة في وحدة تحكم Mpc - Mras المقترحة كأحدث استراتيجية فهى تجمع بين هاتين البنيتين المتتاليتين في قانون تحكم واحد للحصول على شعاع التبديل عن طريق تقليل دالة التكلفة المحددة مسبقًا.

بعد مقدمة عن التحكم التنبؤى MPC و معيار التحسين يتم عرض نظام Mras بالتفصيل مع تطوير استقراره من أجل اقتراح طريقتين بدالتين مختلفتين للتكلفة تجمعان بين المراقبين في مراقب واحد لتوحيد المقادير المراد قياسها وذلك من أجل تحقيق السرعة المثلى.

يتكون النهج الأول من تغذية كميات مدخلات نموذج التحكم التنبؤى بكميات مخرجات النظام التكيفى المرجعى للنموذج من أجل تحقيق السرعة النموذجية.

في النهج الثانى نقترح وحدة تحكم تقوم بتقدير السرعة عن طريق استبدال وحدات التحكم PI التقليدية بنموذج تحكم تنبؤى يقوم بحساب تقدير جديد للسرعة بناءً على مخطط MRAS باستخدام قياسات تيار الجزء الثابت والتوتر الكهربايى فقط ثم تحسين شعاع التوتر الذى يقلل من خطأ التيار